

Title	A Study on Characterization of the Plasma MIG Welding Process
Author(s)	Mamat, Sarizam Bin
Citation	大阪大学, 2018, 博士論文
Version Type	VoR
URL	https://doi.org/10.18910/70761
rights	
Note	

Osaka University Knowledge Archive : OUKA

<https://ir.library.osaka-u.ac.jp/>

Osaka University

Doctoral Dissertation

A Study on Characterization of the Plasma MIG
Welding Process

Mamat Sarizam Bin

June 2018

Division of Materials and Manufacturing Science
Graduate School of Engineering,
Osaka University

Doctoral Dissertation

A Study on Characterization of the Plasma MIG
Welding Process

Mamat Sarizam Bin

June 2018

Division of Materials and Manufacturing Science
Graduate School of Engineering,
Osaka University

Table of Contents

	Page
Chapter 1 Introduction and literature review	
1.1 Background	1
1.2 Plasma MIG welding	2
1.3 Problem statement	5
1.3.1 Challenging issues in controlling heat input into base metal	5
1.3.2 The requirement of low heat input joining in actual application in industry ...	6
1.4 Objectives of the study	8
1.5 Focus and structure of the thesis	9
Chapter 2 Experiment procedure	
2.1 Welding method	10
2.1.1 Plasma MIG welding	10
2.1.2 Conventional MIG welding	11
2.2 Temperature measurement	12
2.2.1 Droplet temperature measurement through two –color temperature Measurement method	12
2.2.2 Plasma temperature measurement through spectroscopy analysis by using Fowler Milne method	13
2.3 Metal transfer observation	15
2.3.1 Shadowgraph method	15
2.3.2 Camera observation method	16
Chapter 3 Study on factors affecting the droplet temperature in plasma MIG welding process	
3.1 Introduction	17
3.2 Materials and welding conditions	18
3.3 Simulation model	20
3.4 Experimental results	24
3.4.1 Correlation between MIG current and wire feeding speed	24
3.4.2 Droplet diameter measurement	26
3.4.3 Droplet temperature measurement	28
3.4.3.1 Dependences of droplet temperature on MIG current and wire feeding speed	28

3.4.3.2 Droplet surface temperature distribution	33
3.4.4 Taper formation around the neck of the wire	36
3.4.5 Plasma temperature measurement in surrounding of MIG wire	40
3.5 Simulation results	44
3.6 Discussion	47
3.6.1 Effects of the plasma flow in plasma MIG welding	47
3.6.2 Effects at low MIG current (from 160 A to 180 A)	48
3.6.3 Effects at medium MIG current (from 190 A to 220 A)	54
3.6.4 Effects at high MIG current (above 230 A)	59
3.6.5 Suggested mechanism of droplet temperature reduction in plasma MIG welding	65
3.7 Conclusion	66

Chapter 4 Mechanism in reducing the droplet temperature in pulse plasma

MIG welding process

4.1 Introduction	67
4.2 Materials and welding conditions	68
4.3 Experimental results	70
4.3.1 Droplet temperature measurement	70
4.3.2 Measurement of droplet diameter	71
4.3.3 Metal transfer observation	72
4.3.4 Taper formation and metal vapor during base current	77
4.4 Discussion	78
4.4.1 Effect of plasma flow to the droplet temperature reduction in pulse plasma MIG welding	78
4.4.2 Mechanism of droplet temperature reduction in pulse plasma MIG welding	80
4.5 Conclusion	81

Chapter 5 The application of pulse plasma MIG welding process to control the IMC thickness in Al/Steel dissimilar joining

5.1 Introduction	82
5.2 Materials and welding conditions	83
5.3 Experimental results	85
5.3.1 Observation of metal transfer behavior in aluminum pulse plasma MIG welding	85

5.3.2 Study on the weldability of Al/Steel dissimilar welding	88
5.3.3 Formation of Intermetallic Compound (IMC)	90
5.3.3.1 Pulse MIG welding	90
5.3.3.2 Pulse plasma MIG welding	91
5.3.3.3 IMC thickness measurement	93
5.3.4 Characterization of IMC through EPMA	97
5.3.4.1 Pulse MIG welding	97
5.3.4.2 Pulse plasma MIG welding	99
5.3.4.3 IMC formation under different MIG current in pulse Plasma MIG welding	101
5.4 Discussion	113
5.4.1 Formation of IMC in pulse plasma MIG welding	113
5.4.2 Control of IMC thickness by plasma MIG welding process	115
5.5 Conclusion	117
Chapter 6 Conclusion	118
Reference	121
Appendix	126
List of publications	134
Acknowledgement	137

Chapter 1

Introduction and literature review

1.1 Background

Nowadays, arc welding is an indispensable method to join a material in various industries such as oil and gas, ship building, automobile and so on. When it comes to controlling quality of the joining, an appearance of weld area such as weld bead profile, height of reinforcement and any other visual defects will be the first consideration in judging the joint quality. However, there are some other defects to be normally present in weld area and beyond the limitations of visual inspection due to its small size, or due to its location inside the joint. Among these, stress riser defect such as crack is one of the most attracted one because of its potential to deteriorate the mechanical properties and leads to the sudden damage of the structures. This brittle failure basically occurs due to the three main reasons: the design stress value that more than maximum stress, the existence of defects, and low material's fracture toughness. For the second and third, it is believed that by controlling the defects formation due to welding process, the mechanical properties of the joining can be improved. Due to that, high quality of welding is required especially for joining the critical structures which dealt with high pressure and so on.

To obtain a high quality of welding, there is a necessity to protect the weld area from the presence of any active gas. The presence of active gas such as oxygen and nitrogen deteriorates the mechanical properties of the joining and become one of the reasons for the formation of welding defects in weld area [1]. For the time being, in a real practice, the welding by using the Gas Tungsten Arc Welding (GTAW) and Plasma Arc Welding (PAW) processes are conducted under the oxygen free condition. However, the disadvantage of these welding processes, which are relatively slower in mass production compared with the Gas Metal Arc Welding (GMAW), increase a production cost. Therefore, GMAW process with its ability to speed up during the production is highly evaluated by the industries.

Nevertheless, GMAW with pure argon as a shielding gas suffers problems such as unstable arcs and shallow penetration. Despite of knowing the consequence, in industry they use mixed gas with small percentages of active gas as shielding gas to stabilize the arc and get a better penetration. However, the effort to resolve the unstable arc with inappropriate penetration using GMAW process leads to many development of new advanced technology. For example, the introduction of plasma MIG welding process is also one of the efforts to enhance the arc stability in GMAW. The plasma MIG welding is a hybrid welding process to realize the plasma welding and MIG welding in a single torch. The idea is to benefit the advantages of both processes and furtherance the possibility of using MIG welding to the extent that previously never being achieved by the conventional one [2].

1.2 Plasma MIG Welding

Basically, the unstable arc in MIG welding process is primarily caused by the uncontrolled cathode spot behavior on the surface of base metal during welding process leading to the disturbance of the MIG wire tip during metal transfer. By using a mixed gas that contained small percentages of active gas, these problems can be solved, but by sacrificing the quality of the joining, which in fact is not realistic in quality control. For this reason, the plasma MIG welding with its capability to hinder the oxygen content in welding arc, and at the same time remain the quality of the weld joint was introduced.

The plasma MIG is a hybrid welding process to be invented in 1970s to enhance the limitation in conventional MIG welding process as well as to improve its stability problem [2–4]. The first introduced model of this system used a non-consumable tungsten electrode attached at the side of the filler wire. The current is supplied into the system through this tungsten electrode and also through the MIG wire. Through this, the lower part of the MIG wire is surrounded by high temperature of argon plasma. Thus the metal transfer process including droplet formation, growth, detachment and transfer takes place within the argon plasma [5]. The technology then has undergone numerous improvements over the decades to make it suitable for practical use. The present developed system enables the plasma and MIG welding employed in a single plasma MIG torch [6,7]. In this plasma MIG torch, the plasma electrode was positioned just below the contact tip. The current is directly supplied to this plasma electrode and ionized an argon gas that passing through the inside of it. This plasma flow enables to control the shape of the arc via the electromagnetic force. This electromagnetic force acting inward is able to fix the position of the MIG arc to lead to a stable metal transfer. The stable metal transfer is crucial in welding process in general since the control of welding quality can be expected. It is proved that the use of plasma MIG welding can decrease the spatter formation, reduces the fume generation, increases the wettability and improves the penetration.

Fig. 1.1 shows a schematic illustration of plasma MIG welding system depicting its main components. The system consists of two welding machine as a power source for the plasma welding and MIG welding. These two power sources are programmed to be operated in different characteristics, the one which supplies the current to the plasma electrode is operated in constant current characteristic, and the other which supplies the current to contact tip in MIG welding is operated in constant voltage characteristic. Meanwhile, the other important feature of this plasma MIG welding system is the configuration of the plasma MIG torch, which is designed in such a way to enable the different gases in different layer to be supplied through it at the same time. Therefore, the control of gases can be done individually. These gases are ionized when they passing through the plasma electrode during welding and overwhelmed the MIG arc, thus to stabilize the arc.

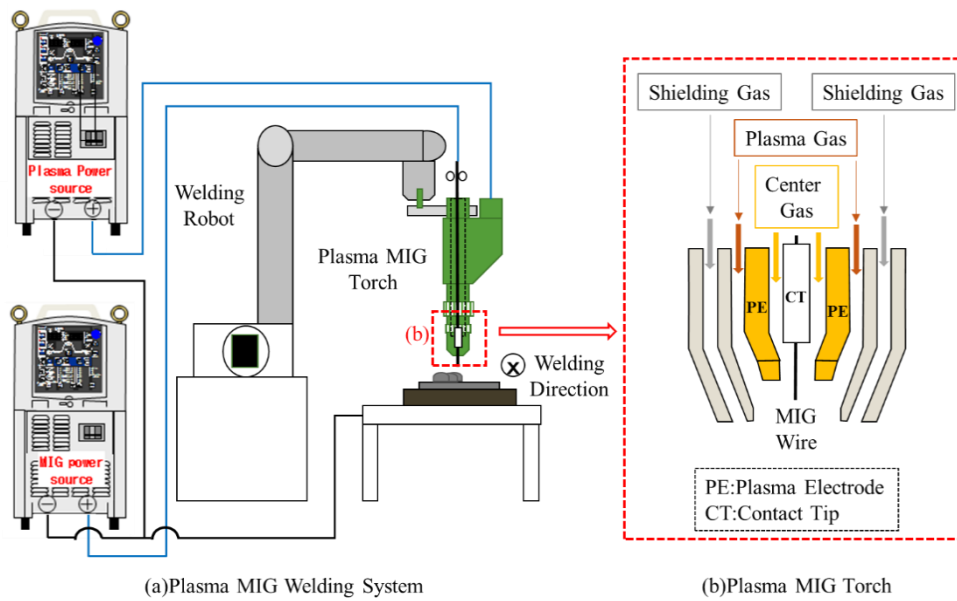
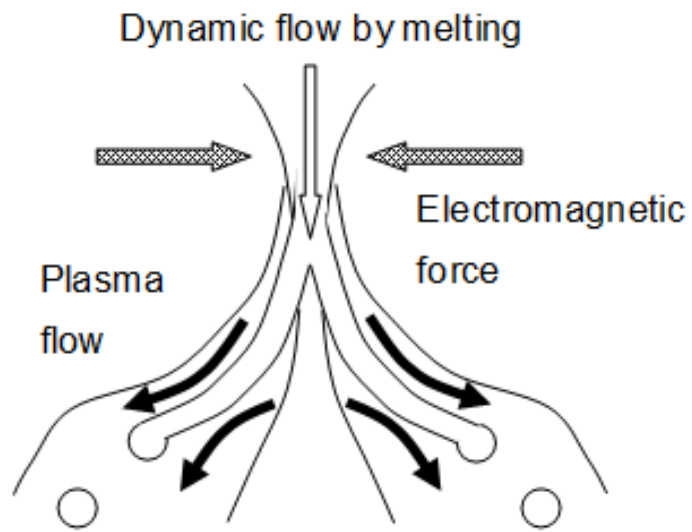


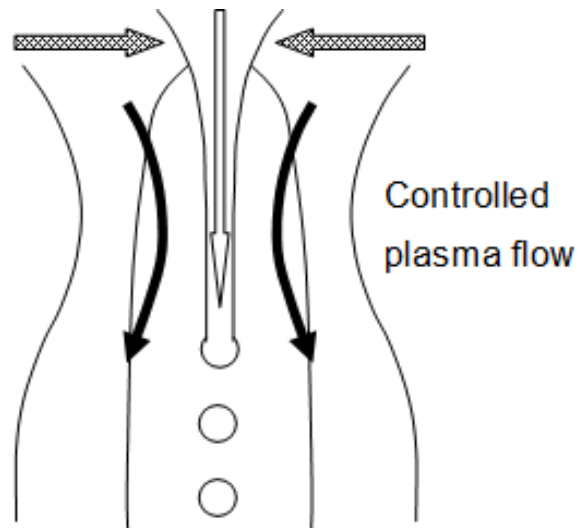
Fig. 1.1 Schematic illustration of (a) plasma MIG welding system and, (b) plasma MIG torch

Fig. 1.2 shows schematic illustrations of the metal transfers in conventional MIG welding and plasma MIG welding processes. The unstable arc in MIG welding is caused due to the uncontrolled cathode spots on the surface of the base metal. It then results in the disturbed movement of the molten wire tip during metal transfer. Meanwhile, in the plasma MIG welding process, the use of the plasma enables to fix the molten wire tip by the electromagnetic force. This improved stability then was confirmed to attribute to the reduction of fume generation and spatter formation.

The use of this plasma is also expected to contribute to the controllable welding process, especially in controlling the droplet temperature through the change in the metal transfer process. In order to study the quality of weld metal, in terms of visual appearance such as good cap profile, optimum reinforcement height and sufficient root penetration that fulfills the standard requirement, the behavior of droplet itself is necessary to be investigated, because the temperature of droplet is known to be one of the possible factors that able to affect the formation of the weld metal especially through the change in the amount of heat input into base metal and its drop position in weld pool.



(a) Conventional MIG welding



(b) Plasma MIG welding

Fig. 1.2 Schematic illustrations of metal transfers in (a) conventional MIG welding process and (b) plasma MIG welding process

1.3 Problem statement

1.3.1 Challenging issues in controlling heat input into base metal

The conventional MIG welding process suffers the unresolved problems of unstable arc generation, large amounts of fume formation and high heat input into the welded metal. The plasma MIG addresses some of these problems, especially in controlling the heat input. The hybrid process creates a stable metal transfer, avoiding localized fluctuation of the heat input into the metal weld, hence improving the quality of the weldment. It has been reported that the heat content in the metal droplet contributes almost 40 percent of the total heat input in the weld zone during MIG welding [8]. The heat content in the metal droplet corresponds to the temperature of the droplet. Since the parameters of the plasma MIG welding system can be freely controlled, there is a possibility of controlling the droplet temperature, and subsequently, controlling the heat input into the base metal.

Several studies have been conducted to evaluate the metal transfer behavior and the droplet temperature in MIG/MAG welding process for various purposes such as to control the fume generation [7,8], to predict the weld pool geometry by relating the droplet temperature and surface tension [9,10] and to measure the energy transfer into weld metal [9,11]. The temperature measurements in these studies were conducted either by optical pyrometry or calorimetry methods. Irrespective of the measurement methods, the range of the droplet temperatures were found to be between 2,000 K to 3,000 K, depending on the shielding gas composition and other welding parameters such as wire feeding speed, welding current, voltage, and contact tip to work distance (CTWD). The droplet temperature has been reported to be directly influenced by the welding current and the time in which the droplet is exposed to the surrounding arc (arc time), where a high welding current and arc time results in increased droplet temperature [9]. Specifically, Yamazaki et al emphasized that the arc heating method has a large influence on the droplet temperature. In CO₂ welding, concentrated arc heating is created by the high current density at the arc root, resulting in increased droplet temperature. In contrast, uniform arc heating in MAG welding results in a homogeneous temperature distribution, decreasing the average droplet temperature [10]. Similar observations were made by Siewert et al and Soderstrom et al in their respective studies [9,11].

In conventional MIG welding, the droplet temperature is dependent on the welding parameters selected for the welding process. The behaviors of the metal transfer and factors that affect the droplet temperature in conventional MIG have been explained well by various researchers. Most studies have tried to compromise with the issue of high droplet temperature by proposing suitable welding applications that can cater for such welding output. For example, to improve the wettability at the weld toe or the depth penetration, which can be obtained by increasing the droplet temperature [12,13]. On the contrary, there are also studies which attempt to control the process by reducing the heat input to the base metal, utilizing various methods such as AC-GMAW [14–17]. This has resulted

in the decrease of droplet temperatures. However, the mechanism for controlling the droplet temperature remains undescribed. In plasma MIG welding, there is a possibility to accurately control the droplet temperature based on the settings of the process parameter. This is because the welding parameters, such as plasma electrode diameter, plasma current, and CTWD, can be freely adjusted. The welding process with controllable droplet temperature, which leads to reducing the heat input into base metal benefits the low heat input joining such as dissimilar joining or cladding process.

1.3.2 The requirement of low heat input joining in actual application in industry

The industry player in all sectors nowadays are facing many challenging issues in their production to cater recent needs such as environmental pollution, safety and cost saving. The same goes with manufacturers involved in transportation industry such as shipbuilding, aircraft, automotive and so on. For example, in automotive companies, the rising price of the fuel gives an impact to them to develop a new technology as well as new materials to be used in production line so as to reduce the weight of their products thus to improve fuel efficiency [20]. Another option that commonly used nowadays is to join the materials dissimilarly. The dissimilar joining can benefit both advantages and minimizes the drawbacks.

The features of the steel with its mechanical property that can be tailored to many purposes of use makes steel a versatile material and widely used in industry. The steel is also well-known to its good weldability and easy to be handled during welding. Meanwhile, the aluminum on the other hand is not as strong as steel, but its weight is much lighter than the steel. Alongside this, it is resistant to corrosion and rust. Therefore, a joining of these two metals is an option to benefit both advantages.

However, because of the large differences in physical and chemical properties in these two metals, the joining of aluminum to steel is not as easy as a normal fusion welding. The differences in thermal conductivity, lattice transformation, large difference between the melting point (660°C for aluminum and 1530°C for steel) and nearly zero solid solubility of iron in aluminum are creating large discrepancy between both metals thus causing the welding defect such as distortion and crack [21,22]. The other problem with this joining is a formation of a brittle intermetallic compound (IMC) layer at its joint interface [23,24]. The formation of this IMC causes the dissimilar joining of aluminum and steel difficult to be conducted by using the normal fusion welding such as conventional MIG or TIG welding processes due to the severe formation of the IMC [23]. However, the use of Al-Si filler wire which contains of higher silicon composition is reported to be able to decrease the growth rate of IMC [25–27]. It was mentioned in earlier studies [28–30] that the IMC thickness must be controlled below $10\ \mu\text{m}$ to ensure the strength of the joint.

There are many works have been done to control the IMC thickness during welding. Katayama et al used the focused laser beam as well as the design of joint groove to suppress the melting of the metal in order to control the amount of fusion metal [31], thus control the IMC thickness. Park

et al reported that the use of AC pulse MIG welding was able to increase the deposition rate and decrease the heat input applied to the base metal through adjustment on EN ratio. Through this welding method, a thin IMC thickness was produced [32]. While, Long Wan et al have utilized the parameter setting in Friction Stir Lap Welding (FSLW) by decreasing the welding speed and increases the rotation speed, which results in the reduction in heat input and strain rate. As a result, the improved joint strength with thin IMC thickness layer has welded.

The above aforementioned studies are aiming the same goal, which is to control the IMC thickness by reducing the heat input. Mathieu et al reported in their numerical simulation study that the temperature distribution in aluminum weld metal played an important role to influence the characteristic of the IMC layer [33]. During dissimilar welding, the heat input into the weld metal consists of thermal conduction from the arc and the heat transfer related to heat content of metal droplet [34]. In regards to this, Tsujimura et al reported that the heat transfer related to the heat content of the metal droplet in MIG welding covered approximately 40% of the total heat input into the weld metal [8]. Therefore, it is suggested that the heat input control by controlling the droplet temperature through the plasma MIG welding can be applied in Al/Steel dissimilar welding.

1.4 Objectives of the study

The purposes of this study are as mentioned as follows:

- 1) To study the basic characteristic of the plasma MIG welding process and its ability to reduce the heat input into base metal. In order to simplify the phenomena, bead on plate plasma MIG welding of carbon steel is carried out in DCEP mode. The investigation aims to clarify the factors affecting the droplet temperature reduction and its mechanism.
- 2) To verify the effect of different welding system (DCEP and pulse DCEP) towards the arc behavior and the consistency of the factors affecting the droplet temperature.
- 3) To apply the pulse plasma MIG welding system to join the aluminum and carbon steel dissimilarly. The effect of low heat input caused by the pulse plasma MIG welding system is utilized in order to join the materials that sensitive to the high heat input.

1.5 Focus and structure of the thesis

This study focusses on the advantage to use the plasma MIG welding in comparison with conventional MIG welding in terms of the heat input reduction into base metal. From literatures, we understood that the droplet temperature was closely related to the heat input into base metal. Therefore, in this study, the droplet temperature is measured as a way to confirm the merit to use plasma MIG welding and its ability to reduce the heat input. The high speed video camera is used to clarify the phenomena during welding. The system of the welding is changed from normal DCEP system to pulse DCEP system to observe the difference in phenomena. Finally, by using pulse DCEP system, the aluminum is welded and tried to benefit to use the plasma MIG welding system to the Al/Steel dissimilar welding.

Therefore, this thesis consists of six chapters. The first chapter describes the issue in current welding condition, the significance of this study and also the purpose of this study. The second chapter describes the methods that being used in the experiments. The result of the experiments is presented in chapter 3, 4 and 5. In chapter 3, the measurement to the droplet temperature is done and the factors that influenced the droplet temperature reduction in plasma MIG welding are scrutinized. In this chapter, DCEP system is used to weld the low alloy carbon steel. Next, in chapter 4, the welding system is changed from DCEP to pulse DCEP and the difference in welding system is clarified to bring the same effect to the droplet temperature reduction. By utilizing the results in both chapter 3 and 4, chapter 5 elucidates the application of pulse plasma MIG welding to join the Al/Steel dissimilarly. Chapter 6 concluded all the findings in chapter 3, 4 and 5.

Chapter 2

Experimental procedure

2.1 Welding method

2.1.1 Plasma MIG welding

A schematic illustration of the plasma MIG welding system used is shown in **Fig. 2.1 (a)**. The system is mounted on a welding robot (Almega, OTC Daihen) and the welding movements are pre-programmed into the control unit. The system consists of two power sources for MIG current and plasma current, a plasma MIG welding torch, a MIG wire feed unit and a water cooling unit. The MIG power source (DP-500, Daihen) is operated under a constant voltage characteristic whereas the plasma power source (DP-500, Daihen) is under a constant current characteristic. The plasma MIG welding torch (PLM-500, TBi) is designed to enable both welding methods (MIG welding and plasma welding) to be employed in an axially single torch. In the interior of the torch, there is a contact tip which is positioned in the center and is surrounded by a plasma electrode placed just below the contact tip. This torch is purposely designed to enable the separation of the supplied gas into three layers, namely center gas, plasma gas and shielding gas, as shown in **Fig. 2.1 (b)**. Using this arrangement, gas types and their flow rates can be controlled independently. In the experiments, both power sources are operated in a Direct Current Electrode Positive (DCEP) mode. The negative polarity of both power sources is connected to the base metal, while the positive polarity of the MIG power source is connected to the contact tip and that of the plasma power source is connected to the plasma electrode.

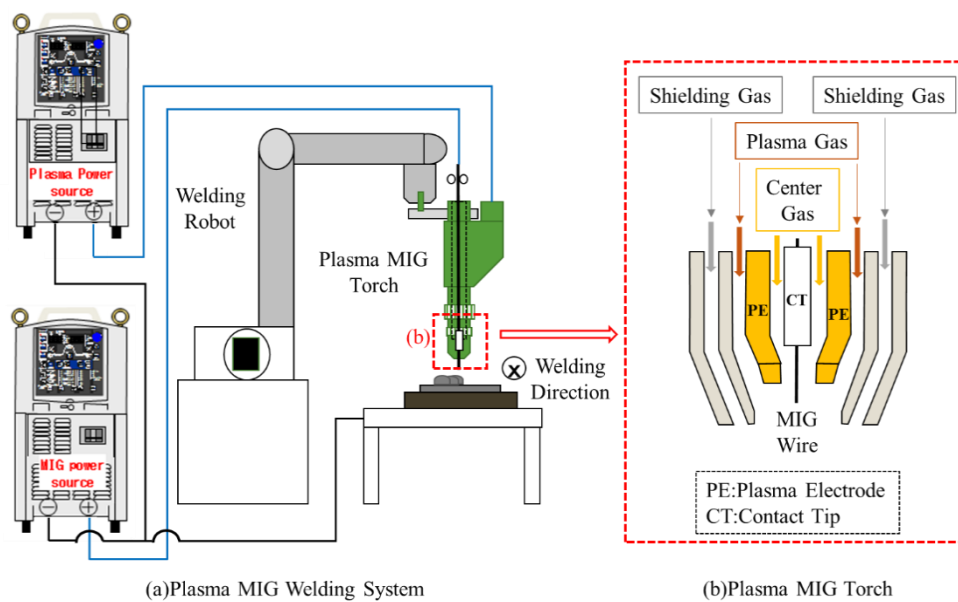


Fig. 2.1 Schematic illustration of (a) plasma MIG welding system and, (b) plasma MIG torch

2.1.2 Conventional MIG welding

In this study, to assure the reliability of the comparison of the phenomena between the plasma MIG welding and the conventional MIG welding, all the welding parameter must be set to be the same. For this reason, the plasma MIG welding system is also used for the conventional MIG welding. There is a function in the plasma MIG welding system to turn off the plasma current. Thus the system is also able to work as the conventional MIG welding. However, since the same plasma MIG torch is used, the plasma electrode is remained in its position. Here, in order to avoid any constriction effect of the shielding gas due to this plasma electrode, the large diameter of plasma electrode is used during welding using the conventional MIG welding.

2.2 Temperature measurement

2.2.1 Droplet temperature measurement through two-color temperature measurement method

Droplet temperature measurement is conducted using a two-color temperature measurement method. A color HSVC (Miro eX, Phantom), set at 2,000 fps with an exposure time of 20 μ s, is used to capture an image of the droplet. The recorded image resolution is at 512x512 pixels corresponding to a captured image size of 10x10 mm. A macro optical camera lens (Sigma DG 28-300 mm, Nikon) is used for the adjustment of image magnification. The distance from the camera lens to the wire tip is approximately 100 mm, as shown in **Fig. 2.2**. The camera system is set perpendicular to the arc axis and the welding direction to capture the image of the area from the wire tip to the weld pool. An image of a free flight droplet is captured immediately after the arc disappears. However, in some cases, an image of a pendant droplet is also recorded due to the difficulty in capturing the droplet in free flight. The recorded images are then analyzed using a temperature measurement software (Thermera-HS, Mitsui Photonics, Ltd) to obtain the temperature distribution on the droplet surface. To ensure the accuracy of the measured droplet temperature, the experiment was conducted approximately 5 ~7 times for every setting of WFS.

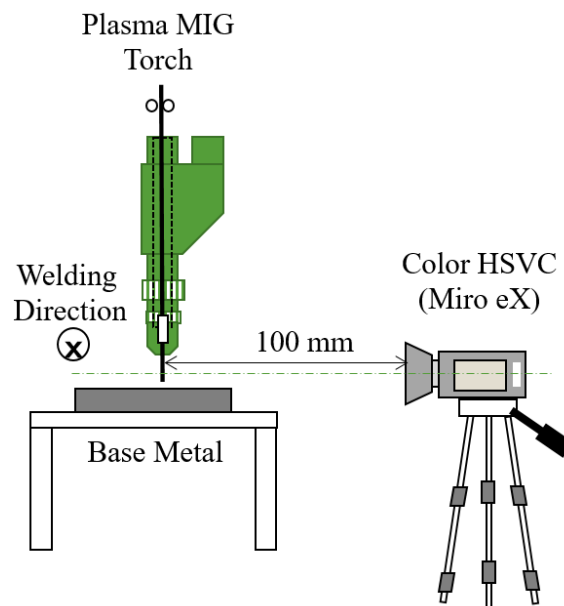


Fig. 2.2 Schematic illustration of the experimental configuration of the droplet temperature measurement

The two-color temperature measurement method has been used in past studies to measure molten steel temperatures [35, 36]. In this method, three images in wavelength ranges corresponding to red (R), green (G) and blue (B) are captured simultaneously by different color sensors equipped in the camera. The central wavelengths of spectral sensitivities of R, G and B sensors are 600 nm, 540 nm and 460 nm, respectively. The camera system is equipped with low-pass and high-pass filters to limit wavelength ranges of the spectral sensitivities to increase measurement accuracy. The droplet surface is presumed as a grey body and its temperature is determined from a ratio of surface radiation intensities measured with different color sensors through the calibration data. The droplet surface temperature can be calculated because the differences in the central wavelengths between R and G or G and B are relatively small (approximately 60 nm or 80 nm) and the emissivity can be assumed to be the same for both wavelengths. In this study, the intensity ratio of R to G is used to obtain the droplet surface temperature since the intensity of B was observed to be very low. The calibration data was obtained in advance by using a standard light source (tungsten ribbon lamp) to ensure high accuracy of the measurement in the experiments.

2.2.2 Plasma temperature measurement through spectroscopy analysis by using Fowler Milne method

The plasma temperature in the surrounding of the MIG wire is also measured by using Fowler Milne method [37]. **Fig. 2.3** shows a schematic illustration of the experimental set-up for the plasma temperature measurement. A HSVC (GX-1, Nac Image Technology), set at 8,000 fps with an exposure time of 50 μ s, is used to capture the image. The recorded image resolution is at 384x288 pixels corresponding to the actual captured image size of 12x12 mm. A macro lens (AF Micro Nikkor 200 mm, Nikon) is used for the adjustment of image magnifications. The band-pass filter is used to observe ArI spectrum at 696.5 nm. The distance from the camera lens to the wire tip is approximately 600 mm. The camera system is set perpendicular to an arc axis and welding direction. The plasma temperature is calculated from the ArI spectrum intensity distribution after Abel inversion by using Fowler Milne method.

The Fowler-Milne method is able to determine the temperature distribution of Ar plasma under the LTE assumption from the normalized intensity of ArI spectrum at 696.5 nm as a function on the plasma temperature as shown in **Fig. 2.4**. In case of ArI spectrum at 696.5 nm, the maximum intensity is found at 15,000 K. By finding the absolute intensity at this temperature in the observed image, the temperature distribution can be determined from the ratio of the local intensity to the maximum intensity. Although the plasma temperature in the plasma MIG welding is expected not to reach 15,000 K, the maximum intensity can be determined from that in Ar TIG welding instead. Keeping the same observation setting, the plasma MIG welding torch is removed to be replaced with the TIG torch to observe the above maximum intensity.

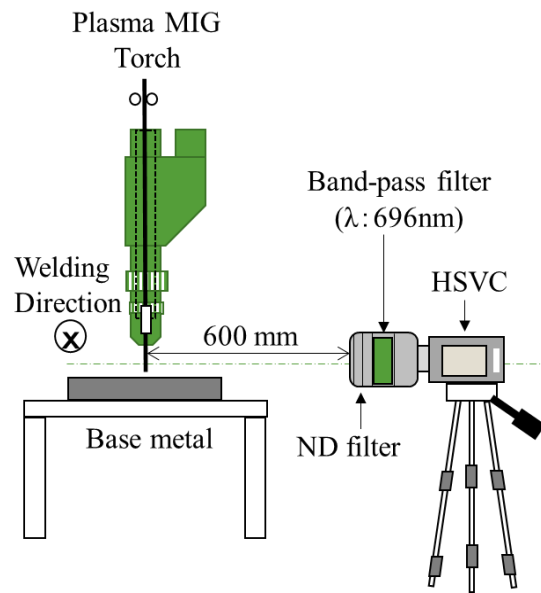


Fig. 2.3 Experiment set-up for plasma temperature measurement

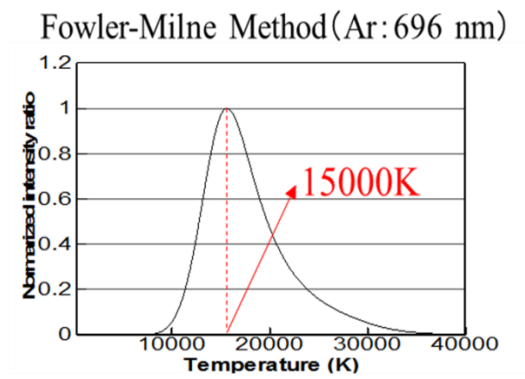


Fig. 2.4 Normalized intensity of ArI spectrum at 696.5 nm as a function of plasma temperature

2.3 Metal transfer observation

2.3.1 Shadowgraph method

Metal transfer observation is conducted using a HSVC (Memrecam-Q1V, Nac Image Technology), a telephoto micro lens (AF Micro Nikkor 200 mm, Nikon) attached with a band-pass filter with the nominal center wavelength at 640 nm, and a high-frequency pulsed diode laser light source system (Cavilux HF system, Cavitar). The image resolution setting is 640x480 pixels to capture an image size of 17x13 mm at a framerate of 2,000 fps. The high-frequency pulsed diode laser light source is placed in line with the optical axis of the HSVC and perpendicular to the arc axis as well as the welding direction. The configuration of the experiment is shown in **Fig. 2.5**. The pulse frequency of the laser light source is synchronized to the camera's frame rate at 2,000 pulses per second. The collimated 640 nm wavelength laser is directed at the arc and a shadowgraph of the wire and the metal droplet can be captured by the camera. The image recorded shows the behavior of the metal transfer in the absence of the intensive arc radiation.

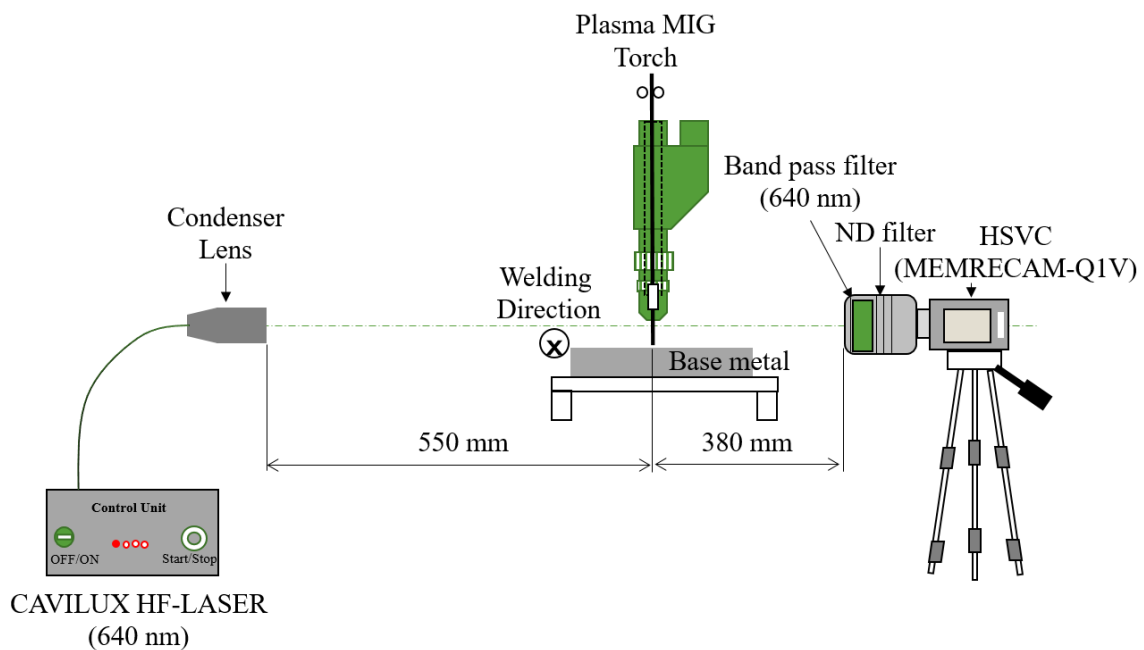


Fig. 2.5 Schematic illustration of the experimental configuration of the metal transfer observation by using the shadowgraph method

2.3.2 Camera observation method

The metal transfer behavior is also observed using the color HSVC (Miro eX, Phantom) without the use of the high-frequency pulsed diode laser light source system to show the arc appearance as well as the metal transfer behavior. In this experiment, the behavior of the metal transfer, superimposed on the image of the arc, can be observed. The color HSVC (Miro eX, Phantom) is set to capture at a frame rate of 2,000 fps with an exposure time of 30 μ s. The image resolution is set at 640x480 pixels, corresponding to an image size of 17x13 mm. A telephoto micro lens (AF Micro Nikkor 200 mm, Nikon) is used for the image magnification, positioned at approximately 500 mm from the wire tip, as shown in **Fig. 2.6**. ND filters are used to attenuate the light from the arc, to enable visualization of the droplet formation, growth and detachment processes in the presence of the arc. Comparison can then be made with the results of the shadowgraph experiments.

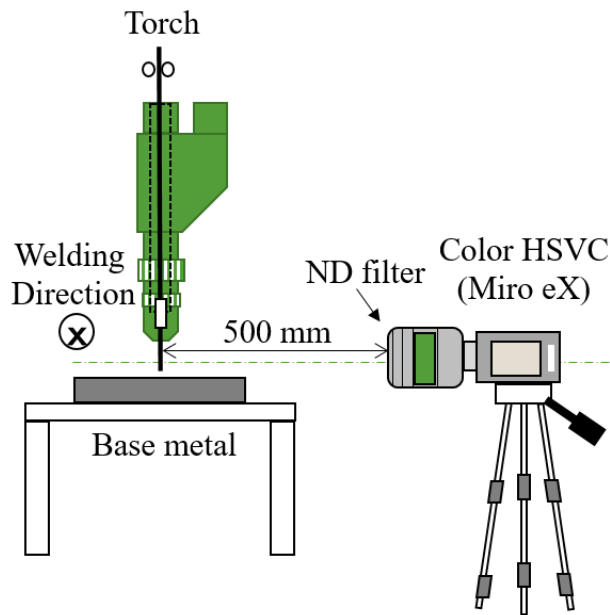


Fig. 2.6 Schematic illustration of the experimental configuration of the metal transfer observation using the color HSVC

Chapter 3

Study on factors affecting the droplet temperature in plasma MIG welding process

3.1 Introduction

This chapter focusses on discussing factors affecting the droplet temperature in the plasma MIG welding process in comparison with that in the conventional MIG welding in terms of the heat input reduction into the base metal. From literature study, the droplet temperature is found to be closely related to the heat input into the base metal. In the plasma MIG welding, there is a possibility to accurately control the droplet temperature based on the settings of the process parameter. This is because the welding parameters, such as torch nozzle diameter, plasma electrode diameter, plasma current, CTWD and so on, can be freely adjusted. In this study, the mechanism to control the droplet temperature in plasma MIG welding is discussed based on the measurements of the droplet temperature for a wide range of MIG currents with different plasma electrode sizes. Measurements of the droplet temperatures are conducted using a two color temperature measurement method. The droplet temperatures in plasma MIG welding are then compared with that of conventional MIG welding. Furthermore, in order to confirm the validity of the mechanism suggested through the experimental study, numerical analysis is also carried out.

This chapter is divided into 7 sections. Section 3.1 describes the introduction. The materials and welding condition are outlined in section 3.2 and the numerical simulation model is described in section 3.3. The experimental results and the simulation results are described in section 3.4 and 3.5, respectively. The discussion is presented in section 3.6. Finally, section 3.7 concludes the findings.

3.2 Materials and welding conditions

A mild steel filler wire (YGW12) with a diameter of 1.2 mm is chosen to be welded onto a mild steel plate (SS400) with wire feeding speed (WFS) ranging from 700 to 1,100 cm/min (corresponding to MIG current of 130 - 250 A). Welding speed (WS) of 50 cm/min is achieved by using an actuator to move the base metal plate at a constant speed. The contact tip to work distance (CTWD) is set at 30 mm, and MIG voltage is set within the range from 25 to 35 V to ensure a constant arc length of approximately 10 mm. Argon gas is introduced into the three layers at flow rates of 5 l/min (center gas), 10 l/min (plasma gas) and 10 l/min (shielding gas) individually from three gas cylinders. The plasma current supplied through the plasma electrode is DC100 A. Two different plasma electrode diameters (PEDs) of 3 mm and 7 mm are used in these experiments to evaluate the influence of the PED on the droplet temperature.

The plasma MIG welding system can be operated with the plasma current switched off, turning it into a conventional MIG welding system. Thus, the conventional MIG welding can also be conducted using the same apparatus and identical welding parameters without the presence of the plasma current. In the conventional MIG experiments, the PED of 7 mm is kept installed in the torch, although it is not used in the process.

The details of the welding conditions for all cases are summarized in **Table 3.1**.

Table 3.1 Details of welding conditions

1. Machine Setting	i. Polarity	DCEP
	ii. Plasma Current	Conventional MIG : 0 A Plasma MIG : 100 A
	iii. Plasma Electrode Diameter (PED)	Conventional MIG : ϕ 7 mm Plasma MIG : ϕ 7 mm, ϕ 3 mm
	iv. Wire Feeding Speed (WFS)	740 – 1080 cm/min (in a gap from 20 or 40 cm/min)
	v. MIG Current	140 – 250 A
	vi. MIG Voltage	25 – 35 V
	vii. Welding Speed (WS)	60 cm/min
	viii. Contact Tip to Work Distance (CTWD)	30 mm
	ix. Wire Stick Out Length	20 mm (approximately)
	x. Argon Gas Flow	Center Gas : 5 litre per minute Plasma Gas : 10 litre per minute Shielding Gas : 10 litre per minute
2. Camera Setting	i. Temperature measurement Method for Droplet	Two color temperature measurement method (2000 fps)
	ii. Metal Transfer Observation	a. Shadowgraph (2000 fps) b. Color observation (2000 fps)
	iii. Plasma Temperature Measurement Method	Fowler Milne method (8000 fps)
3. Materials	i. Base Metal	Mild Steel
	ii. Filler Wire	JIS YGW ϕ 1.2 mm

3.3 Simulation model

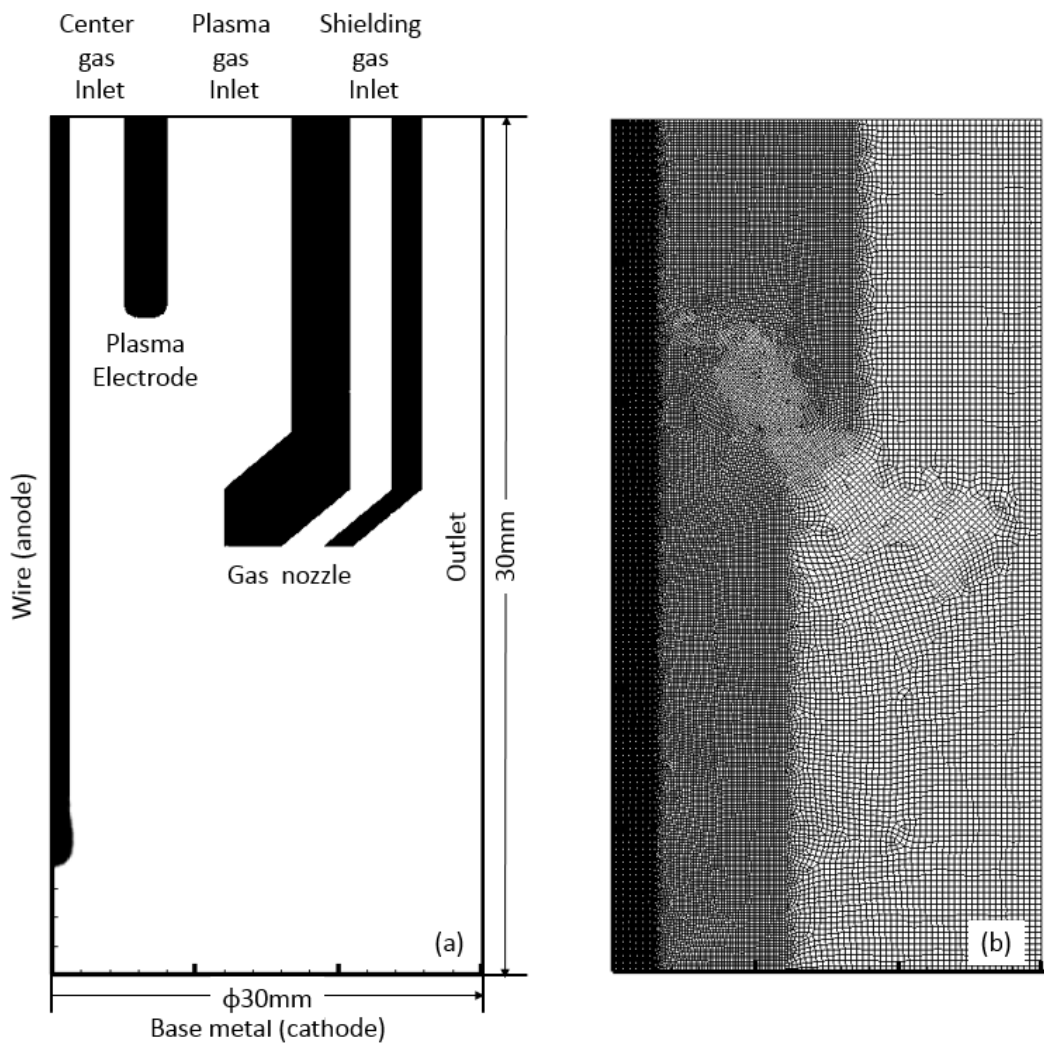
In this section, the numerical simulation on basic characteristics of the plasma MIG welding is also carried out to discuss especially influence of the presence of the plasma on the metal transfer process, droplet temperature and the arc temperature. For comparison, that of the conventional MIG welding is also conducted by setting the plasma current to be 0.

Fig. 3.1 shows an axisymmetric two-dimensional simulation domain (z, r) with a radius of 15mm and a height of 30 mm consisting of an arc region, a wire region, a plasma electrode region and nozzle regions. Regions for feeding the wire, a center gas inlet, a plasma electrode, a plasma gas inlet, shielding gas inlet and nozzles are defined on the top boundary. On the axis, the wire region with a diameter of 1.2 mm and an initial extension of 25 mm corresponding to an arc length of 5 mm is defined. The side boundary is a pressure outlet. The bottom boundary corresponds to the surface of the base metal. The region inside the base metal is not calculated. Non-uniform mesh is used; the maximum and minimum sizes are 0.2 mm and 0.05 mm, respectively.

Table 3.2 summarizes simulation conditions. The wire composition is Fe. The wire feed speed is 5 m/min. The contact tip to work distance is 30 mm. The plasma electrode diameter is 5 mm. The center gas, the plasma gas, and the shielding gas are pure Ar and introduced from the top boundary at a flow rate of 5, 10 and 10 L/min. The MIG current of DC280 A and the plasma current of DC100 A are given at the top boundary. The plasma current is 0 in case of the conventional MIG welding. The bottom boundary is set to be 0 V.

Distributions of flow velocity, temperature, metal vapor concentration and current density are obtained by solving time-dependent conservation equations of mass, momentum, energy, mass of metal vapor and current expressed as follows. The current conservation equations for the MIG current and the plasma current are solved independently. The principle of superposition is applied to determine electric potential distribution. The magnetic field is obtained from calculation of vector potential. The plasma is assumed to satisfy the LTE condition. The thermodynamic and transport properties of the arc under the LTE condition are calculated as a functions of temperature and metal vapor concentration [38]. Fe is assumed as the metal vapor composition to calculate the above properties. The surface tension coefficient of the molten metal of the wire is set to be 1.2 N/m without depending on temperature. The thermodynamic and transport properties of mild steel are used for the wire [39, 40]. VOF method is used for tracking the free surface. ANSYS Fluent 18.1 is used for the calculation.

Table 3.3 summarizes boundary conditions. Where $u_{\text{center gas}}$, $u_{\text{plasma gas}}$, $u_{\text{shielding gas}}$ and u_{wf} are velocities corresponding to the center gas flow rate, the plasma gas flow rate, the shielding gas flow rate and the wire feed speed. j_{MIG} and j_{plasma} are current density corresponding the MIG current and the plasma current. P_{atm} is an atmospheric pressure.



(a) Two-dimensional axisymmetric domain

(b) Mesh

Fig. 3.1 Simulation region and mesh

Mass conservation:

$$\frac{\partial \rho}{\partial t} + \nabla \cdot (\rho \vec{u}) = 0 \quad (1)$$

Momentum conservation:

$$\frac{\partial \rho \vec{u}}{\partial t} + \nabla \cdot (\rho \vec{u} \vec{u}) = -\nabla p + \nabla \cdot \vec{\tau} + \rho \vec{g} + \vec{j} \times \vec{B} + \vec{F}_s + \vec{F}_{sl} \quad (2)$$

Energy conservation:

$$\frac{\partial \rho h}{\partial t} + \nabla \cdot (\rho h \vec{u}) = \nabla \cdot (k \nabla T) + \vec{j} \cdot \vec{E} - Q_r + Q_s \quad (3)$$

Mass conservation of metal vapor:

$$\frac{\partial \rho Y}{\partial t} + \nabla \cdot (\rho Y \vec{u}) = \nabla \cdot (\rho D \nabla Y) + M_{evapmetal} \quad (4)$$

Current conservation:

$$\nabla \cdot \sigma \nabla \Phi = 0 \quad (5)$$

Ohm's law:

$$\vec{j} = -\sigma \nabla \Phi = \sigma \vec{E} \quad (6)$$

Vector potential:

$$\nabla^2 \vec{A} = -\mu_0 \vec{j} \quad (7)$$

Magnetic field:

$$\vec{B} = \nabla \times \vec{A} \quad (8)$$

Where ρ : mass density, \vec{u} : velocity, p : pressure, $\vec{\tau}$: viscus stress tensor, \vec{g} : gravity, \vec{j} : current density, \vec{B} : magnetic field, \vec{F}_s : a source term for surface tension force, \vec{F}_{sl} : a source term to express the behavior of the solid region, h : enthalpy, k : thermal conductivity, T : temperature, \vec{E} : electric field, Q_r : a source term for arc radiation, Q_s : a source term for electron condensation, surface radiation and latent heat of vaporization on the wire surface, Y : mass fraction of metal vapor, D : diffusion coefficient of metal vapor, $M_{evapmetal}$: a source term for evaporation of metal calculated simply by Hertz–Knudsen–Langmuir equation, Φ : electric potential, \vec{A} : vector potential.

Table 3.2 Simulation conditions

	Welding process	
	Conventional MIG	Plasma-MIG
Wire composition	Fe	
Wire diameter [mm]	1.2	
Wire feed speed [m/min]	5	
CTWD [mm]	30	
Plasma electrode diameter [mm]	5	
MIG current [A]	DC280	
Plasma current [A]	0	DC100
Gas composition	Ar	
Center gas flow rate [L/min]	5	
Plasma gas flow rate [L/min]	10	
Shielding gas flow rate [L/min]	10	

Table 3.3 Boundary conditions

Boundary		Mass and momentum	Mass fraction of metal vapor	Energy	Electric potential	Magnetic potential
Top	Wire	$\vec{u}=\vec{u}_{wf}$	$Y=0$	300K	$-\sigma\partial\Phi/\partial n=j_{MIG}$	$\partial A_i/\partial n=0$
	Center gas inlet	$\vec{u}=\vec{u}_{center\ gas}$	$Y=0$	300K	$\partial\Phi/\partial n=0$	$\partial A_i/\partial n=0$
	Plasma electrode	—	—	300K	$-\sigma\partial\Phi/\partial n=j_{plasma}$	$\partial A_i/\partial n=0$
	Plasma gas inlet	$\vec{u}=\vec{u}_{plasma\ gas}$	$Y=0$	300K	$\partial\Phi/\partial n=0$	$\partial A_i/\partial n=0$
	Shielding gas inlet	$\vec{u}=\vec{u}_{shielding\ gas}$	$Y=0$	300K	$\partial\Phi/\partial n=0$	$\partial A_i/\partial n=0$
Side	Outlet	$P=P_{atm}$	$\partial Y/\partial n=0$	300K	$\partial\Phi/\partial n=0$	$A_i=0$
Bottom	Base metal	$\vec{u}=0$	$\partial Y/\partial n=0$	300K	$\Phi=0$	$\partial A_i/\partial n=0$

3.4 Experimental results

3.4.1 Correlation between MIG current and wire feeding speed

Fig. 3.2 shows the dependence of MIG current to WFS in conventional MIG welding, and plasma MIG welding with PEDs of 7 mm and 3 mm, as represented by the green, black and blue color lines, respectively. In general, the MIG current of plasma MIG welding is lower than that of the conventional MIG welding in almost all levels of WFS, except for WFS around 1,100 cm/min. The results of the plasma MIG welding showed a decrease by maximally 24% at WFS of 800 cm/min, 18 % at WFS of 900 cm/min and 8% at WFS of 1,000 cm/min, as compared to those of the conventional MIG welding. However, almost no observable difference in the MIG current was obtained at 1,040 cm/min corresponding to 230 A. There was also no significant difference in the MIG current observed for the use of different PEDs in the plasma MIG welding.

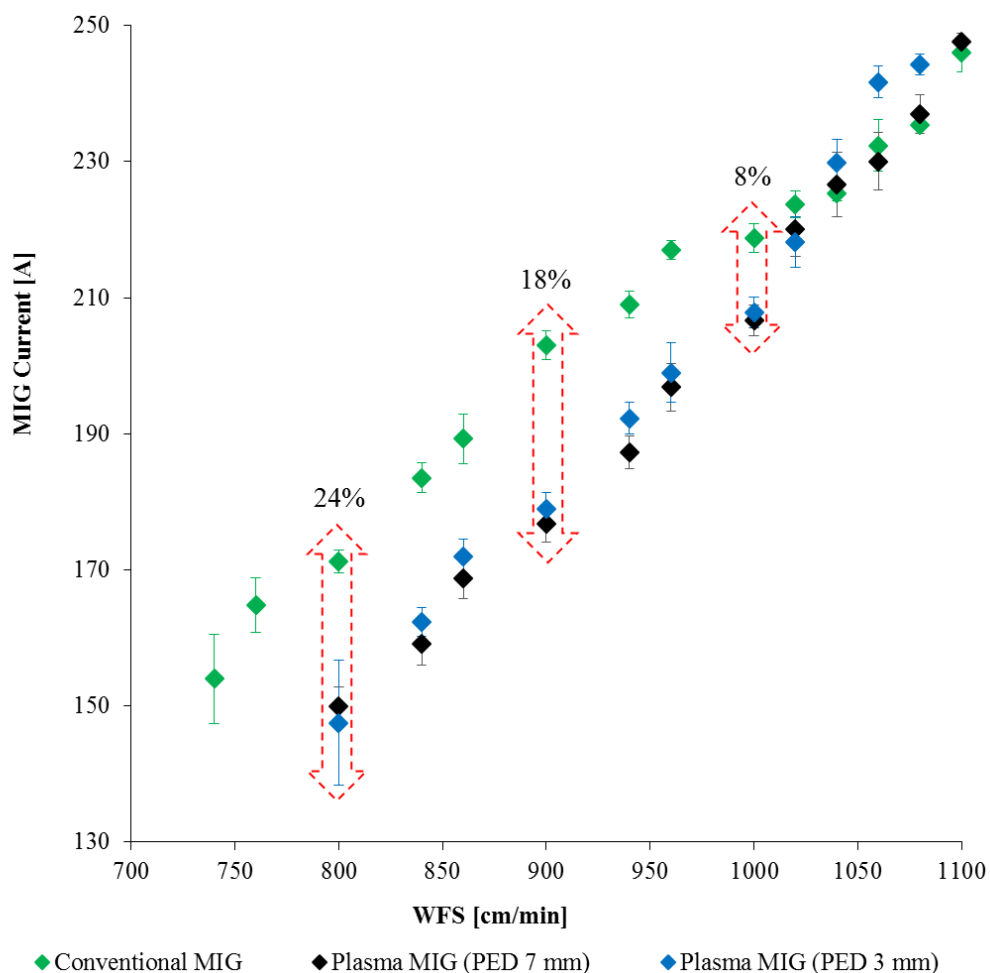


Fig. 3.2 Dependence of MIG current to wire feed speed in conventional MIG welding and plasma MIG welding with plasma electrode diameters of 7 mm and 3 mm

The reduction in the MIG current can be attributed to the increased temperature of the MIG wire that enhances the wire melting rate. Such phenomena is reported in the study of J.Ni et al, where the MIG wire was preheated using a TIG arc positioned above the contact tip [41]. In this study, the plasma around the MIG wire causes a similar effect of preheating of the wire. Hence, for the same value of WFS, a lower MIG current is sufficient to melt an equal amount of the MIG wire in the plasma MIG welding as compared to conventional MIG welding. However, increasing the WFS reduces the duration of exposure of MIG wire to the plasma, thus decreasing the plasma preheating effect on the wire. Consequently, for high WFS, a high MIG current is required to melt the wire, approaching that of conventional MIG welding. In general, the results obtained suggests that the plasma MIG can enhance the melting rate of the MIG wire as compared to conventional MIG welding.

3.4.2 Droplet Diameter Measurement

Droplet diameter measurements for the three welding conditions are conducted together with the droplet temperature measurements. The droplet is considered to be rotated during falling down as presented later in section 3.3.1 and also described in the literature [10]. Although the shape of the droplet is basically almost round, it sometimes become slightly distorted and elliptical. Therefore, in the droplet diameter measurement, the droplet diameter is defined as the average value of the horizontal and vertical droplet lengths, measured using an image processing software. The droplet diameters as a function of MIG current are shown in **Fig. 3.3**. The wire diameter used in the experiment is denoted by the red dashed line. It is observed that the droplet diameter decreases with increasing MIG current for all welding conditions. For the lowest MIG current level, the droplet diameter in the conventional MIG welding is larger than the droplet diameter in the plasma MIG welding. As the MIG current increases, this droplet diameter decreases dramatically to be slightly smaller than the wire diameter at the MIG current of 196 A, after which the diameter remained relatively constant with increasing current. In contrast, the droplet diameter in plasma MIG welding shows a more gradual decrease as the current increases until it approaches the MIG wire diameter at 216 A and 226 A in the plasma MIG welding with PED of 7 mm and 3 mm, respectively.

A spray transfer mode predominates as the droplet diameter becomes smaller than the wire diameter [42–44]. In this measurement, the spray transfer mode started at the MIG current of 196 A in the conventional MIG welding, 216 A in the plasma MIG welding with PED of 7 mm, and 226 A in the plasma MIG with PED of 3 mm. The transition from globular transfer to spray transfer was observed as the MIG current increases from around 160 A to 190 A in the conventional MIG welding. The use of the small PED in the plasma MIG welding tends to increase the transition MIG current to a higher value. In the plasma MIG welding, the droplet diameter gradually decreases with the increase in the MIG current. This indicates that the mode of the metal transfer changes smoothly from a globule transfer to a spray transfer, stabilizing the metal transfer as the MIG current increases.

Fig. 3.4 shows the comparison of droplet diameter in the conventional MIG welding, and the plasma MIG welding with PED of 7 mm and 3 mm at the specific MIG currents: 160 A, 200 A and 230 A. The large standard deviation in the droplet diameter was observed in low MIG current of 160 A in all welding process. Especially, that in the conventional MIG welding is found to be the largest which is considered to be caused by unstable metal transfer due to the transition from globular transfer to spray transfer.

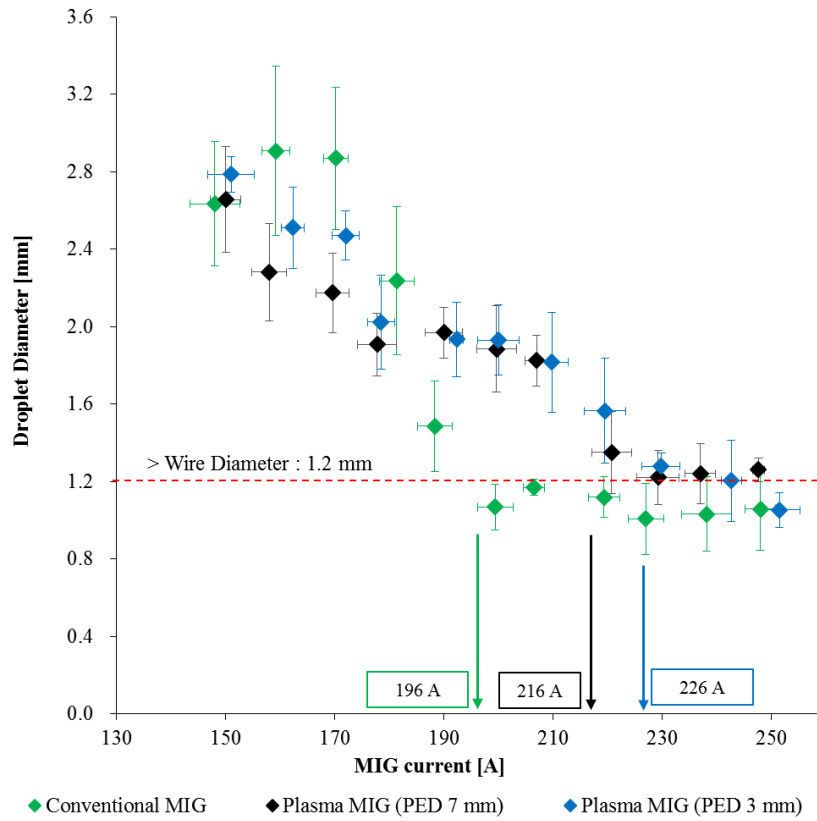


Fig. 3.3 Droplet diameter measurement as a function of MIG current in conventional MIG welding, plasma MIG welding with PED of 7 and 3 mm

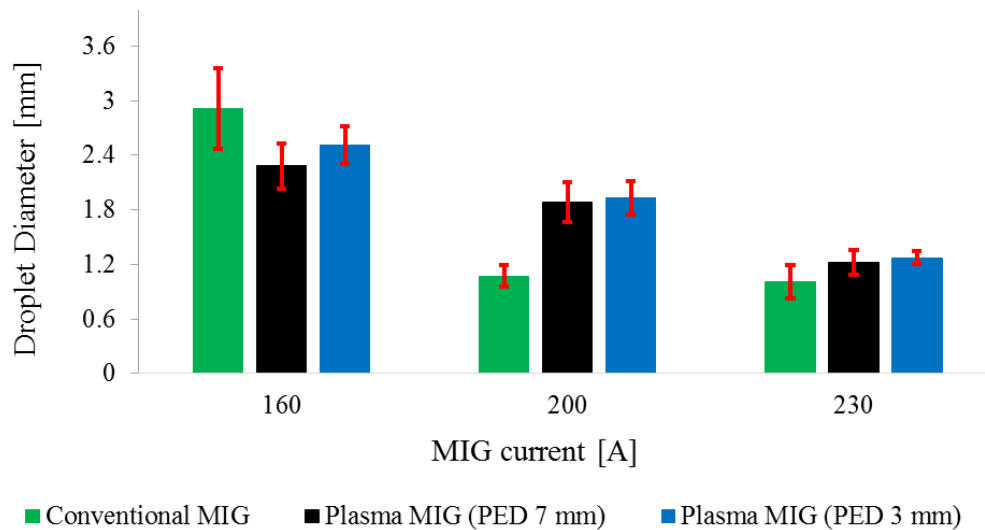


Fig. 3.4 Comparison of droplet diameter in conventional MIG welding, plasma MIG welding with PED of 7 mm and 3 mm at 160 A, 200 A and 230 A

3.4.3 Droplet temperature measurement

3.4.3.1 Dependences of droplet temperature on MIG current and wire feeding speed

The use of the two-color temperature measurement method enables the direct measurement of the droplet temperature immediately after the arc vanishes. In this study, temperatures of free flight droplets were measured for almost all cases. However, in some experiments, the temperature of pendant droplets was also measured when it was difficult to capture the image of the free flight droplet, especially for low MIG current experiments. **Fig. 3.5** shows the dependence of droplet temperature to MIG current in the conventional MIG welding, and the plasma MIG welding with PED of 7 mm and 3 mm.

In the conventional MIG welding, the droplet temperature initially shows a positive linear relationship with the MIG current during globular transfer. It then decreases from 160 A at globular/spray transition to a minimum value at 170 A. As the MIG current is further increased, the droplet temperature rises steeply until it stabilized at temperatures above 216 A (in spray transfer mode). This observation is similar to the findings of past studies [13].

The evolution of the droplet temperature in the plasma MIG welding with PED of 7 mm shows a slightly different trend as compared to that of the conventional MIG welding in terms of temperature volatility in the globular/spray transition. In the plasma MIG welding, a smooth transition from globular to spray transfer is facilitated by the absence of the minimum temperature. Similar to the results in the conventional MIG welding, the droplet temperature remained relatively constant once the MIG current increases from 220 A up to 250 A.

In the plasma MIG welding with PED of 3 mm, the droplet temperature increases gradually and monotonically from low to high MIG current. The droplet temperature became almost the constant above the MIG current of 230 A which was larger than that in the plasma MIG welding with PED of 7 mm.

Generally, it is seen that the droplet temperatures in the conventional MIG welding are higher as compared to those in the plasma MIG welding, irrespective of the transfer mode. The maximum droplet temperature in the conventional MIG welding is 2781 K at 246 A, while the maximum droplet temperatures in the plasma MIG welding are 2646 K at 216 A for PED of 7 mm and 2495 K at 244 A for PED of 3 mm. Thus, the difference between the maximum droplet temperature in the conventional MIG welding than those in the plasma MIG welding with PED of 7 mm and 3mm are +135 K and +286 K, respectively. These maximum droplet temperatures were achieved in the spray transfer mode.

Fig. 3.6 shows the comparison of droplet temperature in the conventional MIG welding, and the plasma MIG welding with PED of 7 mm and 3 mm at the specific MIG currents: 160 A, 200 A and 230 A. It is seen that the standard deviation in the droplet temperature becomes larger in low MIG current in all welding process. This large standard deviation is considered to be linked to the standard

deviation in the droplet diameter. Especially, that in the conventional MIG welding is found to be the largest which may be related to the metal transfer transition. The droplet temperature becomes more stable with less standard deviation after the transfer starts to be completely spray.

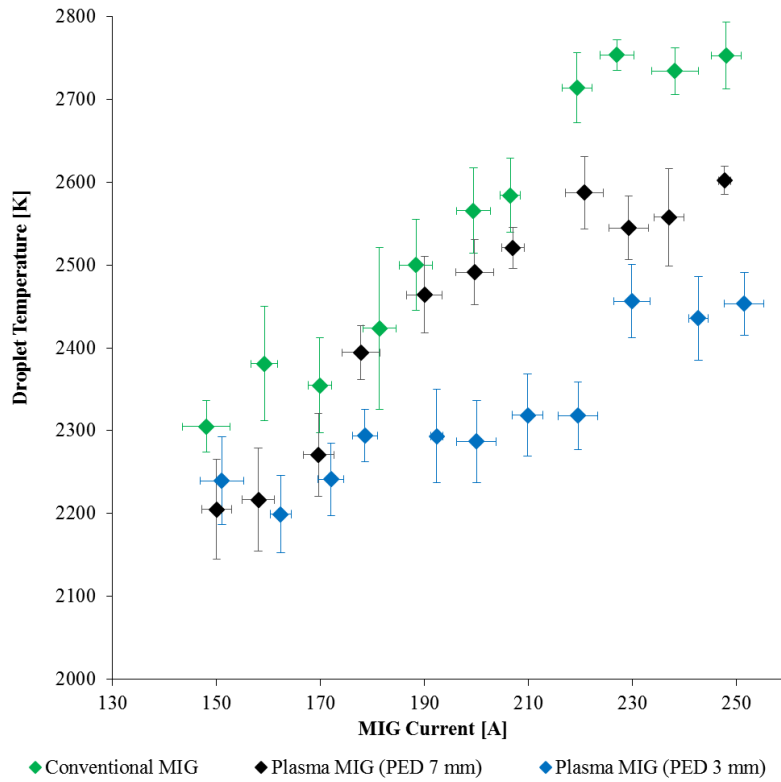


Fig. 3.5 Dependence of droplet temperature to the MIG current in conventional MIG welding and plasma MIG welding with PED of 7 mm and 3 mm

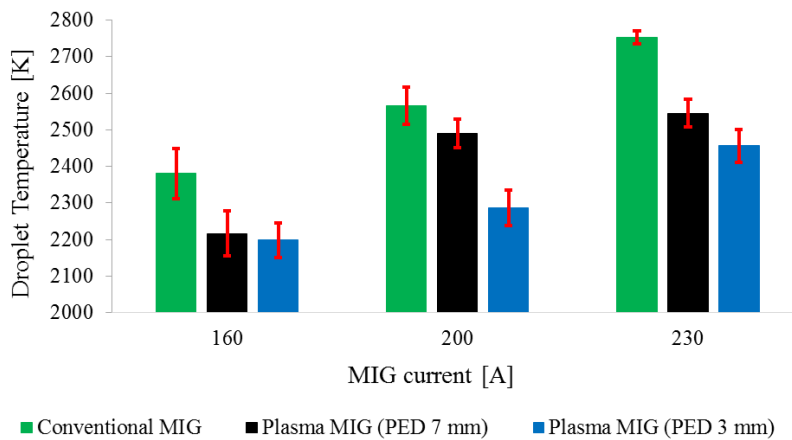


Fig. 3.6 Comparison of droplet temperature in conventional MIG welding, plasma MIG welding with PED of 7 mm and 3 mm at 160 A, 200 A and 230 A

In the droplet temperature measurement, there are possible factors to cause the change in the droplet temperature during the free flight, which lead to the increase in the standard deviation. The radiation and metal vapor evaporation from the droplet surface cool the droplet. Contrarily, the thermal conduction from the surrounding arc heats the droplet. In order to discuss influence of these cooling and heating processes on the droplet temperature, two kinds of analysis were additionally carried out.

The first analysis was done to a single free flight droplet after the arc around 230 A turned off. The duration of the observation is from just after the detachment from the wire tip until it impinges on the base metal. The evolution of the droplet temperature is presented as a function of the distance from the base metal in **Fig. 3.7**. As shown in the figure, the temperature distribution on the droplet surface is not completely uniform. The measured droplet temperature was found to fluctuate periodically by approximately 100 K during the free flight in all three cases, due to the rotation of the droplet with the non-uniform surface temperature distribution [10], despite of the constant droplet enthalpy. On the other hand, there was no clear tendency for the temperature to monotonically decrease by the cooling process during the free flight. However, this fluctuation is considered to be one of the factors to increase the standard deviation of the temperature measurement.

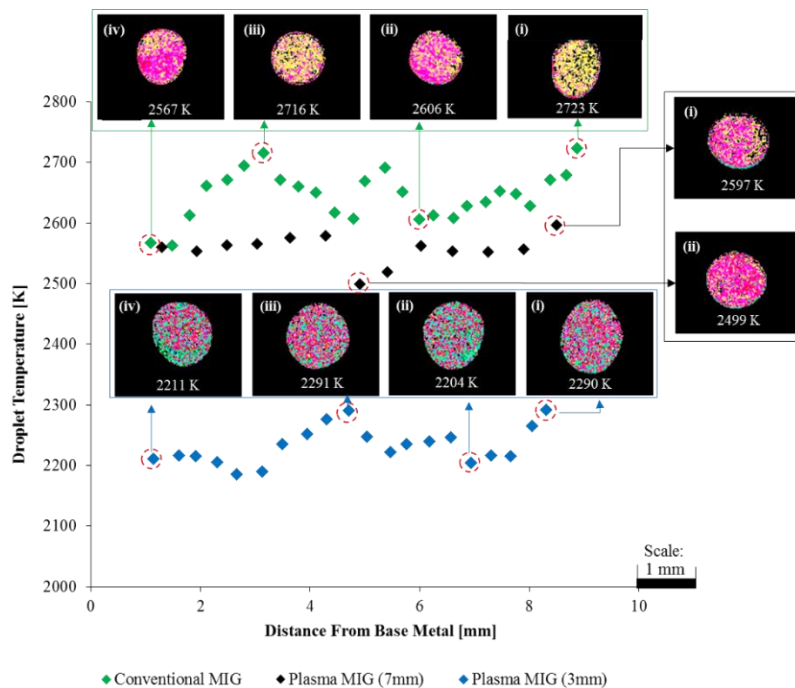


Fig.3.7 Temperature evolution of a single droplet during free flight in conventional MIG welding, plasma MIG welding with PED of 7 and 3 mm

The second analysis was done to free flight droplets observed immediately after turning off the arc at MIG current ranging from 220 A to 230 A. The measured droplet temperature arranged as a function of the distance from the base metal is shown in **Fig. 3.8**. It should be noted that the difference in droplet temperatures larger than approximately 100K shows that the droplet temperatures are actually different exceeding the range of the fluctuation. If the thermal conduction from the surrounding arc to the droplet during the free flight significantly affects the droplet temperature, the droplet temperature should increase with decrease in the distance from the base metal. However, the tendency to show this heating process is not observed. Consequently, the measured droplet temperature is considered basically not to be influenced by the distance from the base metal where the droplet is observed, because influence of the cooling and heating processes during the free flight on the droplet temperature can be assumed to be negligible.

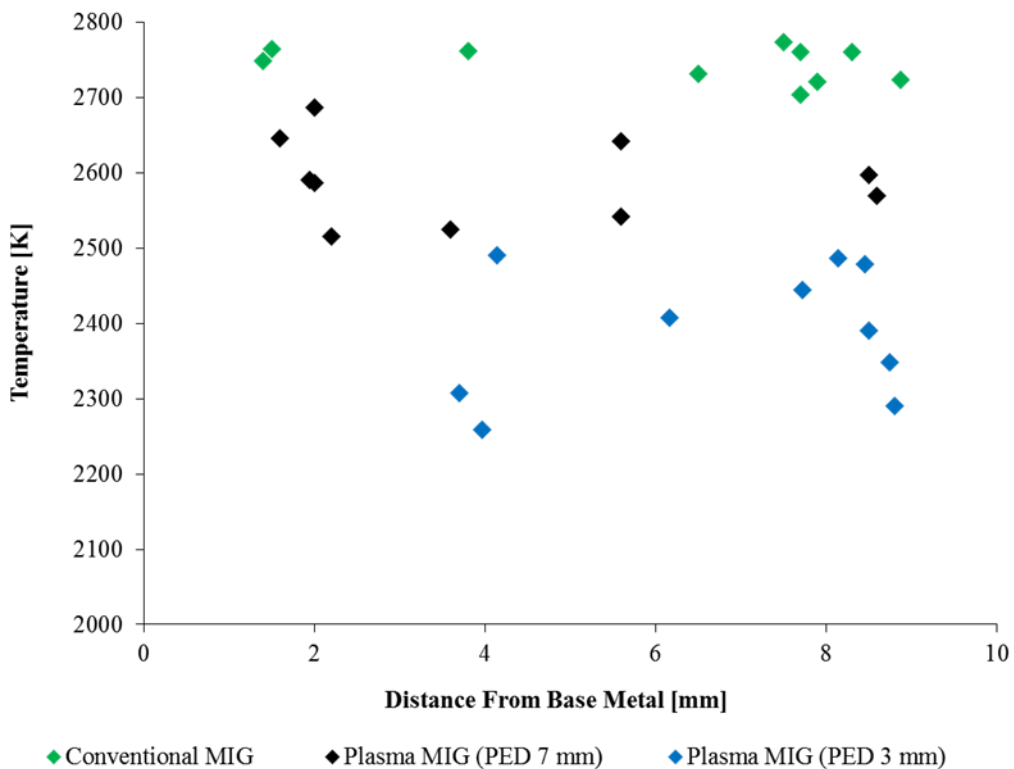


Fig.3.8 Effect of the distance of the droplet from base metal to the droplet temperature of conventional MIG welding, plasma MIG welding with PED of 7 mm and 3 mm at MIG current ranging from 220 A to 230 A

Fig. 3.9 shows dependence of droplet temperature to WFS for each welding condition. The temperature variations for all welding conditions show almost similar tendency with the results in **Fig. 3.5**. For the same WFS, the melting rates of the wire in all conditions are similar. Thus, for a particular WFS, the observed difference in the droplet temperatures between the conventional MIG welding and the plasma MIG welding suggests that the use of plasma reduces the local heat input into the base metal by the droplet. It has been mentioned in past studies that the droplet heat content contributes 30 to 40 percent of the total heat input to the base metal during welding [8].

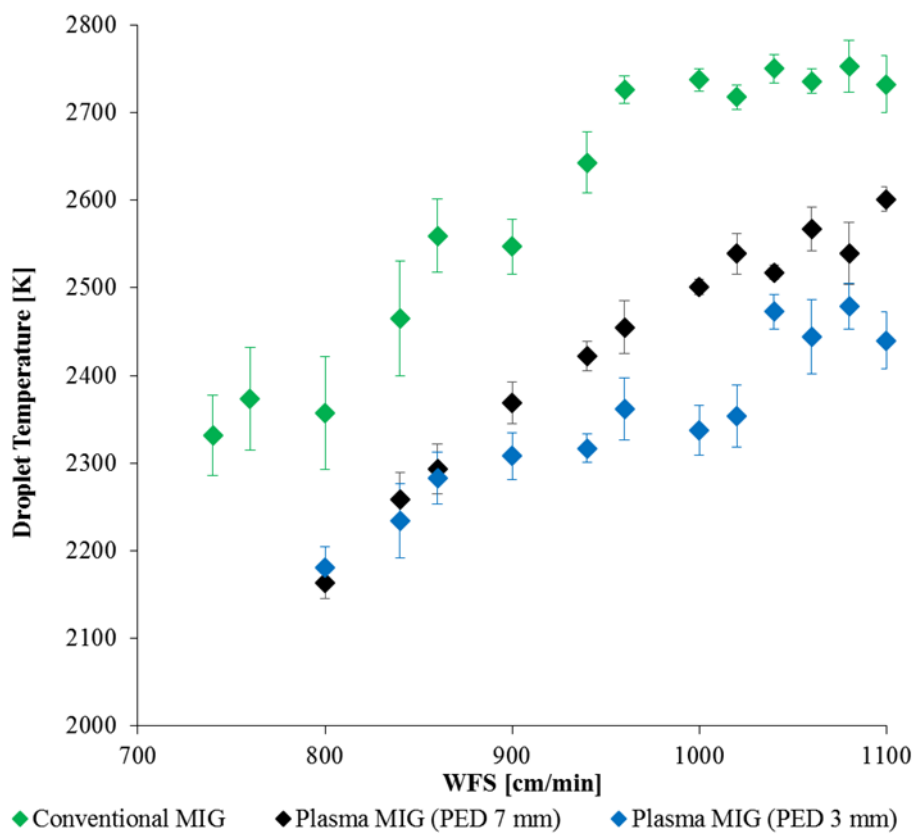


Fig. 3.9 Dependence of droplet temperature to the WFS in conventional MIG welding and plasma MIG welding with PED of 7 mm and 3 mm

3.4.3.2 Droplet surface temperature distribution

It was observed that the application of the plasma reduces the droplet temperature. However, further evaluation of the droplet temperature distribution is required to identify the temperature reduction mechanism. **Fig. 3.10** shows the temperature distribution on the droplet surface at three MIG current levels. The decrease in the averaged droplet temperature in the plasma MIG welding with PED of 7 mm and PED of 3 mm in comparison with that in the conventional MIG welding displayed in %, and the enthalpy of the droplet calculated from the averaged droplet temperature and droplet size are also presented.

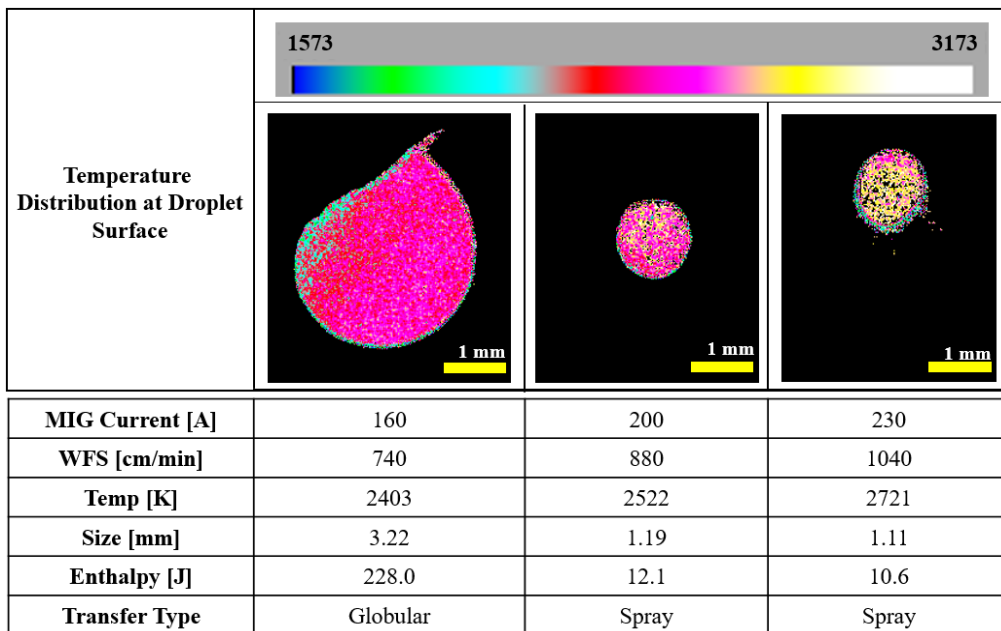
In the conventional MIG welding, the averaged droplet surface temperatures with respect to the MIG currents are 2403 K at 160 A, 2522 K at 200 A and 2721 K at 230 A, as shown in **Fig. 3.10 (a)**. Lower droplet surface temperatures were observed in the plasma MIG welding; the averaged droplet surface temperatures of 2230 K at 160 A, 2423 K at 200 A and 2612 K at 230 A for PED of 7mm as shown in **Fig. 3.10 (b)**, and 2156 K at 160 A, 2327 K at 200 A and 2408 K at 230 A for PED of 3 mm as shown in **Fig. 3.10 (c)**. The decrease in the averaged droplet temperature is found to reach approximately 8 % ~ 12 % in case of PED of 3mm.

The enthalpies of the droplet in the conventional MIG welding with respect to the MIG currents are seen to be 228.0 J at 160 A, 12.1 J at 200 A and 10.6 J at 230 A. Those in the plasma MIG welding are 140.5 J at 160 A, 51.1 J at 200 A and 11.3 J at 230 A for PED of 7 mm, and 127.3 J at 160 A, 64.8 J at 200 A and 12.4 J at 230 A for PED of 3 mm. Although the droplet temperature increases with the MIG current, the enthalpy decreases inversely. This is because the largest droplet diameter is obtained at relatively low MIG current levels, and the droplet diameter significantly decreases as the MIG current increases. It is also found that, in case of 230 A, the enthalpy becomes higher in the plasma MIG welding especially with PED of 3mm than that of the conventional MIG welding despite of the lower droplet temperature and the same WFS. Also in this case, the heat input to the base metal caused by the droplet per unit time in the plasma MIG welding becomes lower than that in the conventional MIG welding due to lower metal transfer frequency.

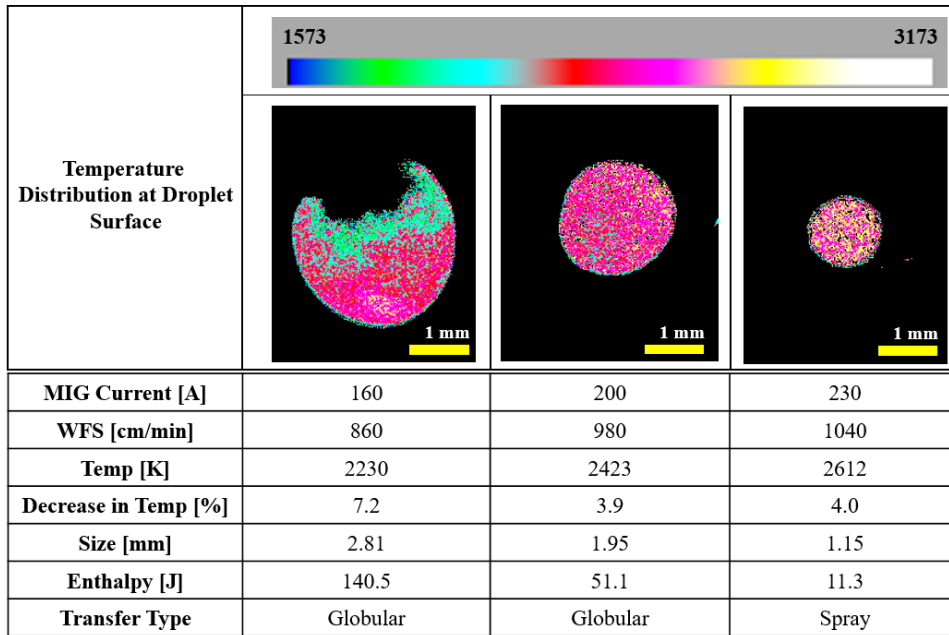
Two major differences were observed in the conventional MIG welding and the plasma MIG welding: (1) the droplet shape in the globular transfer mode, (2) the temperature distribution on the droplet surface. The droplet in the conventional MIG welding has an elongated shape with a uniform temperature distribution, whereas the droplet in the plasma MIG welding has a rounded shape with a non-uniform temperature distribution. These differences can be attributed to the arc heating process which closely influenced the droplet temperature. It is mentioned that the temperature largely affects the surface tension of the droplet [1,45,46]. During the welding, the arc attachment in the conventional MIG welding is observed to cover the whole of the droplet and the arc heating tends to be more concentrated to the droplet rather than to the wire. This may cause an increase in droplet temperature and reduces the surface tension of the droplet, resulting in the elongated droplet shape in the

conventional MIG welding. It also explains the uniform temperature distribution on the droplet surface in the conventional MIG welding.

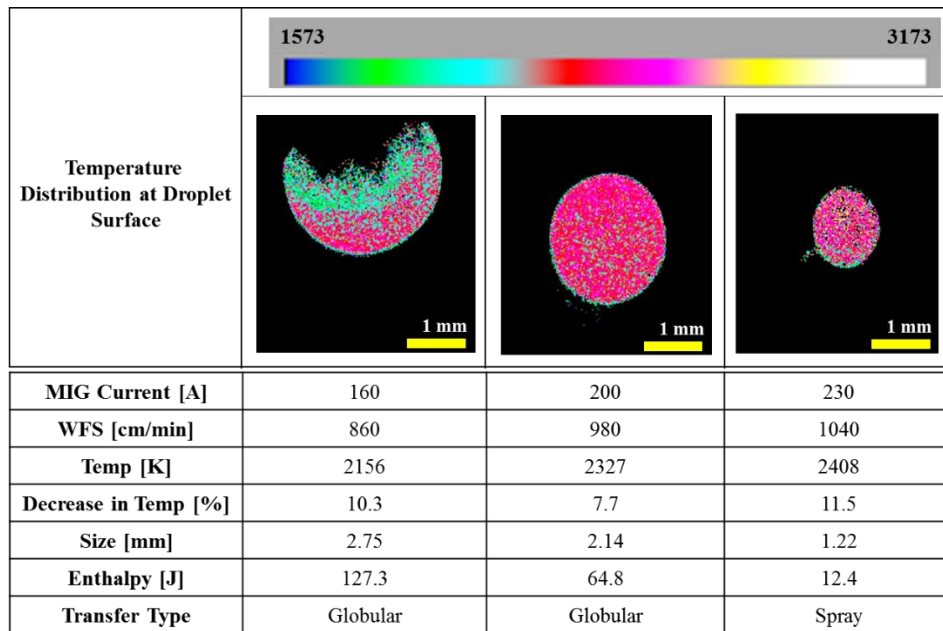
On the other hand, in the plasma MIG welding, the arc attachment was observed to cover not only the droplet but also the upper portion of the wire due to the dispersed arc attachment. Therefore, the arc heating is not fully concentrated to the droplet, resulting in the lower droplet temperature. It influences the surface tension of the droplet surface in the plasma MIG welding to be higher than that in the conventional MIG welding. This leads to the rounded droplet shape in the plasma MIG welding. The difference in the arc attachments observed with the color HSVC is presented in Section 4.



(a) Droplet temperature in conventional MIG welding



b) Droplet temperature in plasma MIG welding with PED of 7 mm

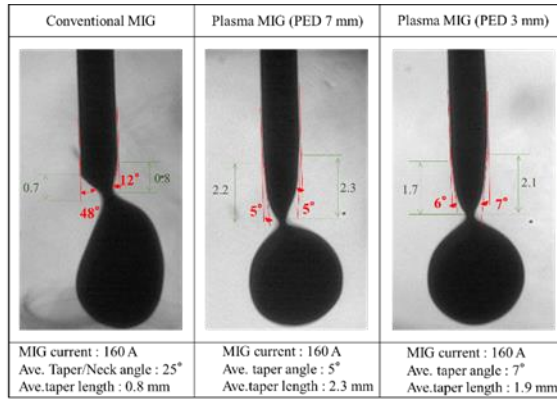


(c) Droplet temperature in plasma MIG welding with PED of 3 mm

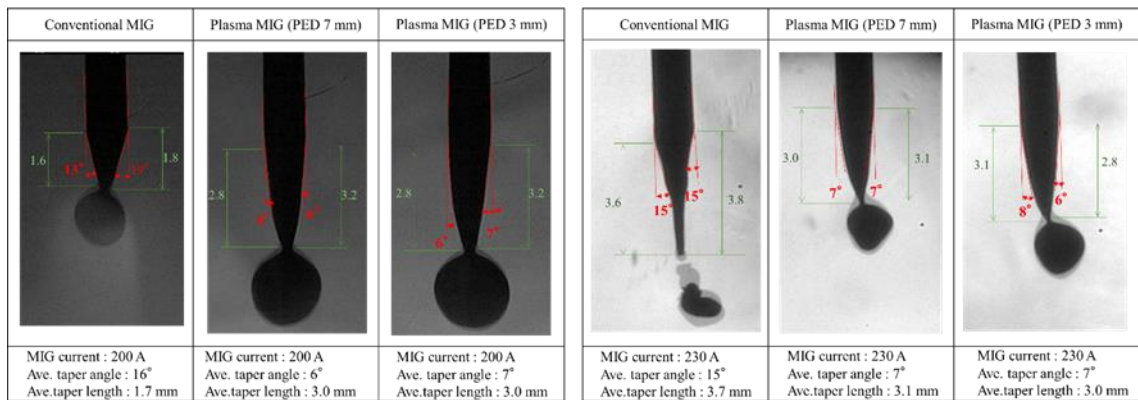
Fig. 3.10 Droplet surface temperature distribution analysis by using two-color temperature measurement method

3.4.4 Taper formation around the neck of the wire

In the previous section, it was suggested that the differences in the droplet temperature distributions and the droplet shapes were caused by the change in the arc attachment. It has been explained that the dispersed arc attachment from the droplet to the wire forms a taper around the neck of the wire [39]. The shadowgraph method enables the observation of the taper formation as well as the metal transfer process. **Fig. 3.11** shows the taper formation in the conventional MIG welding, and the plasma MIG welding with PED of 7 mm and 3 mm at 160 A, 200 A and 230 A. In this figure, the angles and the lengths of the tapers are denoted by red and green markings, respectively. These images were captured at 0.5 ms before the droplet detachment to obtain the maximum taper angle. **Fig. 3.11 (a)** shows the formation of a large taper angle and an average taper of 25° at 160 A in the conventional MIG welding. Unlike the large taper angle in the conventional MIG welding, small taper angles are seen in the plasma MIG welding. The average taper angles in the plasma MIG welding with PED of 7 mm and 3 mm are 5° and 7° , respectively. Furthermore, similar trends were also observed in all welding conditions at 200 A and 230 A, in which the taper angle in the conventional MIG welding were larger than the plasma MIG welding in all conditions. The increase in MIG current largely decreases the average taper angle in conventional MIG welding from 25° at 160 A to 16° at 200 A and 15° at 230 A. On the contrary, the taper angles at 200 A and 230 A at both of PEDs in the plasma MIG welding are almost similar those at 160A.



(a) 160 A



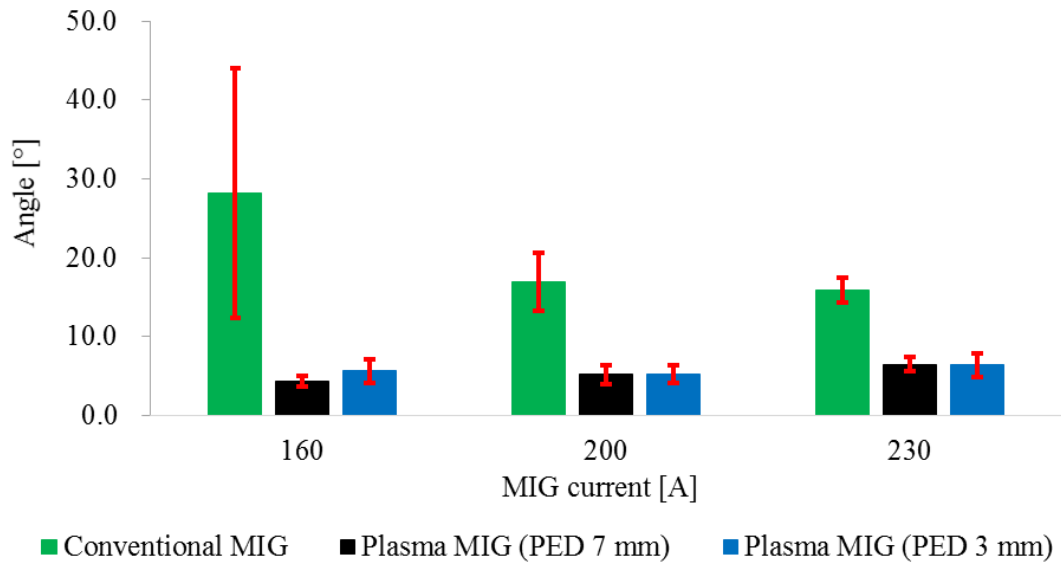
(b) 200 A

(c) 230 A

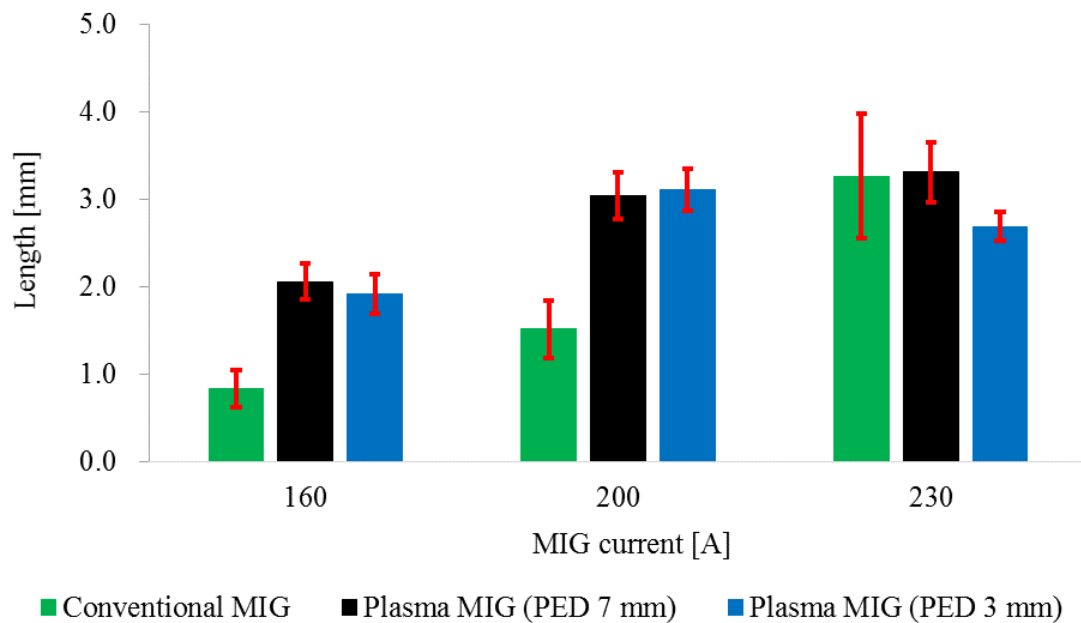
Fig. 3.11 Taper formation in conventional MIG welding, plasma MIG welding with PED of 7 mm and 3 mm at, (a) 160 A, (b) 200 A and (c) 230 A

For the average taper length, the conventional MIG welding was observed to form a very short taper before the droplet detachment at 160 A. The length of the taper increases markedly (from 113% to 200%) by increasing the MIG current. A similar trend was also observed in the plasma MIG welding, in which increasing the MIG current increases the taper length from 30% to 35% for PED of 7 mm and from 37% to 58% for PED of 3 mm.

The average taper angles and taper lengths for the number of samples up to 20 at 160 A, 200 A and 230 A were measured and the results shown in **Fig. 3.12 (a)** and **(b)**. The average taper angles and average taper lengths tend to increase as the MIG current increases, as observed previously. A large standard deviation seen in average taper angle at 160 A in the conventional MIG welding is caused by the unstable axial position of the droplet. Increasing the MIG current decreases this deviation, similar to those in the plasma MIG welding. A smaller standard deviation of the taper angle is considered to indicate the stability of the metal transfer. Furthermore, the large standard deviation of the taper length at 230 A in the conventional MIG welding is caused by the streaming transfer, as the measurement of the taper length would include the length of the molten metal hanging at the wire tip.



(a) Average taper angle



(b) Average taper length

Fig. 3.12 Taper formation behavior in conventional MIG welding, plasma MIG welding with PED of 7 mm and 3 mm, which (a) average taper angle (b) average taper length

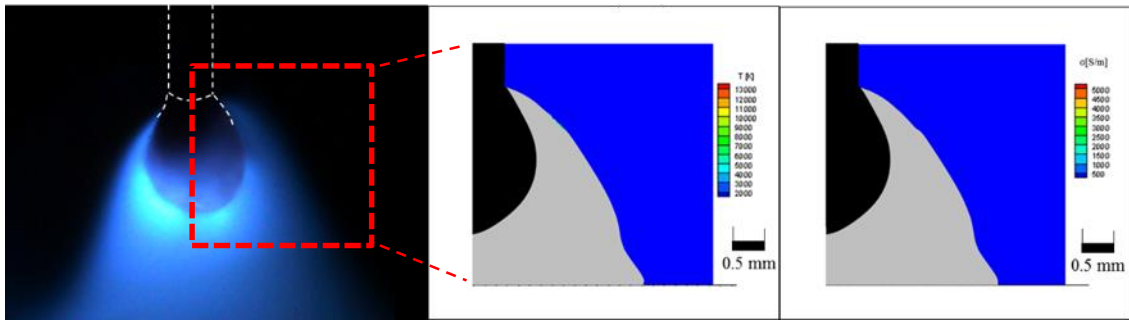
3.4.5 Plasma temperature measurement in surrounding of MIG wire

The plasma temperature in the surrounding of the MIG wire was also measured by using Fowler Milne method, to discuss the difference in the arc attachment. Fowler Milne method can be basically used only for the plasma satisfying the LTE assumption and containing a single gas composition such as pure Ar gas. Ar MIG arc is known to be in a dual structure consisting of low temperature dense metal vapor plasma near the central axis and high temperature pure Ar plasma surrounding the dense metal vapor plasma [47,37]. Fowler Milne method is considered to be applicable to the latter especially exceeding approximately 10,000 K which is necessary temperature to satisfy the LTE assumption. In this way, the plasma temperature in surrounding of MIG wire can be roughly obtained. From the measured plasma temperature, electrical conductivity is also calculated.

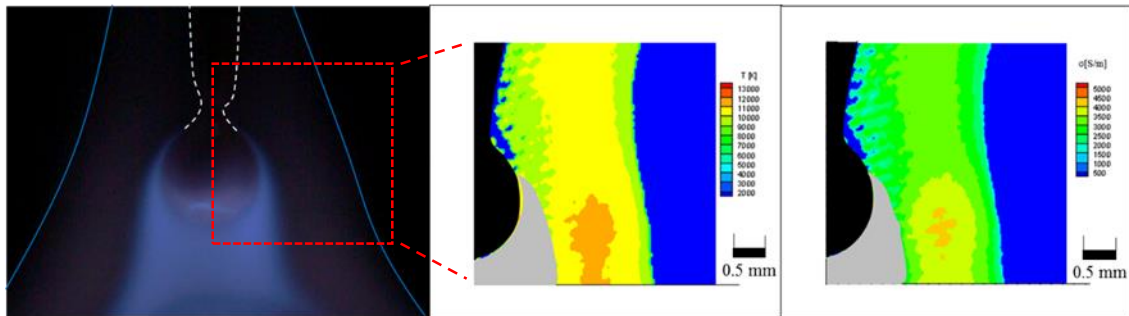
Fig. 3.13, 3.14 and 3.15 show the image captured by color HSVC, the plasma temperature as well as the electrical conductivity surrounding the MIG wire in (a) the conventional MIG welding, (b) the plasma MIG welding with PED of 7 mm, (c) the plasma MIG welding with PED of 3 mm at 160 A, 200 A and 230 A, respectively. The dense metal vapor plasma region found in the image captured by color HSVC is masked in the plasma temperature distribution and the electrical conductivity distribution.

In the conventional MIG welding at 160 A, available plasma temperature and electrical conductivity couldn't be obtained due to very narrow Ar plasma region. However, at 200 A and 230 A, the maximum plasma temperature is found to reach around 13,000 K, which nearly agrees with the result reported in the literatures [47,37]. The high temperature plasma is seen to be confined within the region closed to the taper.

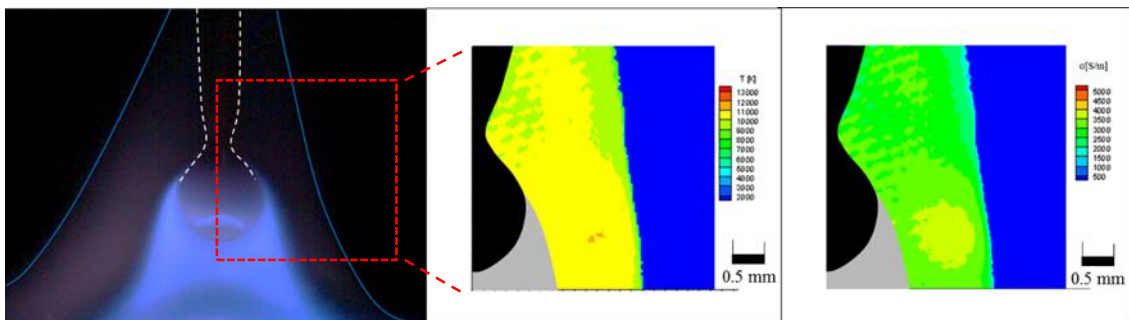
In the plasma MIG welding, although the maximum plasma temperature becomes lower than that of the conventional MIG welding by about 1,000 K, it is thought to still be under the LTE assumption. The high temperature plasma is clearly expanded more upward than that of the conventional MIG welding. The calculated electrical conductivity in this expanded high temperature plasma is found to be at least 3,000 S/m, which is enough for dispersing the MIG current. Furthermore, this electrical conductivity is found to increase with decrease in the plasma electrode diameter. It is considered that this difference affects the degree of the MIG current dispersion to change the droplet temperature.



(a) Conventional MIG welding

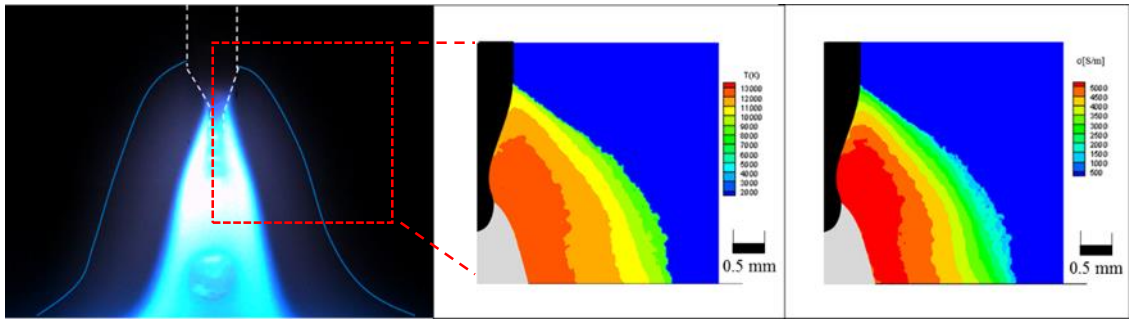


(b) Plasma MIG welding with PED of 7 mm

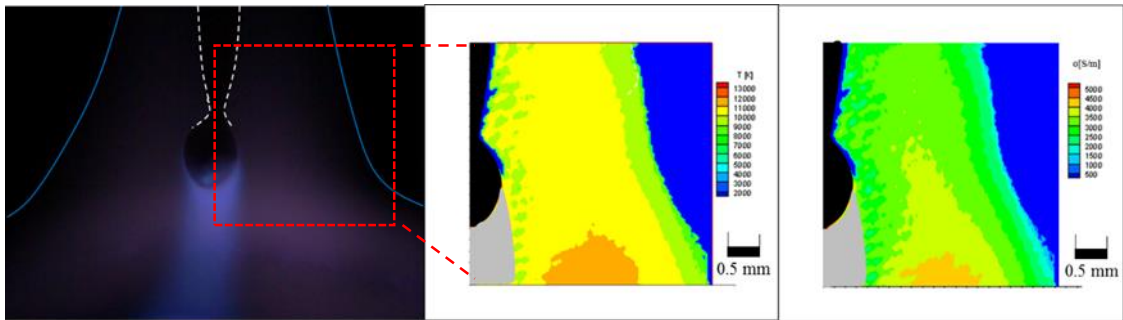


(c) Plasma MIG welding with PED of 3 mm

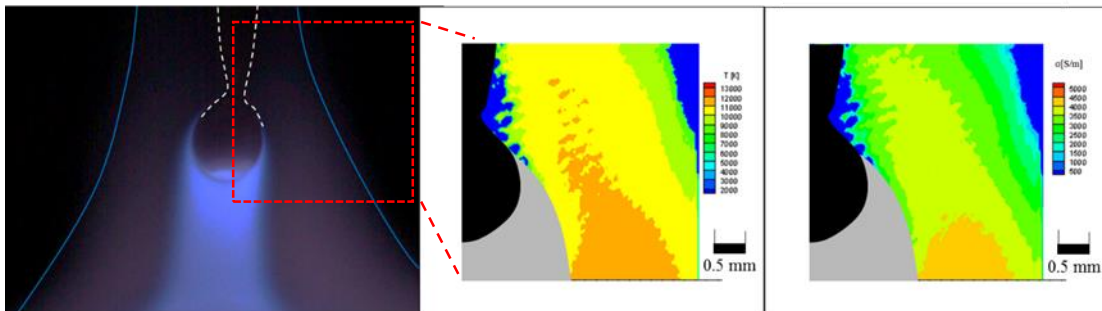
Fig. 3.13 Image captured by color HSVC, plasma temperature as well as electrical conductivity surrounding the MIG wire in (a) the conventional MIG welding, (b) the plasma MIG welding with PED of 7mm, (c) the plasma MIG welding with PED of 3mm at 160 A



(a) Conventional MIG welding

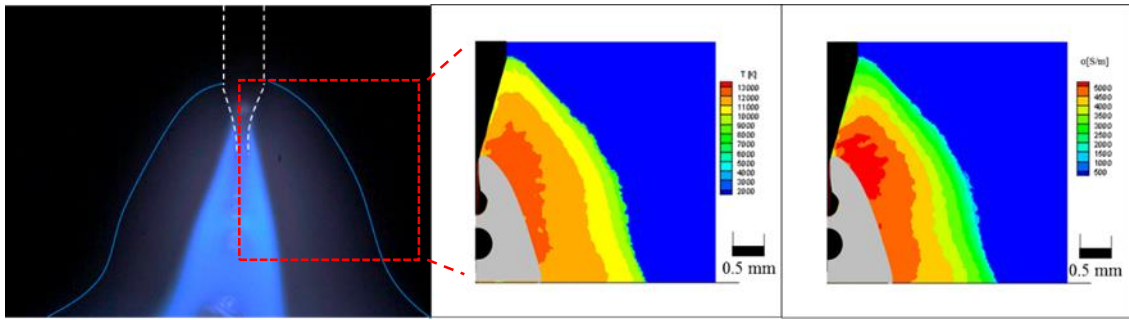


(b) Plasma MIG welding with PED of 7 mm

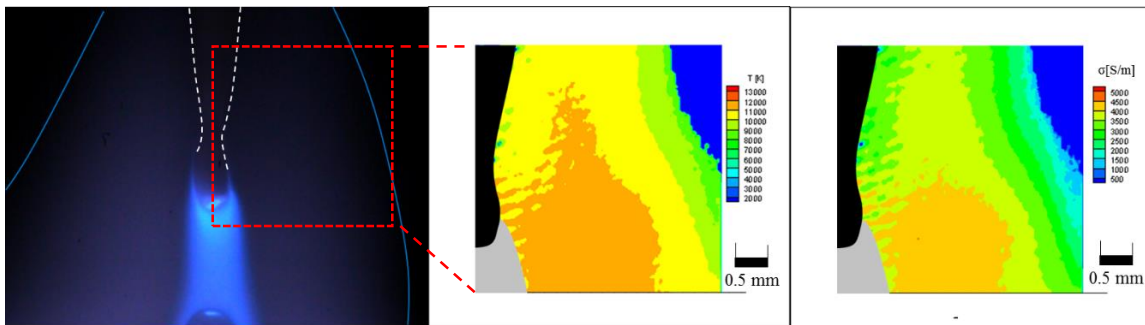


(c) Plasma MIG welding with PED of 3 mm

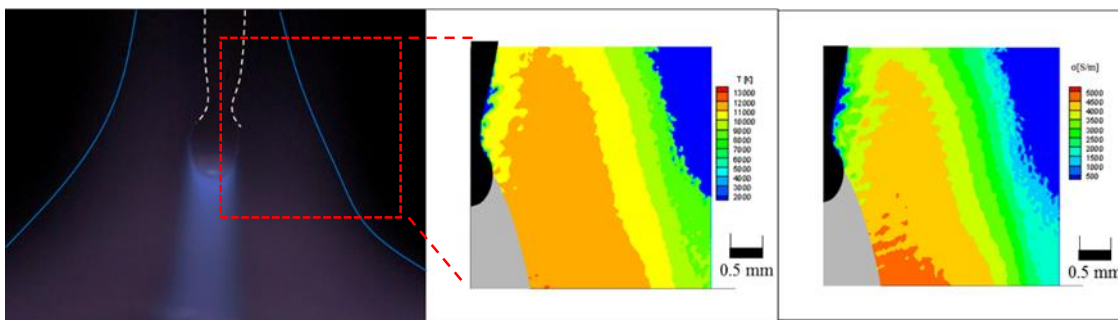
Fig. 3.14 Image captured by color HSVC, plasma temperature as well as electrical conductivity surrounding the MIG wire in (a) the conventional MIG welding, (b) the plasma MIG welding with PED of 7mm , (c) the plasma MIG welding with PED of 3mm at 200 A



(a) Conventional MIG welding



(b) Plasma MIG welding with PED of 7 mm



(c) Plasma MIG welding with PED of 3 mm

Fig. 3.15 Image captured by color HSVC, plasma temperature as well as electrical conductivity surrounding the MIG wire in (a) the conventional MIG welding, (b) the plasma MIG welding with PED of 7mm, (c) the plasma MIG welding with PED of 3mm at 230 A

3.5 Simulation results

Fig. 3.16 shows the temperature distributions immediately after the droplet detachment in the conventional MIG welding and the plasma MIG welding. **Fig. 3.17** shows the metal vapor mole fraction distributions at the same moment as **Fig. 3.16**.

In the conventional MIG welding, the arc temperature reached approximately 12,000K at the maximum. The droplet temperature was raised to approximately 2,900K on average due to the strong heating by the electron condensation and the thermal conduction from the arc plasma. Consequently, large amount of metal vapor was evaporated from the droplet surface and the wire tip. Then the metal vapor was transported to the base metal by the plasma jet. Afterward, the metal vapor transported radially outward. Because of the intensive radiation loss by the metal vapor, the arc temperature around the axis decreased to around 6,000K. These results are found to agree with the results of the experimental observation [48,49].

On the other hand, in the plasma MIG welding, the center gas and shielding gas were ionized in advance in upstream region of the MIG arc, becoming the plasma with temperature of approximately 10,000 K. The arc temperature around the wire tip was lower than that of the conventional MIG welding by approximately 1,000K. This difference implies the decreased current density around the wire tip by influence of the plasma. The droplet temperature is considered to be decreased due to this lower current density. The amount of the metal vapor evaporated from the droplet is seen to be decreased than that of the conventional MIG welding due to the lower droplet temperature. It will lead to smaller amount of fume formation generally known in the plasma MIG welding. **Fig. 3.18** and **Fig. 3.19** show the current density vectors and the current density distributions at the same moment as **Fig. 3.16**.

In the conventional MIG welding, the arc attachment was seen to be concentrated around the wire tip to lead to the higher current density. However, in the plasma MIG welding, the plasma transported to the surrounding of the wire tip increases the electric conductivity in that region. It leads to dispersion of the arc attachment toward the wire root. Consequently, the current density in the plasma MIG welding is found to decrease compared with that of the conventional MIG welding, causing decrease in the droplet temperature and metal transfer frequency.

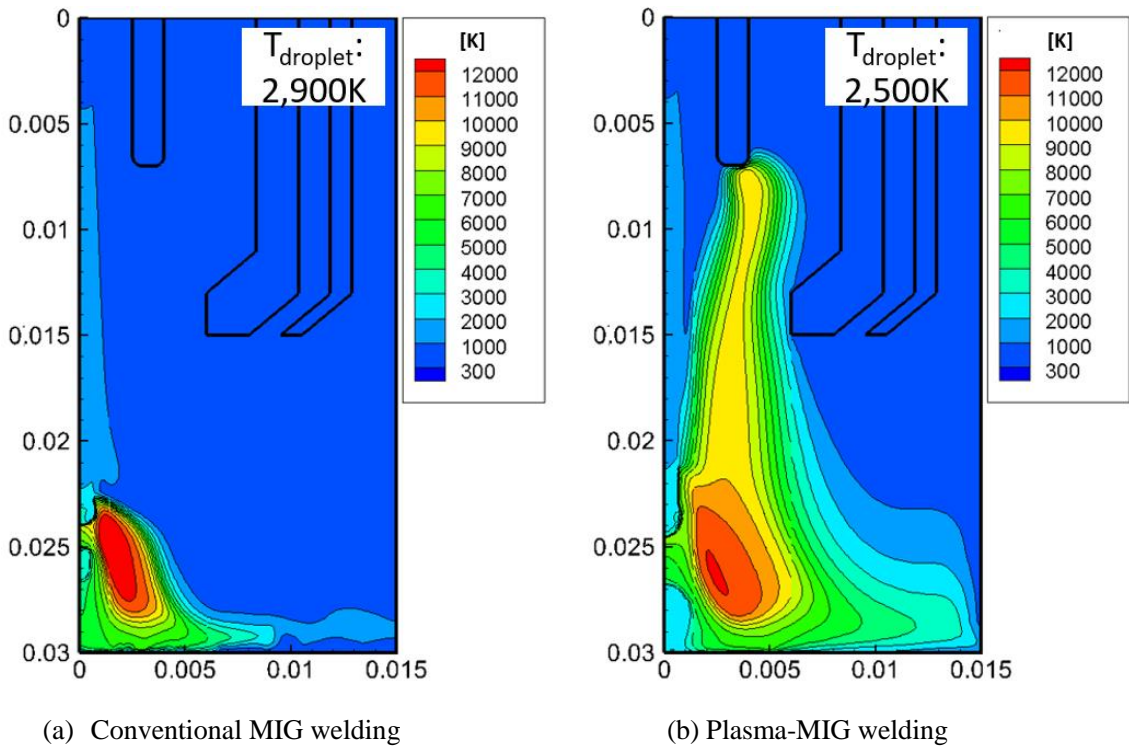


Fig. 3.16 Temperature distributions in (a) conventional MIG welding and (b) plasma-MIG welding

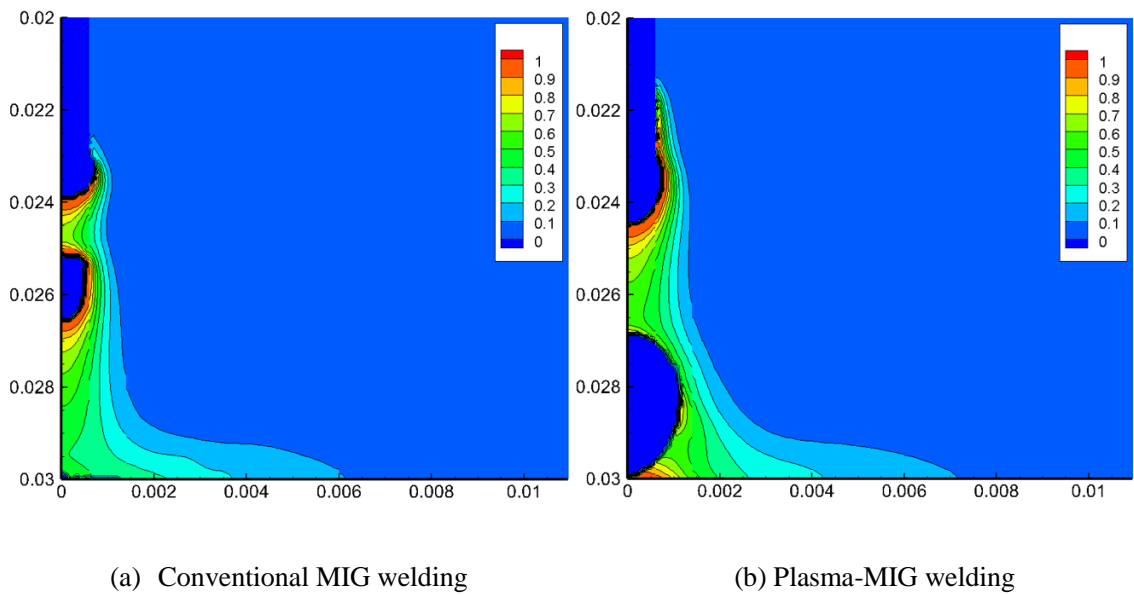


Fig. 3.17 Metal vapor mole fraction distributions in (a) conventional MIG welding and (b) plasma-MIG welding

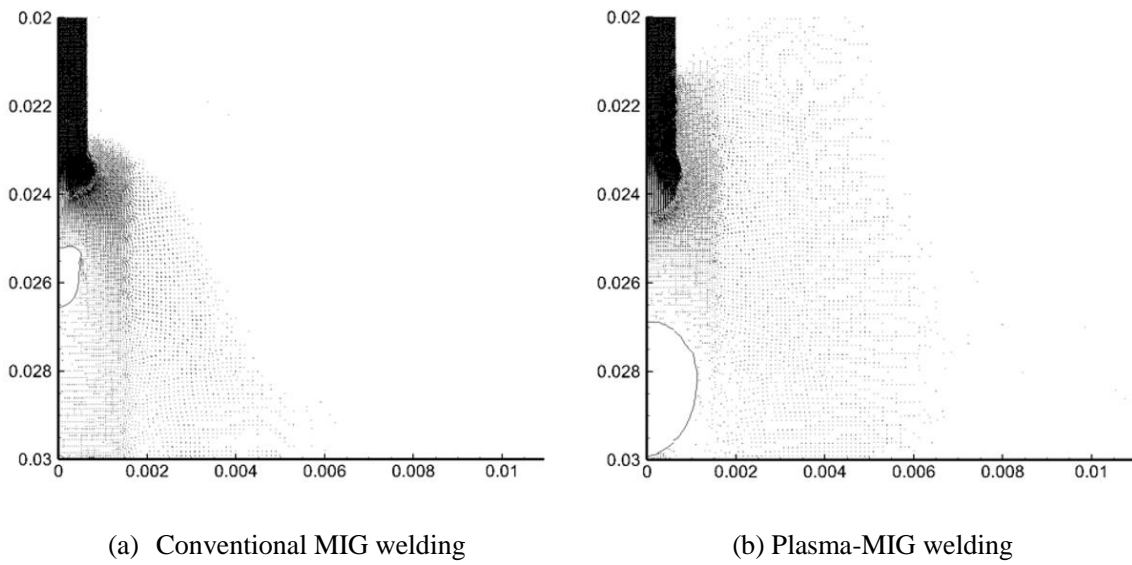


Fig. 3.18 Current density vectors in (a) conventional MIG welding and (b) plasma-MIG welding

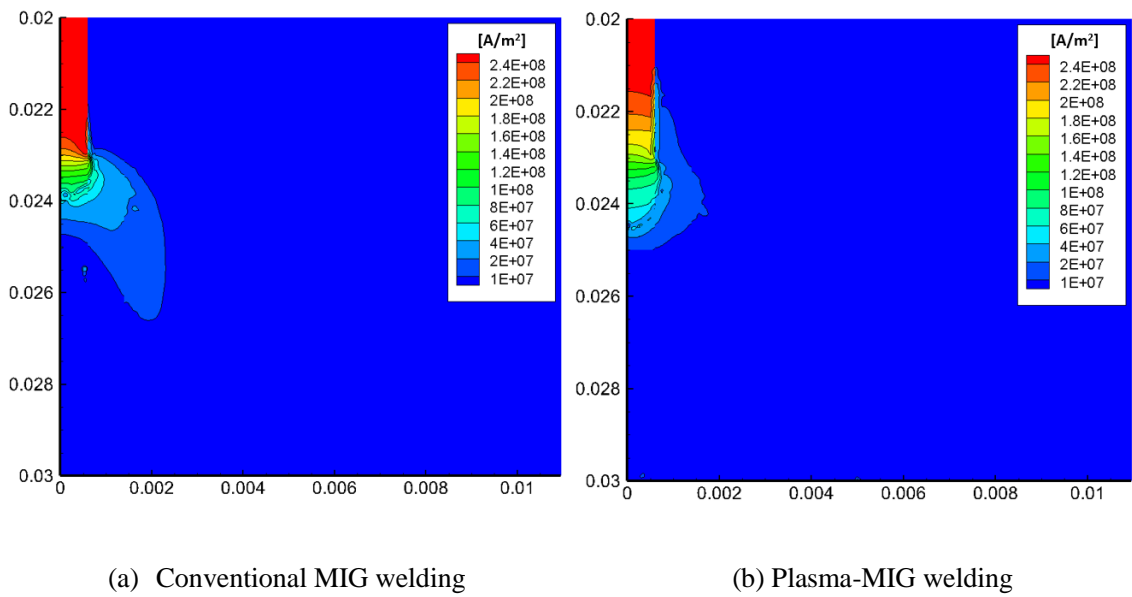


Fig. 3.19 Current density distributions in (a) conventional MIG welding and (b) plasma-MIG welding

3.6 Discussion

3.6.1 Effects of the plasma flow in plasma MIG welding

The experimental results have shown that the presence of plasma in plasma MIG welding causes a decrease in the droplet temperature as well as changes in the wire melting rate, the droplet diameter and the taper formation. To interpret this effect of plasma on droplet temperature, the discussion in this section will be divided into three segments, corresponding to three MIG current ranges according to the metal transfer modes: low MIG current (from 160 A to 180 A), medium MIG current (from 190 A to 220 A), high MIG current (above 230 A), as shown in **Fig. 3.20**.

At low MIG current, the metal transfer mode is in globular transfer for both the conventional MIG welding and plasma MIG welding. However, at medium MIG current, the transfer mode in the conventional MIG welding changes into projected spray transfer while remaining in the globular mode in the plasma MIG welding. At high MIG current, both the transfer modes in the conventional MIG welding and plasma MIG change into streaming transfer and projected spray transfer, respectively.

The presence of the plasma surrounding the wire in the plasma MIG welding is considered to be a major factor in changing the heating process of the droplet. This causes a difference in the metal transfer mode as compared to conventional MIG welding, leading to the variation in the droplet temperatures.

	Low MIG current (160 A – 180 A)			Medium MIG current (190 A – 220 A)				High MIG current (230 A ~)	
MIG current [A]	160	170	180	190	200	210	220	230	240
Conventional MIG	G	G	G	P	P	P	S	S	S
Plasma MIG (PED 7 mm)	G	G	G	G	G	G	P	P	P
Plasma MIG (PED 3 mm)	G	G	G	G	G	G	G	P	P

G : Globular
 P : Projected
 S : Streaming

Fig. 3.20 Metal transfer modes in conventional MIG welding and plasma MIG welding

3.6.2 Effects at low MIG currents (from 160 A to 180 A)

At low MIG currents (from 160 A to 180 A), both the conventional MIG welding and plasma MIG welding are in the globular transfer mode. However, larger droplet size and higher droplet temperature were seen in the conventional MIG welding than those in the plasma MIG welding.

Fig. 3.21 shows the metal transfers at the moment of droplet detachment at 160 A in the conventional MIG welding observed by the color HSVC and the shadowgraph methods. The image taken by the color HSVC presents the arc attachment covering the whole of the droplet and the area near the wire tip. On the other hand, the shadowgraph image clearly shows the wire, necking area and droplet without the effect of the arc. The uniform temperature distribution and a high average temperature on the droplet surface shown in **Fig. 3.10 (a)** are considered to be caused by the large amount of MIG current transferring through the droplet surface rather than through the wire.

A similar behavior of arc attachment was also observed in low MIG current in the plasma MIG welding, as shown in **Fig. 3.22** and **3.23** for plasma MIG welding with PED of 7 mm and 3 mm, respectively. The shadowgraph images of the MIG wire in both PED cases similarly show the formation of the gradual taper, which have the small taper angle and the long taper length, positioned slightly higher along the wire above the droplet. This taper formation suggests that the MIG current could have dispersed from a higher position along the wire to the droplet. A large portion of the heat input into the wire functioned as an anode due the electron condensation by MIG current, and consequently melts the vicinity of the wire surface [50]. Therefore, in the plasma MIG welding, the presence of the plasma surrounding the wire could have expanded the arc to move upwards along the wire surface to disperse the MIG current. This dispersion of MIG current causes a decrease in current density on the droplet surface, leading to the lowered droplet temperature. In addition, the spreading of the heat input gradually to the wire results in a non-uniform droplet surface temperature distribution, as shown in **Fig. 3.10 (b)**.

Fig. 3.24 illustrates the difference of the predicted current path and taper formation at low MIG currents between the conventional MIG welding and the plasma MIG welding. In the plasma MIG welding, a fraction of MIG current diverges at a higher position along the wire to form a current path, bypassing the droplet. This is because the presence of the plasma surrounding the wire increases the electron density near the wire surface, and raises its electrical conductivity. It also results in the dispersion of electromagnetic forces and heat input to the wire and the droplet. As a result, a gradual taper forms at a higher position along the wire above the droplet. The electromagnetic force acts in driving the molten fluid along the taper surface towards the wire tip [51]. Since the comparison is made for the same MIG current, the total heat input to the wire and the droplet by MIG current is considered to be almost the same. Any decrease in the total heat input into the droplet would indicate that heat is diverted to the wire instead. Such mechanism would explain the decrease in the droplet temperature at low MIG current in the plasma MIG welding.

The significantly stronger radiation from the metal vapor covering the droplet, which appears to be blue, is observed in the conventional MIG welding compared with those in the plasma MIG welding with PED of 7 mm and 3 mm. This implies that the metal vapor concentration around the droplet is higher because of the higher droplet temperature. This dense metal vapor decreases the plasma temperature due to strong radiation cooling, leading to low electrical conductivity of the plasma. It is reported that large portion of the total MIG current transfers through between the upper half of the droplet and the neck to the surrounding argon plasma avoiding the dense metal vapor plasma located at the center [52]. This current distribution acts to increase the force for the droplet detachment. Contrarily, the MIG current transferring through the droplet in the plasma MIG welding is considered to be distributed more uniformly over the droplet surface due to the lower metal vapor concentration around the droplet, to decrease the force for the droplet detachment as well as the MIG current dispersion above the neck.

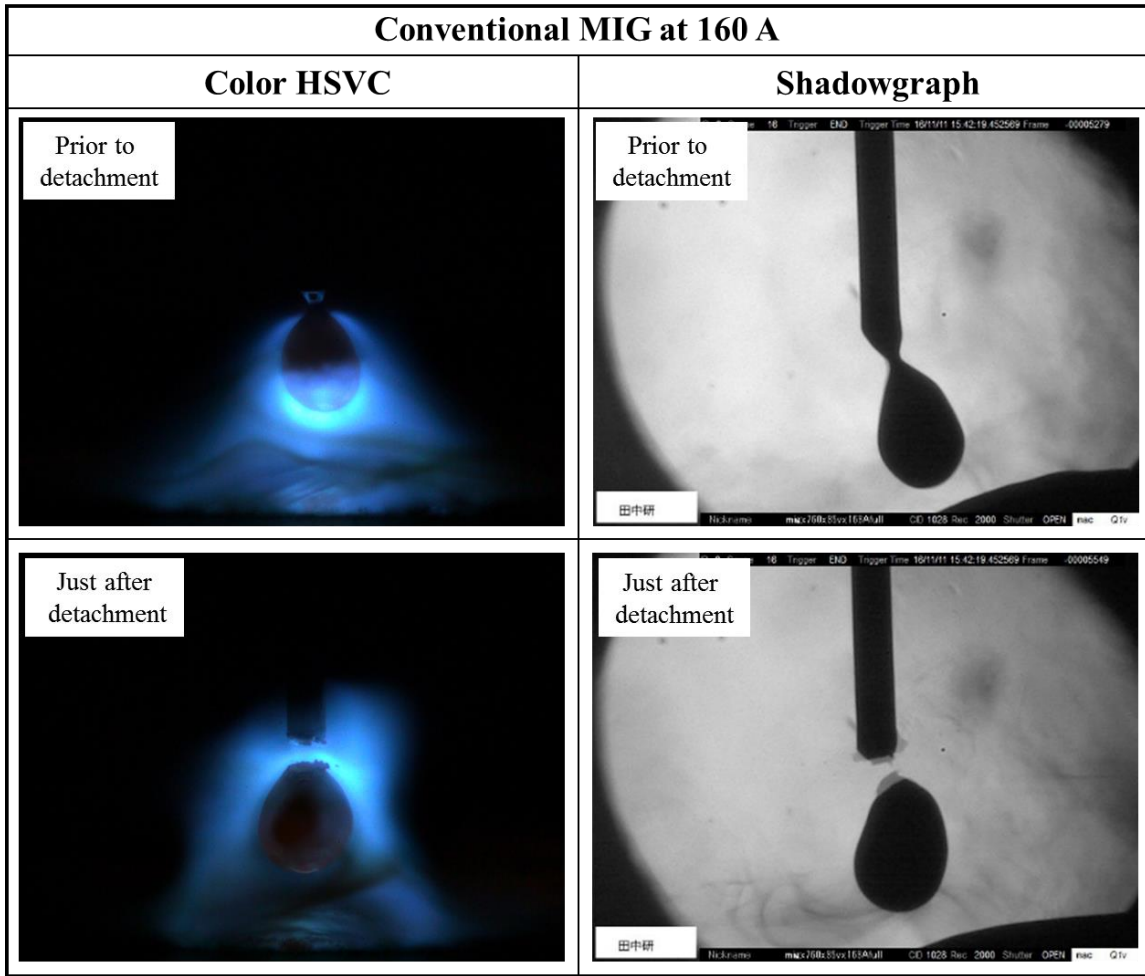


Fig. 3.21 Metal transfer observation at the moment of droplet detachment at 160 A in conventional MIG welding by color HSVC and shadowgraph graph method

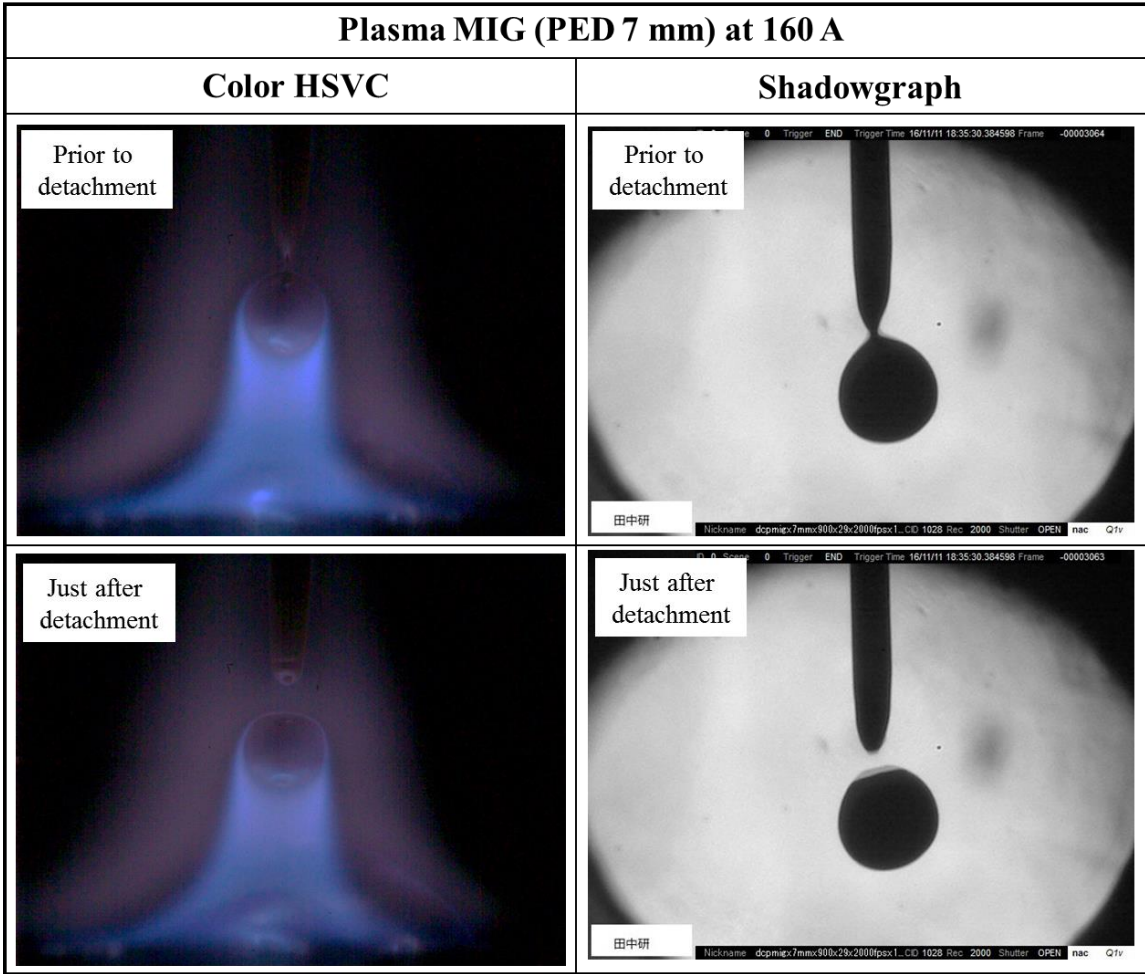


Fig. 3.22 Metal transfer observation at the moment of droplet detachment at 160 A in plasma MIG welding (PED 7 mm) by color HSVC and shadowgraph method

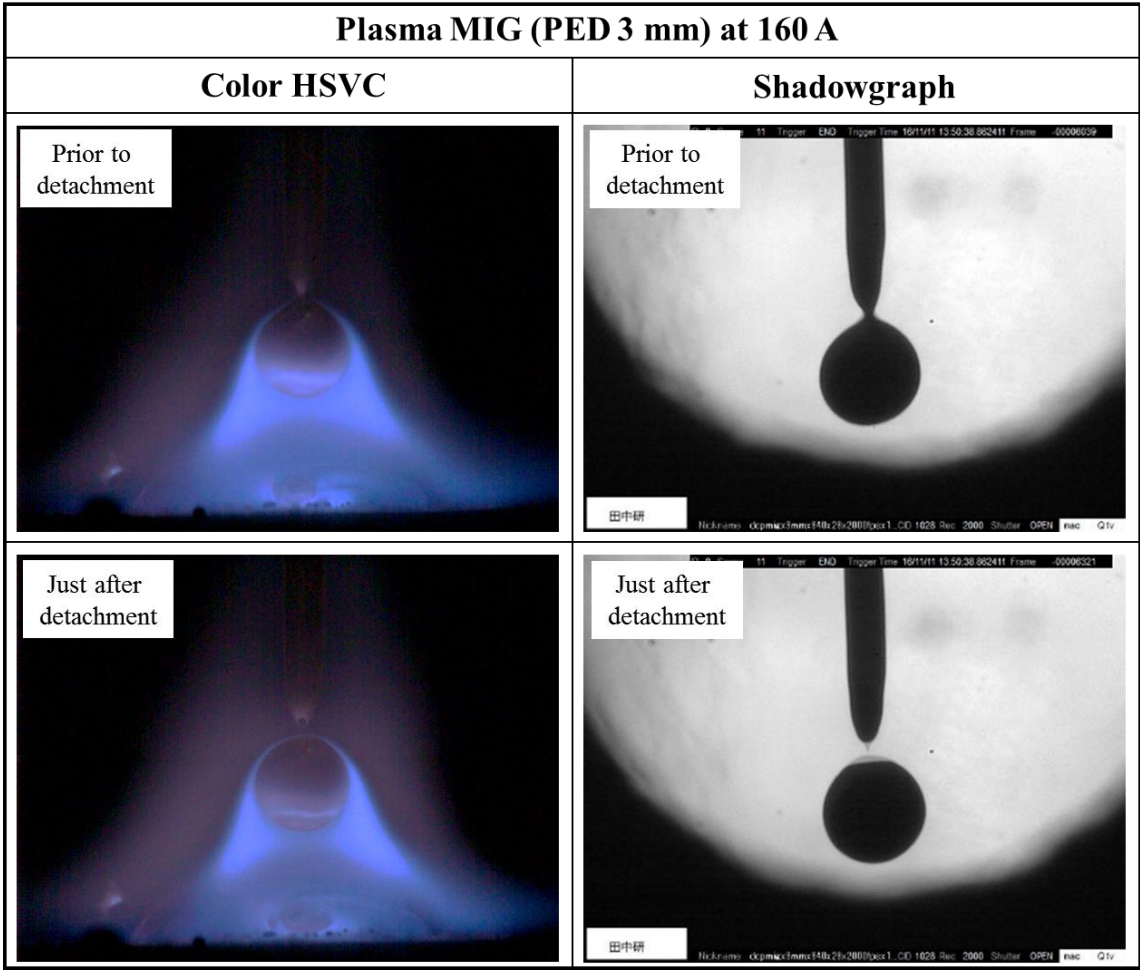
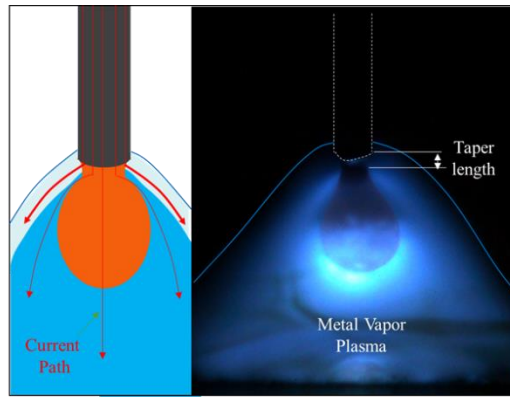
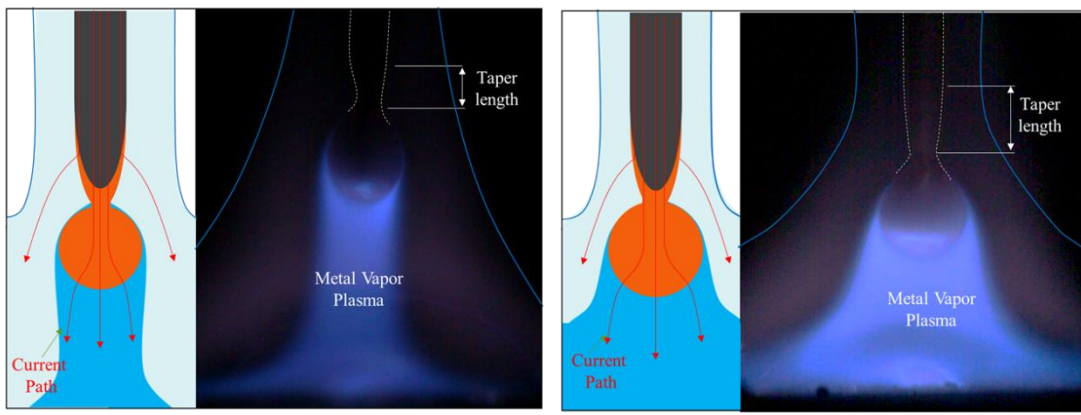


Fig. 3.23 Metal transfer observation at the moment of droplet detachment at 160 A in plasma MIG welding (PED 3 mm) by color HSVC and shadowgraph method



(a) Conventional MIG



(b) Plasma MIG (PED 7 mm)

(c) Plasma MIG (PED 3 mm)

Fig. 3.24 Illustration of a difference in predicted current path and taper formation in low MIG current in (a) conventional MIG welding, (b) plasma MIG welding (PED 7 mm), and (c) plasma MIG welding (PED 3 mm) in low MIG current

3.6.3 Effects at medium MIG current (from 190 A to 220 A)

At medium MIG current (from 190 A to 220 A), different transfer modes were observed in both welding methods. A spray transfer mode predominated in the conventional MIG welding, whereas a globular transfer mode was observed in the plasma MIG welding. In comparison to the plasma MIG welding, the droplet size in the conventional MIG welding is seen to be smaller. However, the droplet temperature in conventional MIG is higher than in the plasma MIG welding.

Fig. 3.25 shows the metal transfer at the moment of droplet detachment at 200 A in the conventional MIG welding observed by the color HSVC and the shadowgraph methods. It can be seen from the image taken by the color HSVC that the arc attachment covers until the side wall of the wire, enabling the divergence of MIG current to bypass the droplet. The dispersion of the heat input and the electromagnetic force to the side wall of the wire causes the taper formation, positioned above the droplet. The shadowgraph image shows the formation of the steep taper, which has a large taper angle and a small taper length, and the detachment of the small-sized droplet. The steep taper and the small droplet size lead to high concentration of MIG current, resulting in a high flux into the droplet which increases the droplet temperature.

The metal transfer at the moment of droplet detachment in the plasma MIG welding is shown in **Fig. 3.26** and **3.27** for plasma MIG welding with PED of 7 mm and PED of 3 mm, respectively. Since the transfer mode of medium MIG current remains unchanged from low MIG current, the same mechanism is described for the metal transfer as well as the mechanism of droplet temperature reduction. However, the droplet size in medium MIG current decreases slightly as compared to the droplet size in low MIG current in both plasma MIG welding.

Fig. 3.28 illustrates the difference in predicted current path and taper formation in medium MIG current for the conventional MIG welding and both plasma MIG welding. Although the dispersion of MIG current is seen in both the conventional and plasma MIG welding, the proportion of the dispersed MIG current to a higher position along the wire is larger in the plasma MIG welding than in the conventional MIG welding. This is verified by the gradual taper formed on the side of the wire in the plasma MIG welding. This current dispersion weakens the electromagnetic force acting on the neck of the wire, lowering the frequency of the droplet detachment and increasing the droplet size.

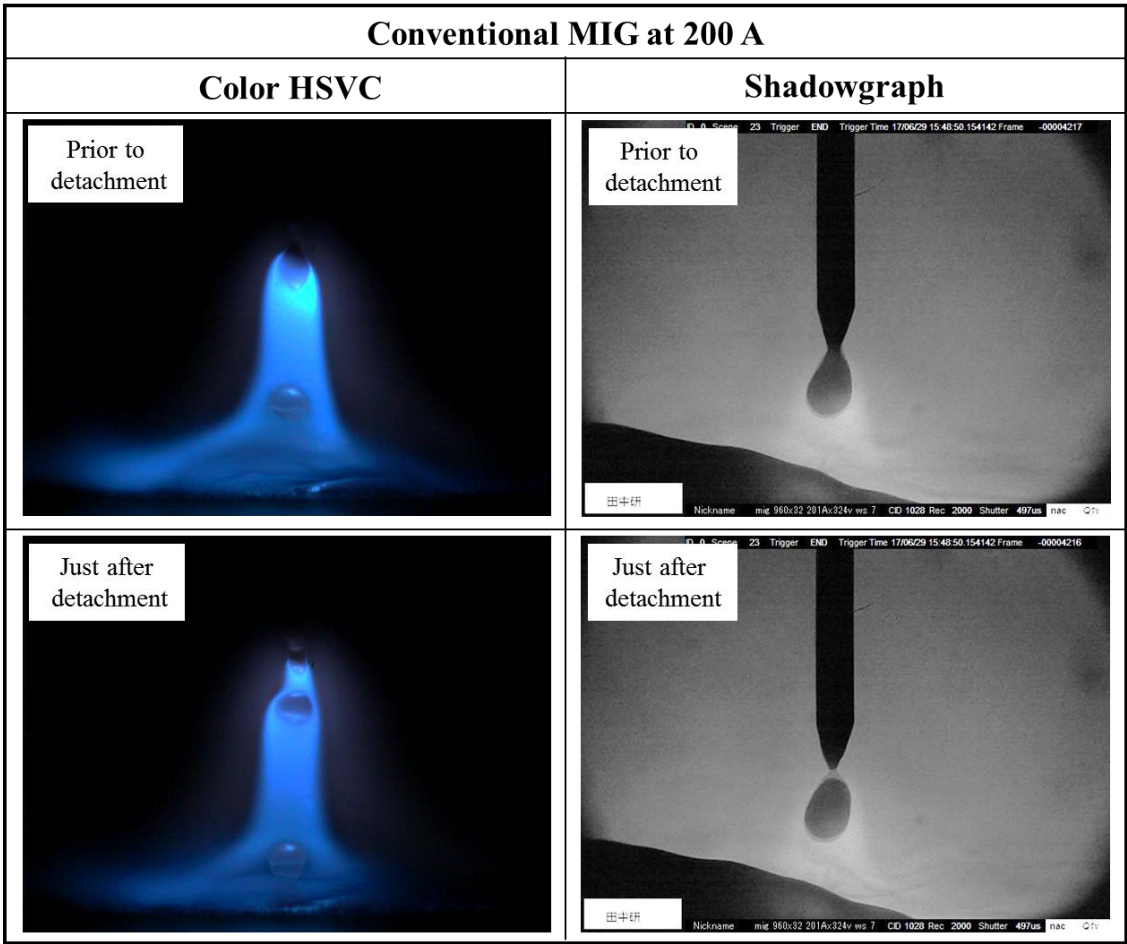


Fig. 3.25 Metal transfer observation at the moment of droplet detachment at 200 A in conventional MIG welding by color HSVC and shadowgraph method

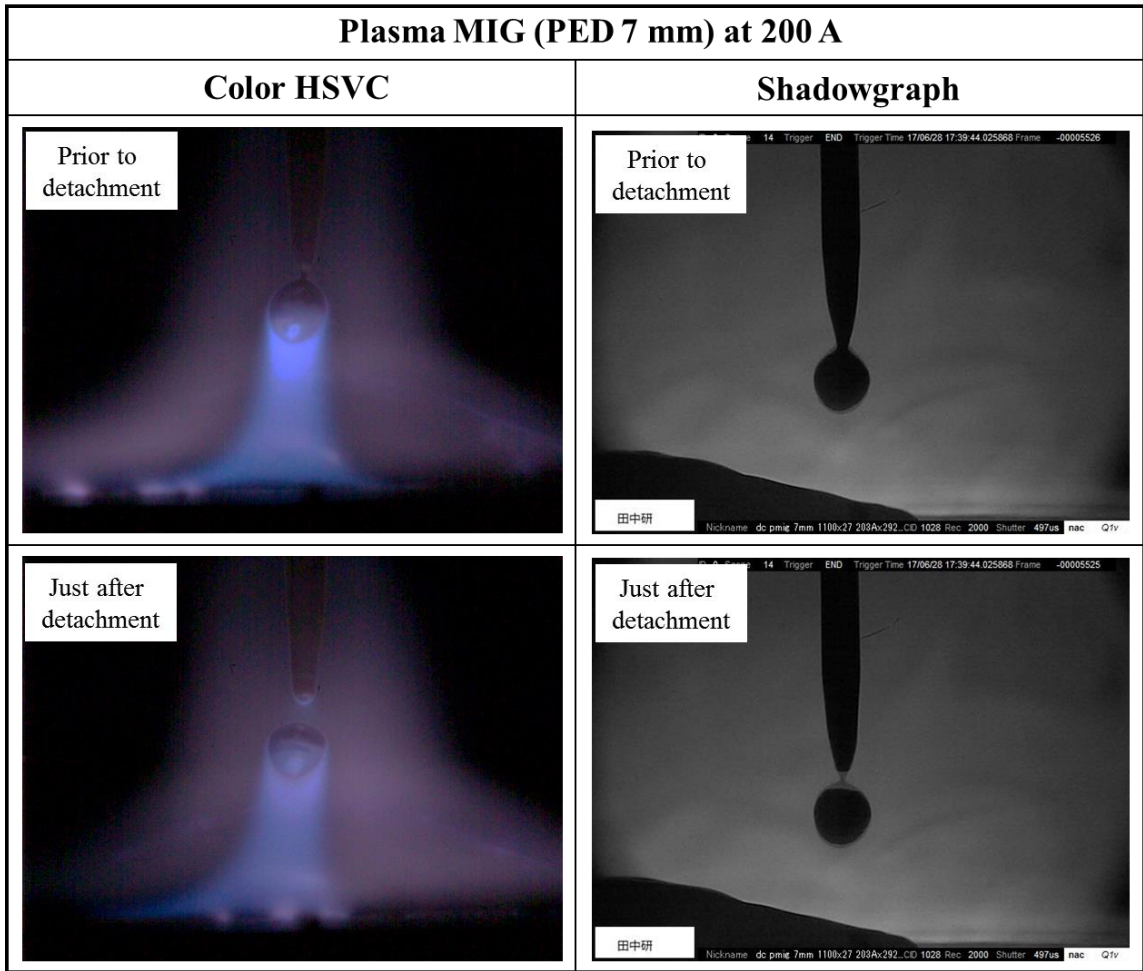


Fig. 3.26 Metal transfer observation at the moment of droplet detachment at 200 A in plasma MIG welding (PED 7 mm) by color HSVC and shadowgraph method

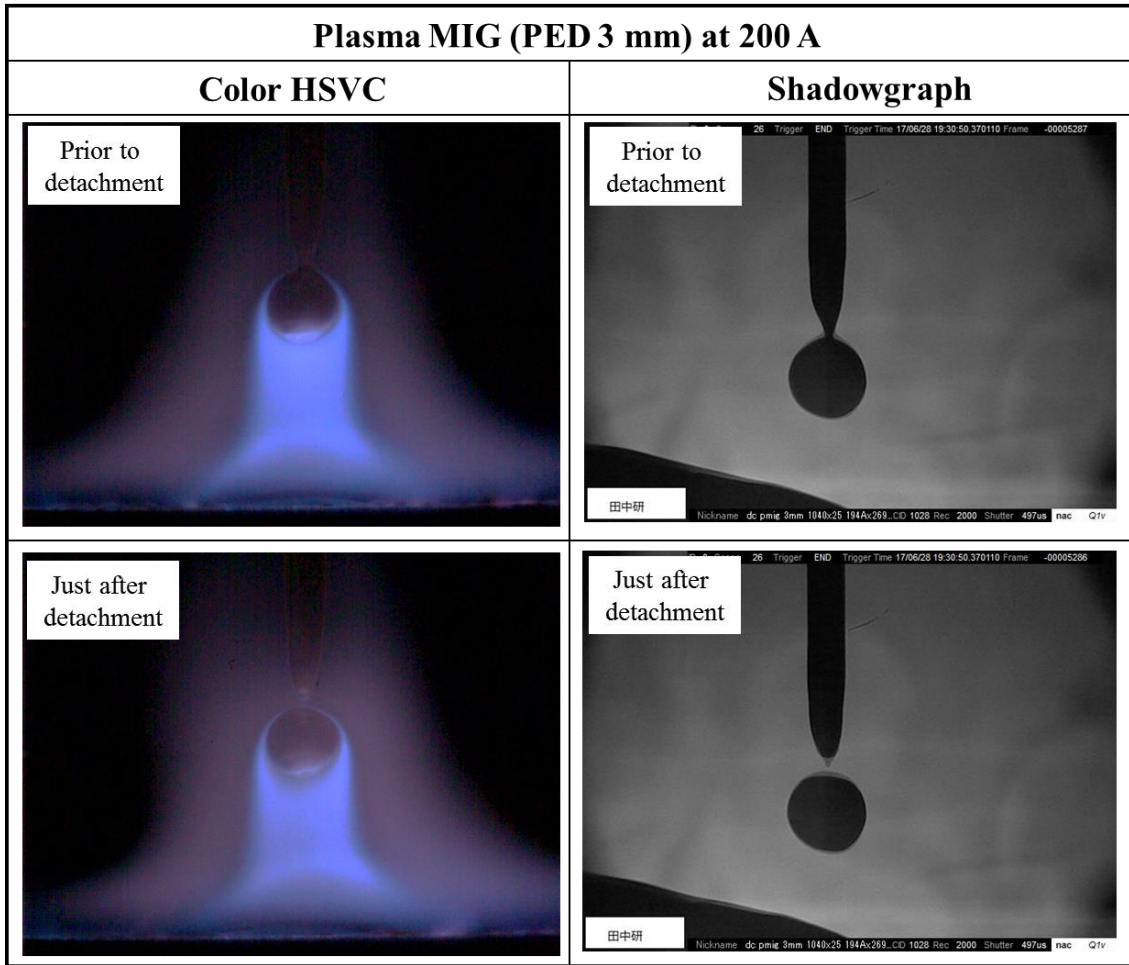
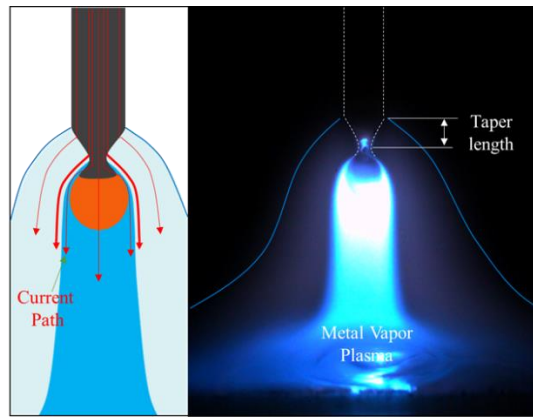
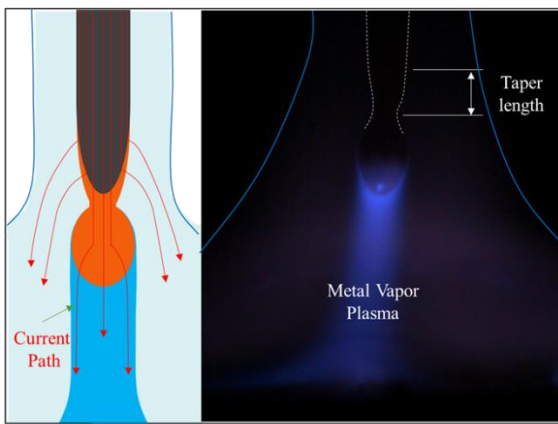


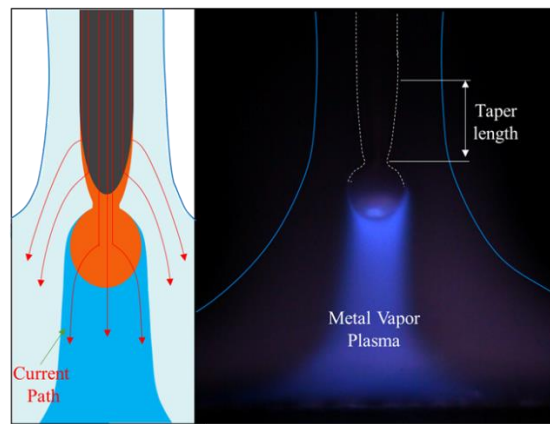
Fig. 3.27 Metal transfer observation at the moment of droplet detachment at 200 A in plasma MIG welding (PED 3 mm) by color HSVC and shadowgraph method



(a) Conventional MIG



(b) Plasma MIG (PED 7 mm)



(c) Plasma MIG (PED 3 mm)

Fig. 3.28 Illustration of a difference in predicted current path and taper formation in (a) conventional MIG welding, (b) plasma MIG welding (PED 7 mm), and (c) plasma MIG welding (PED 3 mm) in medium MIG current

3.6.4 Effects at high MIG current (above 230 A)

At high MIG currents (above 230 A), a spray transfer mode predominates in both welding processes. Specifically, the metal transfer mode evolves from projected spray transfer to streaming transfer in the conventional MIG welding whereas the metal transfer mode changes from globular transfer to projected spray transfer in the plasma MIG welding. As mentioned earlier, the droplet temperature in the plasma MIG welding is, at most, about 400 K lower than that of the conventional MIG welding. In addition, the droplet size in the conventional MIG welding is slightly smaller than the droplet size in the plasma MIG welding.

Fig. 3.29 shows the metal transfer at the moment of droplet detachment at 230 A in the conventional MIG welding observed by the color HSVC and the shadowgraph methods. In the streaming transfer mode, a steep taper is formed with an extended molten metal attached from the wire tip, as seen in the shadowgraph image. In this case, the MIG current is expected to be highly concentrated around the droplet. This results in a large heat flux into the small droplet, raising the droplet temperature.

Fig. 3.30 and **3.31** show the observation of metal transfer behavior in both plasma MIG welding with PED of 7 mm and 3 mm. Apparently, the droplet diameter in both plasma MIG welding approaches the size of the wire diameter. The dispersion of MIG current caused by the plasma prevents concentration of heat input into the droplet, lowering the droplet temperature as compared with that in the conventional MIG welding.

Fig. 3.32 illustrates the difference in predicted current path and taper formation in high MIG current for the conventional MIG welding and plasma MIG welding with PED of 7 mm as well as PED of 3 mm. In case of the streaming transfer mode, the joule heating in the extended molten metal is also possible to increase the droplet temperature. It is considered that a relatively larger fraction of the MIG current conducts through the extended molten metal rather than through the arc surrounding the extended molten metal. It contributes increase the joule heating in the extended molten metal to raise the droplet temperature significantly [18,19], because of the longer extended molten wire with the small cross-sectional area compared with that in the plasma MIG welding as shown in **Fig. 3.33**.

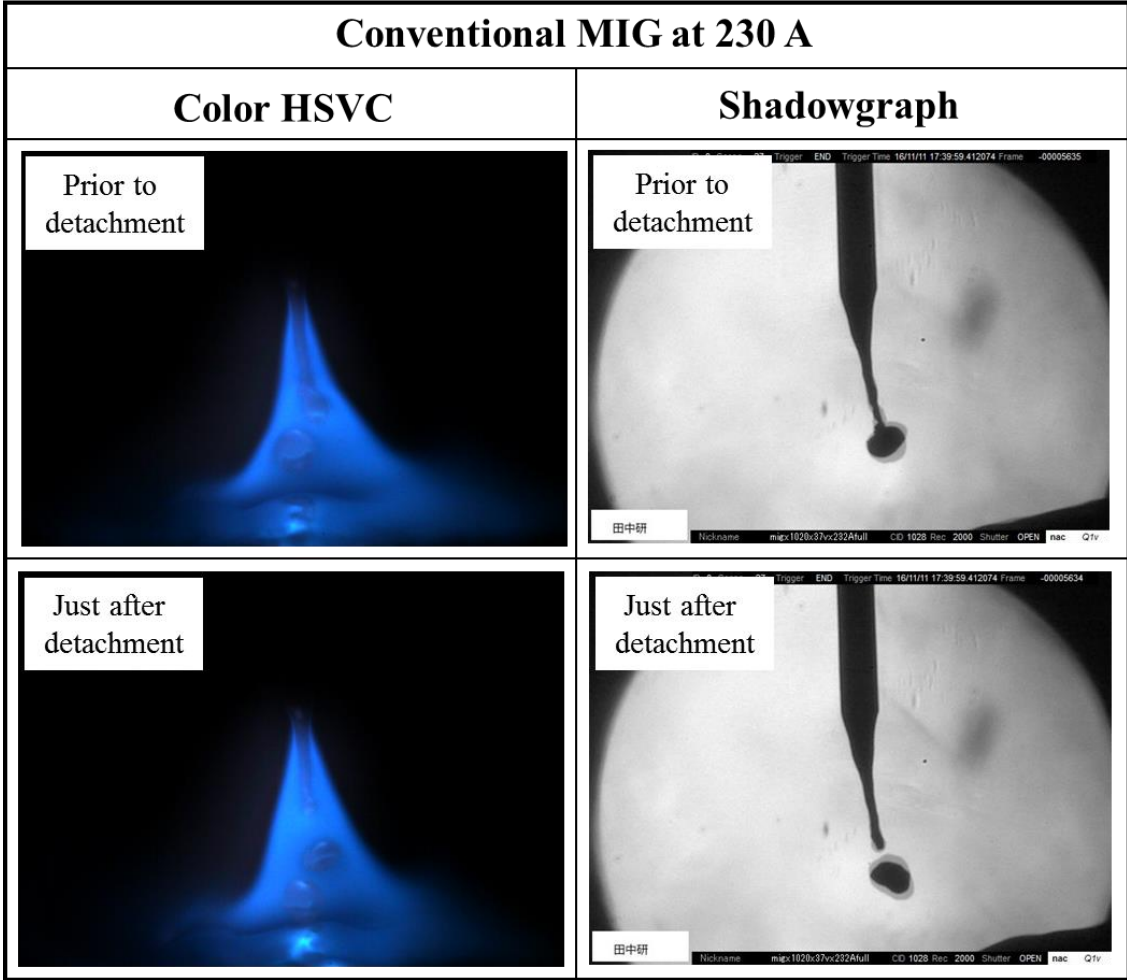


Fig. 3.29 Metal transfer observation at the moment of droplet detachment at 230 A in conventional MIG welding by color HSVC and shadowgraph method

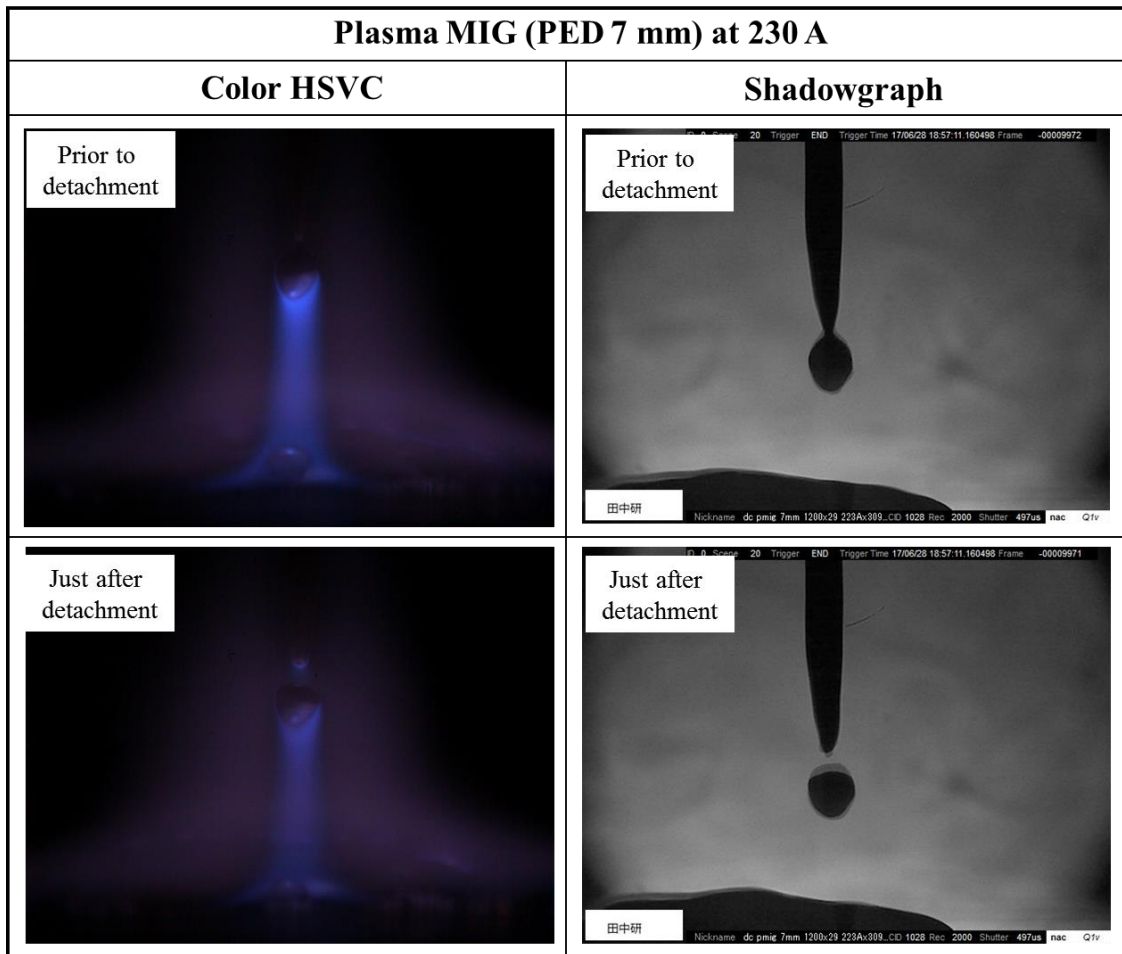


Fig. 3.30 Metal transfer observation at the moment of droplet detachment at 230 A in plasma MIG welding (PED 7 mm) by color HSVC and shadowgraph method

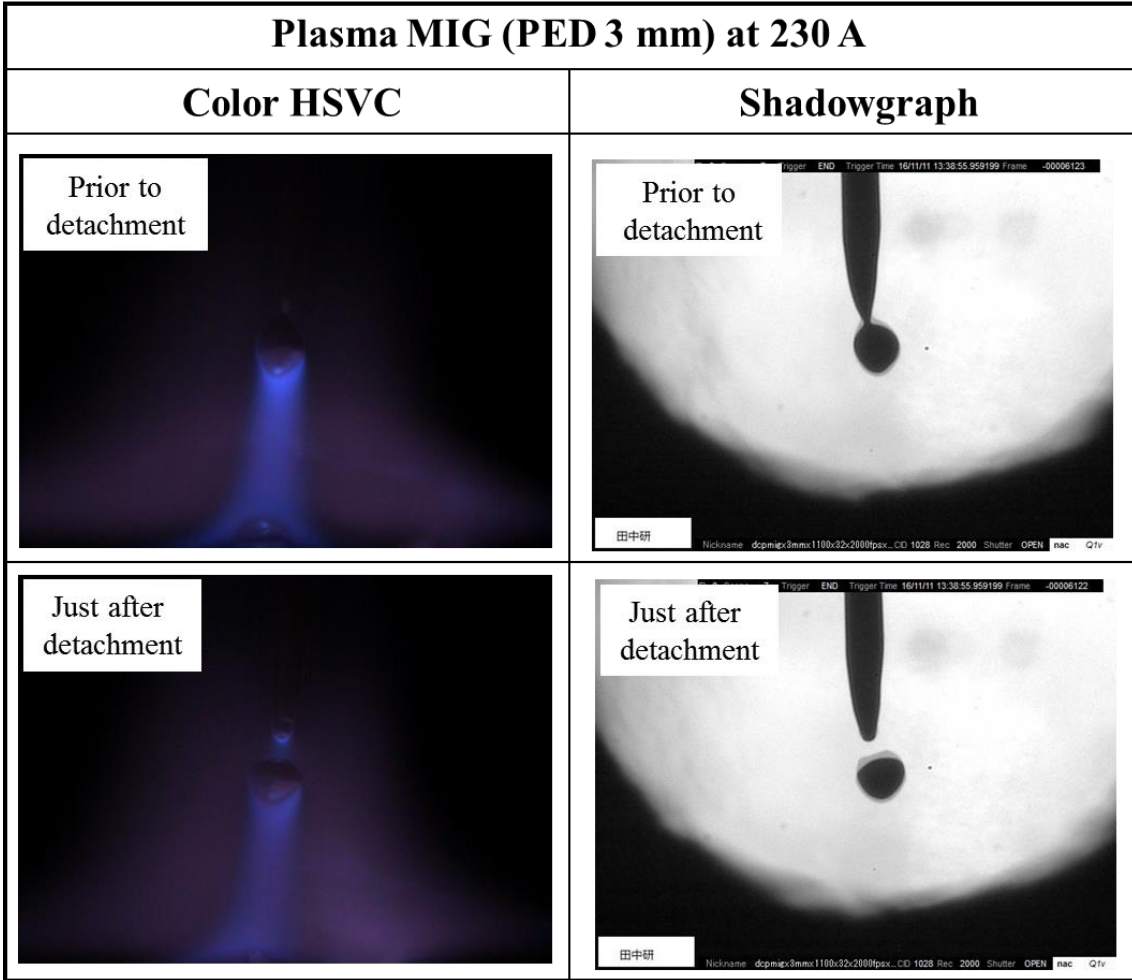
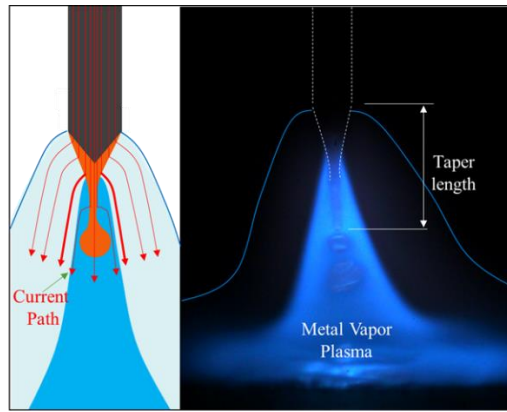
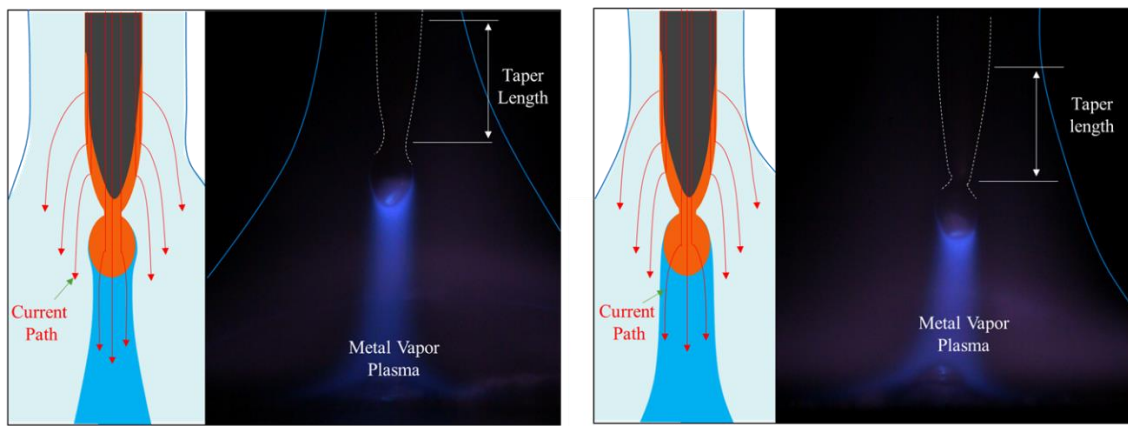


Fig. 3.31 Metal transfer observation at the moment of droplet detachment at 230 A in plasma MIG welding (PED 3 mm) by color HSVC and shadowgraph method



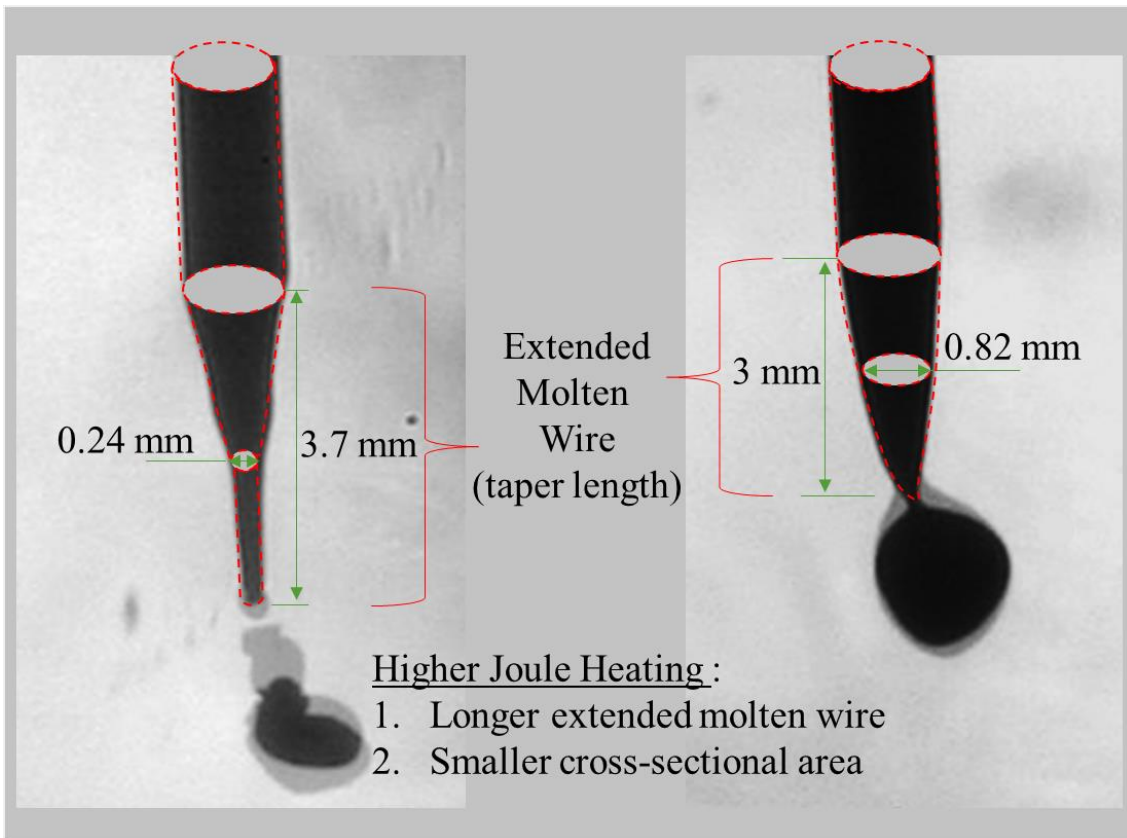
(a) Conventional MIG



(b) Plasma MIG (PED 3 mm)

(c) Plasma MIG (PED 3 mm)

Fig. 3.32 Illustration of a difference in predicted current path and taper formation in (a) conventional MIG welding, (b) plasma MIG welding (PED 7 mm), and (c) plasma MIG welding (PED 3 mm) in high MIG current



(a) Conventional MIG welding at 230 A

(b) Plasma MIG welding at 230 A

Fig. 3.33 Extended molten wire (taper length) measurement and cross-sectional area for (a) conventional MIG welding and (b) plasma MIG welding

3.6.5 Suggested mechanism of droplet temperature reduction in plasma MIG welding

Fig. 3.34 summarizes the suggested mechanisms of droplet temperature reduction in plasma MIG welding. Here, the main reason for the different metal transfer behaviors in the plasma MIG welding is due to the use of the plasma current in the system.

The presence of the plasma surrounding the wire increases the electron density in its vicinity, resulting in the arc attachment to expand upwards along the wire surface to disperse the MIG current. This dispersion of MIG current causes a decrease in current density on the droplet surface, lowering the droplet temperature. This MIG current dispersion forms the gradual taper above the neck of the wire due to the dispersed heat input caused by the electron condensation of the MIG current.

Furthermore, the dispersed MIG current also weakens the electromagnetic pinch force acting on the neck of the wire above the droplet. This leads to a larger droplet diameter with increased surface area through lower frequency of droplet detachment to decrease the MIG current density on the droplet surface, as compared to the conventional MIG welding at the same MIG current. Thus, the lower droplet temperature is caused by the reduction of heat flux into the droplet.

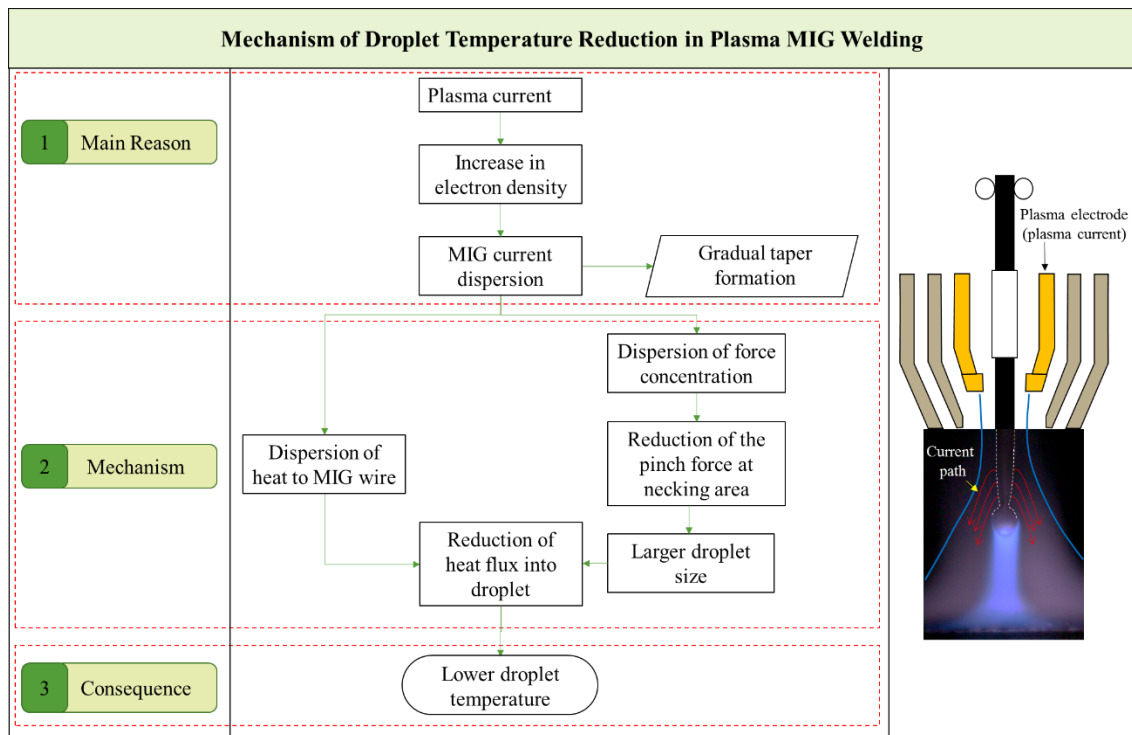


Fig. 3.34 Flow chart on the mechanism of droplet temperature reduction in plasma MIG welding

3.7 Conclusion

In this study, the mechanism to control droplet temperature in the plasma MIG welding was discussed based on the measurements of the droplet temperature for a wide range of MIG currents with different plasma electrode sizes. The measurements of the droplet temperatures were conducted using a two color temperature measurement method. The droplet temperatures in the plasma MIG welding were then compared with that of the conventional MIG welding. The following conclusions can be drawn from the results obtained:

1. The wire melting rate in the plasma MIG welding is higher than that in the conventional MIG welding except for higher WFS range.
2. The droplet temperature in the plasma MIG welding was reduced in comparison with the conventional MIG welding under the same MIG current. Especially, when the small PED was used, the decrease in the droplet temperature reached maximally 500 K.
3. Also for a particular WFS, the droplet temperatures in the conventional MIG welding were lower than those in the conventional MIG welding. It is suggested that the use of plasma contributes to reduce the local heat input into the base metal by the droplet.
4. The presence of the plasma surrounding the wire increases the electron density in its vicinity, resulting in the arc attachment to expand upwards along the wire surface to disperse the MIG current. This dispersion of MIG current causes a decrease in current density on the droplet surface, lowering the droplet temperature.
5. The dispersed MIG current also weakens the electromagnetic pinch force acting on the neck of the wire above the droplet. This leads to a larger droplet diameter with increased surface area through lower frequency of droplet detachment to decrease the MIG current density on the droplet surface, as compared to the conventional MIG welding at the same MIG current. Thus, the lower droplet temperature is caused by the reduction of heat flux into the droplet.
6. The use of smaller diameter of plasma electrode diverges more MIG current and results in the lower droplet temperature.
7. The mechanism to control droplet temperature in the plasma MIG welding was clarified.

Chapter 4

Mechanism in reducing the droplet temperature in pulse plasma MIG welding process

4.1 Introduction

Based on the results of the experimental measurement in DCEP and observation in previous chapter, the presence of plasma surrounding the MIG wire was found to be the main reason to cause the droplet temperature reduction. The presence of plasma flow promotes the divergence of MIG current at a higher position of MIG wire. This phenomenon causes the dispersion of the heat input and electromagnetic force onto the MIG wire surface towards contact tip. The dispersion of the heat input to the MIG wire significantly reduces the total heat input into droplet, which eventually reduces its temperature. Moreover, the dispersion of the electromagnetic force reduces the pinch force acting to the neck area, therefore to result in the larger droplet diameter. The larger droplet decreases the current density on the droplet surface, thus eventually to reduce the droplet temperature as well.

Therefore, in this chapter, by applying the above finding and the concept of the droplet temperature reduction mechanism during DCEP, the significance of the mechanism in pulse plasma MIG welding process is studied. Here, it is aimed to clarify the droplet temperature by using two color temperature measurement methods and then the metal transfer phenomena in pulse plasma MIG welding is also observed to validate the mechanism through the similarity of the phenomena. The result from this study will be a bridge in relating the relevancy of the system to be applied in aluminum welding.

The outline of this chapter is that the introduction is described in section 4.1, the materials and welding method is described in section 4.2. The experimental results are discussed in section 4.3, while the discussion in section 4.4. section 4.5 concludes the findings of this study.

4.2 Materials and welding conditions

A mild steel filler wire (YGW12) with a diameter of 1.2 mm is chosen to be welded onto a mild steel plate (SS400) with wire feeding speed (WFS) at 880 cm/min for pulse MIG welding and 1000 cm/min for pulse plasma MIG welding (corresponding to MIG current of 200 A). The peak current, base current and peak time are set at 500 A, 50 A and 0.8 ms, respectively. This pulse setting is effective for both pulse MIG and pulse plasma MIG welding. Welding speed (WS) of 50 cm/min is achieved by using an actuator to move the base metal plate at a constant speed. The contact tip to work distance (CTWD) is set at 30 mm, and MIG voltage is set within the range from 25 to 35 V to ensure a constant arc length of approximately 10 mm. Argon gas is introduced into the three layers at flow rates of 5 L/min (center gas), 10 L/min (plasma gas) and 10 L/min (shielding gas) individually from three gas cylinders. The plasma current supplied through the plasma electrode is ranging from 25 to 100 A. The pulse MIG welding is realized by setting plasma current of 0. Two different plasma electrode diameters (PEDs) of 3 mm and 7 mm are used in these experiments to evaluate the influence of the PED on the droplet temperature.

The details of the welding conditions for all cases are summarized in **Table 4.1**.

Table 4.1 Details of welding conditions

1. Machine Setting	i. Polarity	Pulse DCEP
	ii. Plasma Current	Pulse MIG: 0 A Pulse plasma MIG: 100 A
	iii. Plasma Electrode Diameter (PED)	Pulse MIG: $\phi 7$ mm Pulse plasma MIG: $\phi 7$ mm, $\phi 3$ mm
	iv. Wire Feeding Speed (WFS)	Pulse MIG: 880 cm/min Pulse plasma MIG: 1000 cm/min
	v. MIG Current	200 A
	vi. MIG Voltage	25 – 35 V (to remain the same arc length)
	vii. Welding Speed (WS)	60 cm/min
	viii. Contact Tip to Work Distance (CTWD)	30 mm
	ix. Wire Stick Out Length	20 mm (approximately)
	x. Argon Gas Flow	Center Gas: 5 liter per minute Plasma Gas: 10 liter per minute Shielding Gas: 10 liter per minute
2. Camera Setting	i. Temperature measurement Method for Droplet	Two color temperature measurement method (2000 fps)
	ii. Metal Transfer Observation	a. Shadowgraph (2000 fps) b. Color observation (2000 fps)
3. Materials	i. Base Metal	Mild Steel
	ii. Filler Wire	JIS YGW $\phi 1.2$ mm

4.3 Experimental results

4.3.1 Droplet temperature measurement

Fig. 4.1 shows a dependence of the droplet temperature to the plasma current at MIG current of 200 A in pulse plasma MIG welding with difference size of PED. The black color refers to the droplet temperature in pulse plasma MIG welding with PED of 7 mm and blue color refers to the droplet temperature in pulse plasma MIG welding with PED of 3 mm. The green color refers to the droplet temperature in pulse MIG welding. The droplet temperature in pulse plasma MIG welding with PED of 7 mm was measured to be higher than the one in pulse plasma MIG welding with PED of 3 mm. At 25 A of plasma current, the droplet temperature in pulse plasma MIG welding with PED of 7 mm was 2356 K and that with PED of 3 mm was 2227 K. The droplet temperature in both pulse plasma MIG welding with PED of 7 mm and 3 mm shows the almost constant temperature against the plasma current above 25 A. The difference of the droplet temperature was maintained almost the similar value of about 110 K to 130 K independent of plasma current above 25 A.

However, the droplet temperature in the case of the pulse MIG welding was observed to be higher than the others. The droplet temperature was measured at 2433 K. The difference in droplet temperature simply showed that the use of pulse plasma MIG welding is also able to reduce the droplet temperature. The smaller PED gives more drops in droplet temperature.

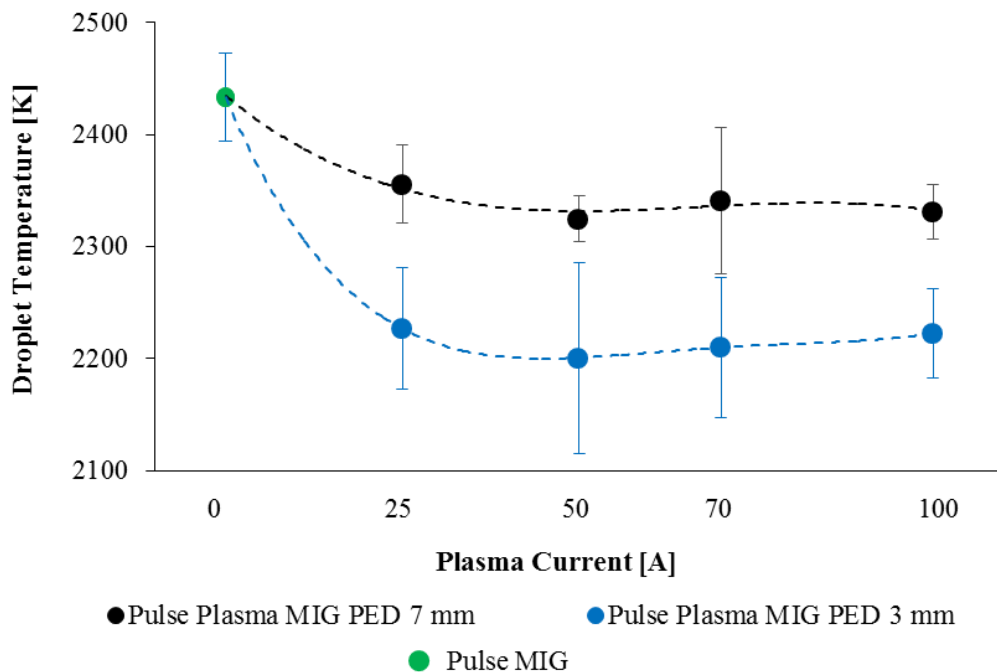


Fig. 4.1 Dependence of droplet temperature to the plasma current at MIG current of 200 A in pulse plasma MIG welding with difference PED (plasma current of 0 refers to pulse MIG welding)

4.3.2 Measurement of droplet diameter

Fig. 4.2 shows the dependence of droplet temperature to the plasma current at MIG current of 200 A in pulse plasma MIG welding with different PED. As being mentioned above, the black color refers to the droplet temperature in pulse plasma MIG welding with PED of 7 mm and blue color refers to the droplet temperature in pulse plasma MIG welding with PED of 3 mm. The green color refers to the droplet temperature in pulse MIG welding. The measurement of this droplet diameter was done concurrently with the droplet temperature measurement. The graph showed that the average value of droplet diameter in pulse plasma MIG welding tended to have larger droplet diameter compared with the one in pulse MIG welding. In other words, the transfer type in pulse plasma MIG welding seems to be different, in which the transfer type in pulse plasma MIG welding tended to be globular but that in pulse MIG welding was almost spray.

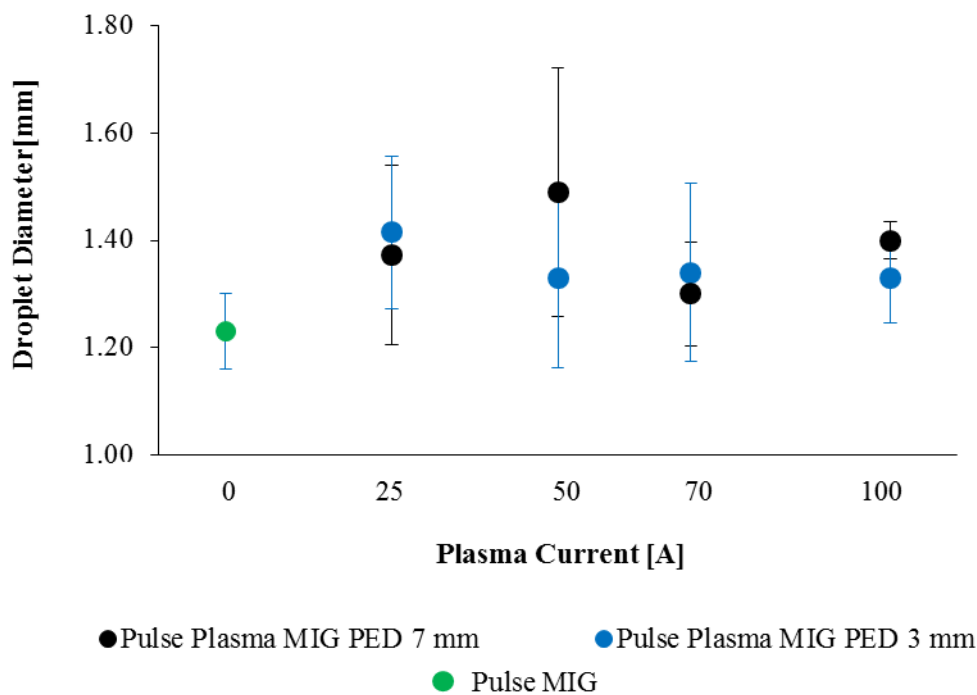


Fig. 4.2 Dependence of droplet temperature to the plasma current at MIG current of 200 A in pulse plasma MIG welding with different PED (plasma current of 0 refers to pulse MIG welding)

4.3.3 Metal transfer observation

From the above results, it was clear that the increase of plasma current has not given any significant change in the droplet temperature in pulse plasma MIG welding. However, by eliminating the plasma flow in surrounding of the MIG wire, the droplet temperature increased dramatically. Therefore, to scrutinize the change of arc phenomenon that might appear during metal transfer and thus influences the droplet temperature, the high speed video camera is used to visualize the metal transfer. To simplify the comparison, the plasma current of 0 in pulse MIG welding and that of 100 A in pulse plasma MIG welding with PED of 3 mm are studied.

Fig. 4.3 shows the cycle of metal transfer in pulse MIG welding process at MIG current of 200 A. **Fig. 4.4** shows MIG current and voltage wave forms. The arc attachment can be seen clearly at MIG wire above the droplet during peak current (c – e). The MIG arc covered the whole of the droplet and during this time, the metal vapor increased markedly. The neck point was observed at the area when the peak current started to decrease (f). The formation of this neck point is thought to be caused by the high concentration of heat and force associated with the position of arc attachment at the area. The droplet detached during the base current period at (l). There was a slight increase in voltage during the droplet detachment as shown by red arrow in **Fig. 4.4**. Relatively smooth metal transfer without spatter formation was seen during the process.

Fig. 4.5 shows the cycle of metal transfer of pulse plasma MIG with PED of 3 mm welding process at 200 A. **Fig. 4.6** shows MIG current and voltage wave forms. The plasma current was supplied at 100 A. The effect of the taper formation at the MIG wire above the wire tip from the earlier cycle could be seen clearly at the early stage of pulse cycle (a-b) when the MIG current started to increase. At the peak current (c-e), compared with during zero plasma current, the presence of plasma flow promotes the arc attachment to expand towards the contact tip. The MIG arc covered only half of the droplet and the metal vapor region in arc axis was slightly smaller compared with that in zero plasma current. The formation of gradual taper was enhanced even though the MIG current started to decrease. The droplet detached during the base current period at (l) with a long taper formation. With regards to the voltage fluctuation during droplet detachment, in pulse plasma MIG welding, as shown in **Fig. 4.6**, there was no change in voltage when the droplet detached suggests the very smooth metal transfer.

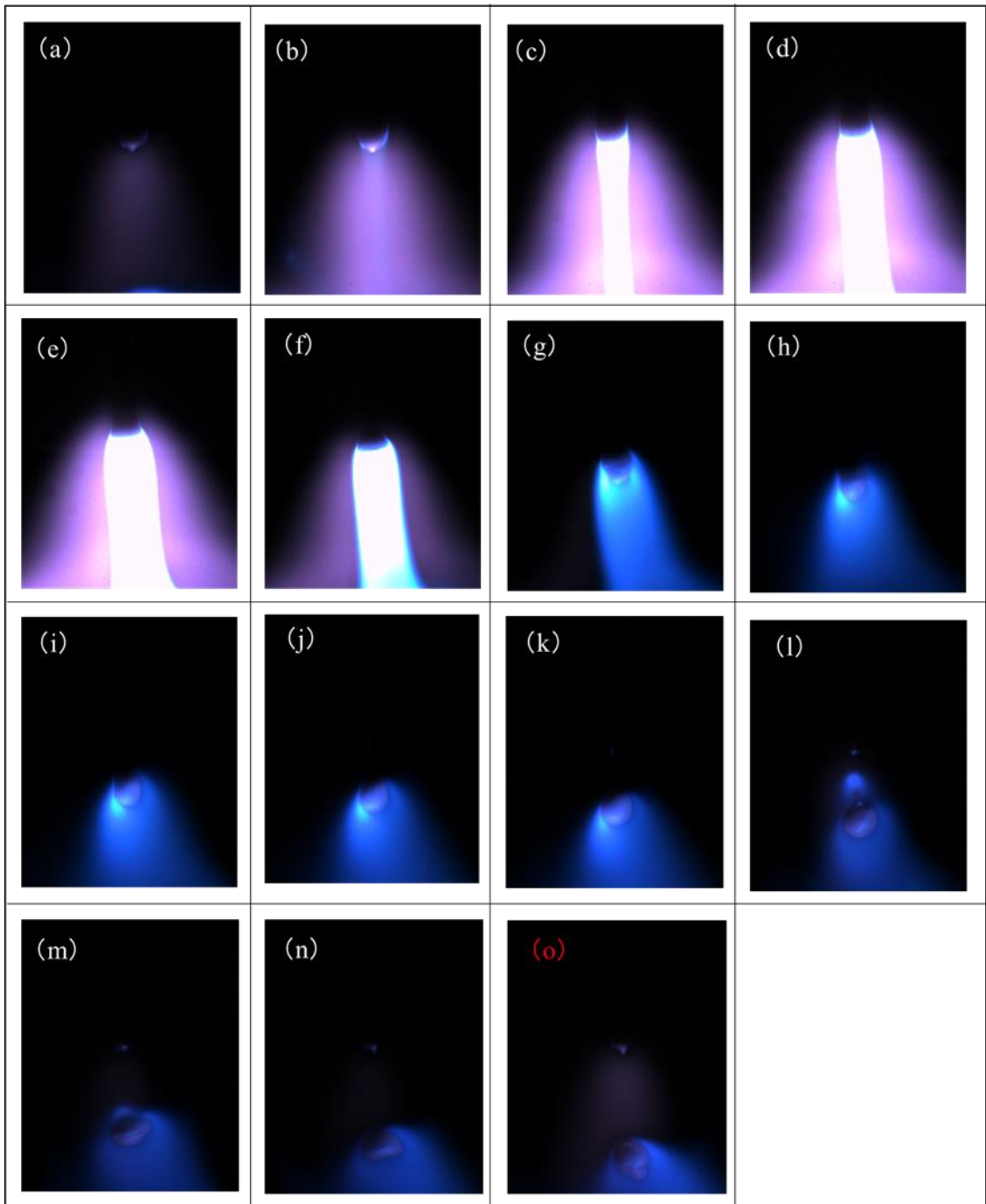


Fig. 4.3 One cycle of metal transfer of pulse MIG welding process at MIG current of 200 A (plasma current of 0)

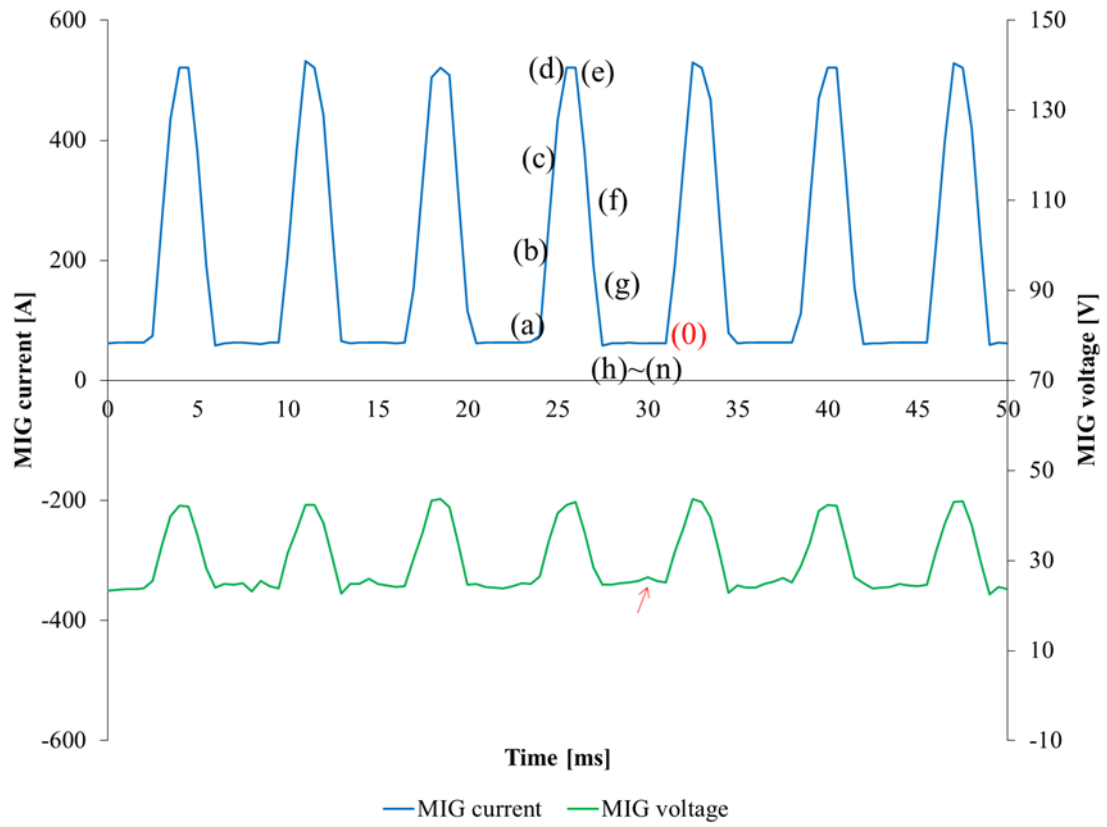


Fig. 4.4 Waveform of a cycle of metal transfer in pulse MIG welding. The alphabet of (a) to (o) refers to each (a) to (o) in **Fig. 4.3**

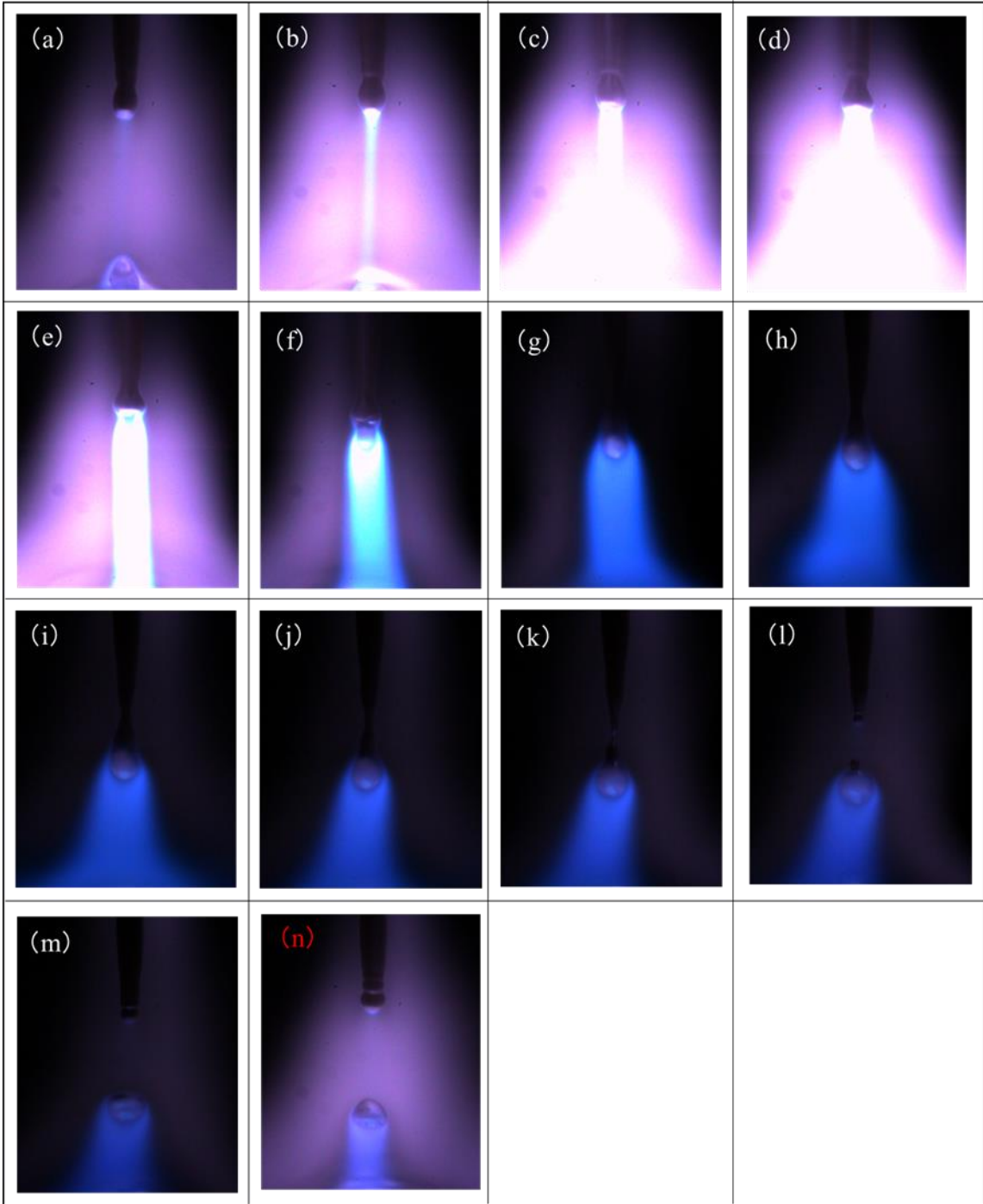


Fig. 4.5 One cycle of metal transfer of pulse plasma MIG welding process at MIG current of 200 A (plasma current set at 100 A)

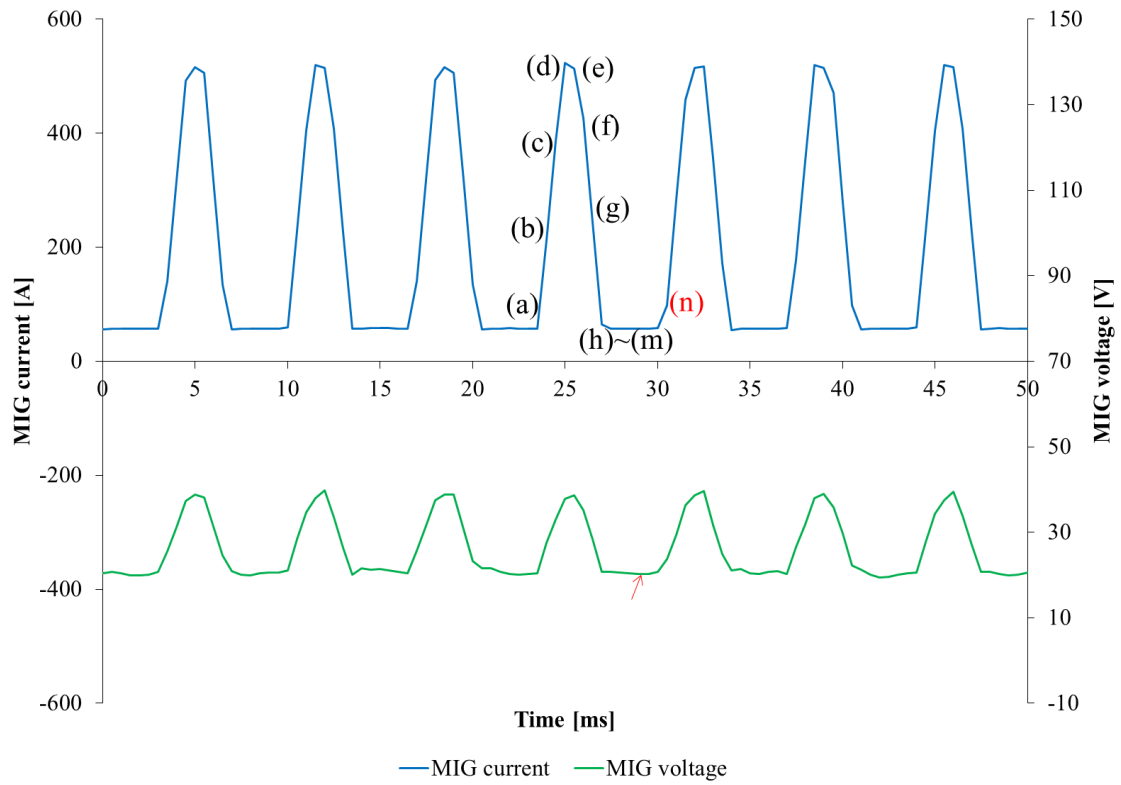


Fig. 4.6 Waveform of a cycle of metal transfer in pulse plasma MIG welding (plasma current set at 100 A). The alphabet of (a) to (n) refers to each (a) to (o) in Fig. 4.5

4.3.4 Taper formation and metal vapor during base current

Fig. 4.7 shows an arc behavior during peak current and prior to the detachment in pulse MIG welding (zero pulse current) and pulse plasma MIG welding (pulse current 100 A). The taper formation behavior in pulse MIG and pulse plasma MIG welding under the effect of an arc was compared by using this figure. The comparison was done during peak current and prior droplet detachment. In pulse MIG welding, it was a small deformation of the MIG wire at the area covered by arc, where the arc attachment can be observed. The MIG wire that was being covered by the arc melted and formed a taper. The constricted area was observed beyond this area and became minimal at neck point. This minimal condition occurred at the moment of prior droplet detachment.

Meanwhile, in pulse plasma MIG welding, the effect of the taper formation from the earlier cycle can be observed during peak current. The MIG wire was slightly deformed at the moment of the peak current, and the readily melted MIG wire at wire tip formed an area as like a neck point due to the effect of arc pressure that worked upward. The presence of plasma flow clearly caused the arc attachment to move upward. The surface of MIG wire was partially melted and moved downward to form a droplet. The formation of gradual taper at the same time created a constriction area in MIG wire and became minimal at the neck point.

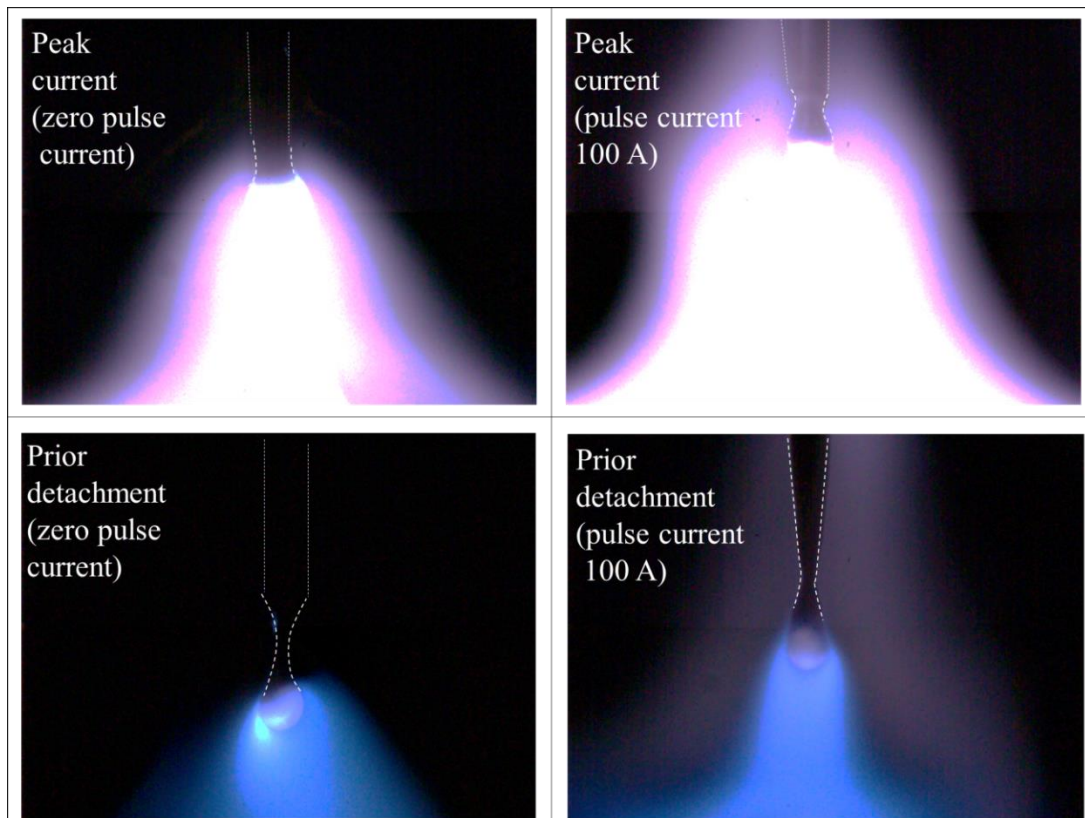


Fig. 4.7 Arc behavior during peak current and prior to the detachment in pulse MIG welding (pulse current of 0) and pulse plasma MIG welding (pulse current 100 A)

4.4 Discussion

Pulse system is an excellence system to enhance the metal transfer stability. Compared with conventional MIG welding mentioned in chapter 3, the use of pulse MIG welding increases the metal transfer stability and capable to reduce the spatter formation. In chapter 3, we compare the conventional MIG welding and plasma MIG welding and found that the use of plasma MIG welding by its plasma flow effect is able to reduce the droplet temperature besides effective to reduce the spatter formation. In order to benefit the plasma MIG welding system to join the thin materials that necessity of low heat input, in this chapter we try to investigate the effect of plasma flow in pulse plasma MIG welding and compare with that zero plasma flow in pulse MIG welding. The metal transfer observation shows the same phenomena as occurred in plasma MIG welding, such as the taper formation has occurred in pulse plasma MIG welding, confirmed that the works of plasma flow in the plasma MIG welding system. Here, the discussion will be focused on the mechanism in reducing the droplet temperature due to the effect of plasma flow in pulse plasma MIG welding.

4.4.1 Effect of plasma flow to the droplet temperature reduction in pulse plasma MIG welding

Main difference between the pulse plasma MIG welding and pulse plasma MIG welding is the presence of plasma flow in surrounding of the MIG wire at all time during welding. The presence of this plasma flow has promoted the MIG current to move out from the high temperature with high electrical resistivity of MIG wire during peak current, thus expand the distribution of electrical conductivity at the wire tip to diffuse at a wider area of the MIG wire. Since the arc attachment at the MIG wire determines by the distribution of electrical conductivity[39], expansion of electrical conductivity's distribution also influences an arc attachment to climb upwards.

This phenomenon is illustrated in **Fig. 4.8**, in which the arc attachment in pulse plasma MIG welding is diffused to a higher position of MIG wire, whereas in pulse MIG welding, the arc attachment concentrated at the flank of the wire electrode. Plasma flow in surrounding of the MIG wire establishes the current path out from the MIG wire and by-passing the droplet, thus reduces the fraction of the total heat flux into the droplet. This mechanism suggests the reduction droplet temperature in plasma MIG welding system. Apart from that, this behavior also causes the dispersion in the electromagnetic force as well as the heat towards the solid wire. The dispersions lead to the multiple effects such as taper formation, higher wire melting rate and larger droplet size.

However, since the peak time is only 0.8 ms before the MIG current starts to decrease to base current, the droplet heating time occurs only in a short time. With this pulse system that limits the heat flux into the droplet results in lower heat content in the droplet. Therefore, the low droplet temperature in pulse plasma MIG welding is caused by the short heating time besides the dispersion of heat that reduce the heat flux into the droplet as an effect of the plasma flow. In addition, as shown in **Fig. 4.7** as well as illustration in **Fig.4.9**, the metal vapor in both welding processes still could be

observed at beneath of the droplet prior the droplet detachment. The evaporation of vapor at wire tip emitted the radiation and significantly cooled the temperature [55].

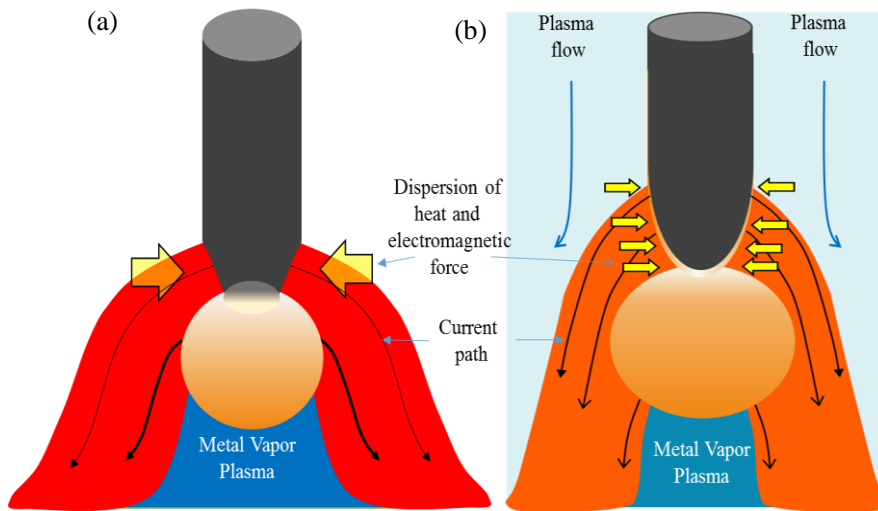


Fig. 4.8 Illustration of the difference in dispersion of heat and electromagnetic force in (a) pulse MIG and, (b) pulse plasma MIG welding, during peak current period

Also, during the base current period, the low MIG current transported through the constricted area thus reduce the current density especially at the neck point. Therefore, the small concentration of electromagnetic force acts at the neck point results in the stable and spatter free metal transfer [52]. As shown in **Fig. 4.9**, the presence of plasma flow during this period enhances the stability of the metal transfer by equal distribution of electromagnetic force in surrounding of the neck point. Therefore, the possibility of the occurrence of an arc disturbance after the droplet detachment can be avoided.

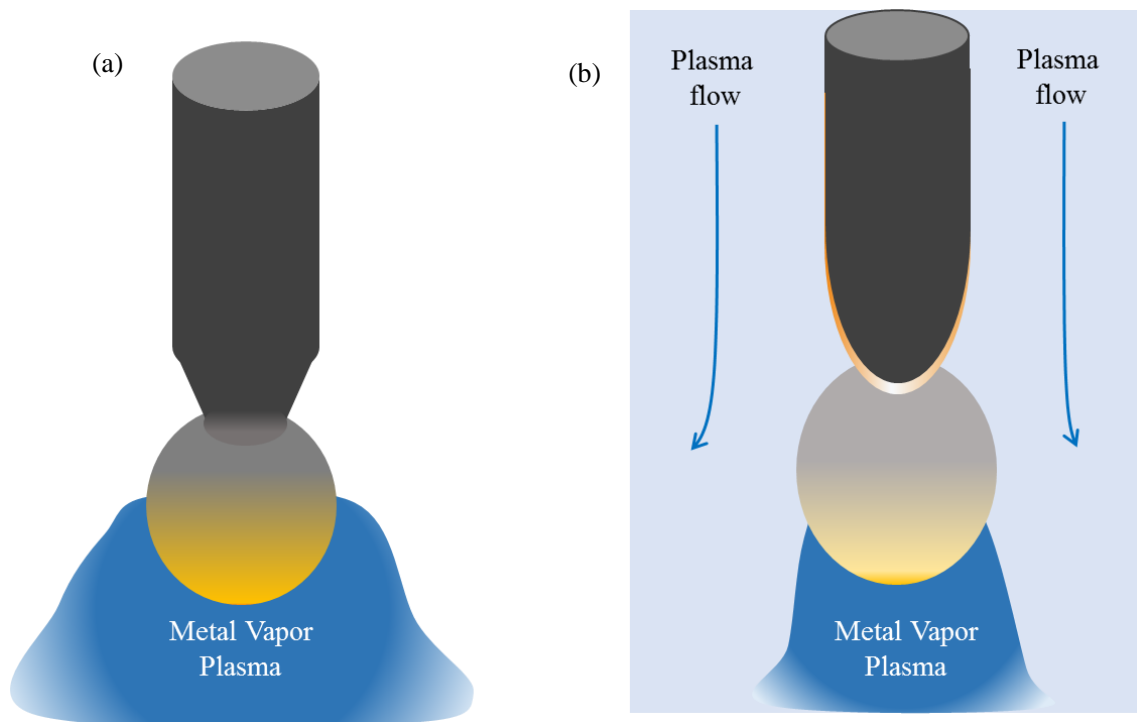


Fig. 4.9 Illustration of metal vapor formation in (a) pulse MIG welding and (b) pulse plasma MIG welding during base current period

4.4.2 Mechanism of droplet temperature reduction in pulse plasma MIG welding

The use of plasma MIG welding system is able to reduce the droplet temperature by reducing the heat flux into droplet through dispersion of heat as well as the electromagnetic force to the MIG wire. The introduction of plasma flow in surrounding of the MIG wire causes these dispersions to occur. Here, by combining the plasma MIG welding system with the pulse welding system experimentally results in reducing the droplet temperature to a hundred Kelvin lower than that when the plasma MIG welding done alone. Through the metal transfer observation, the same phenomena when the plasma MIG welding is used occurred in pulse plasma MIG welding validates the effect of the plasma flow to the system. In addition, the pulse system that reduces the MIG current during base current period limits the heat flux into droplets, indeed cooled the droplet through radiation and convection. Therefore, it is suggested that the use of plasma MIG welding system with the combination of pulse system capable to further reduce the droplet temperature rather than the pulse MIG welding as well as the plasma MIG welding system alone.

4.5 Conclusion

In this chapter, the comparison of the droplet temperature in pulse MIG welding and pulse plasma MIG welding was done. The measurements of the droplet temperatures were conducted using a two color temperature measurement method. The metal transfer phenomena in both welding processes were observed by using color observation method. The following conclusions can be drawn from the results obtained :

1. The use of pulse plasma MIG welding reduces the droplet temperature compared with the one in pulse MIG welding approximately 200 A.
2. The use of pulse system enables the stable metal transfer in both welding process. However, the effect of plasma flow in pulse plasma MIG welding enhances the droplet detachment process by minimizing the arc disturbance at the wire tip.
3. It is suggested that the droplet temperature reduction in pulse plasma MIG welding is dominated by 3 main factors, namely the reduction of heat flux into the droplet through the dispersion of heat and force as an effect of plasma flow surrounding the MIG wire, the limitation of heat flux during base current in pulse system, and the cooling effect during base current.

Chapter 5

The application of pulse plasma MIG welding process to control the IMC thickness in Al/Steel dissimilar joining

5.1 Introduction

It is mentioned that the control of the formation of IMC is a great challenge in joining the aluminum and steel. The use of fusion welding giving high heat input suffers a formation of thick IMC and affecting the joint quality. Here, the necessity of developing a welding method which can reduce a heat input arises. In regards to this, based on the study in previous chapters, it is confirmed that the use of the plasma MIG welding is capable to reduce the droplet temperature by up to 500 K in comparison with conventional MIG welding (refer chapter 3), and that in the pulse plasma MIG welding is found to be approximately 200 K (refer chapter 4). It is suggested that the heat input control by controlling the droplet temperature through pulse plasma MIG welding can be applied in Al/Steel dissimilar welding.

Therefore, in this chapter, the pulse plasma MIG welding system is used to join the aluminum to steel and aims to clarify the relevancy of this method in controlling the IMC formation as well as its thickness at the joint interface.

This chapter is divided into 4 sections. The introduction is described in section 5.1. The materials and welding method is described in section 5.2. The experimental results are discussed in section 5.3, while the discussion in section 5.4. Section 5 concludes the findings of this study.

5.2 Materials and welding conditions

In this chapter, before starting the dissimilar welding between aluminum and steel, a preliminary experiment on aluminum welding is conducted to understand basic characteristics of the welding including the stability of metal transfer. The observation of metal transfer of aluminum droplet is also carried out by using camera observation method and shadowgraph method. The industrial pure aluminum sheet (A1050P) with the size of 300x50x15 mm is welded as bead on plate by using the Al-Si filler wire (A4047WY) with 1.2 mm in diameter. Argon is used in all three layers of gas with the total flowrate was 25 L/min. The detail of the welding parameter is shown in **Table 5.1**.

Following, the dissimilar welding between aluminum and steel is carried out. The plain carbon steel sheet (SPCC) and industrial pure aluminum sheet (A1050P) with the size of 300x100x2 mm and 300x50x2 mm are used. In the experiment, the aluminum sheet is lapped over a steel sheet as shown in **Fig. 5.1**. The surface of workpiece is wiped by using acetone in order to clean it from any contaminated dirt. The Al-Si filler wire, A4047WY with 1.2 mm in diameter is used during welding and the argon gas was used in all three layers, with the total flow rate was 25 L/min. The detail of the welding parameter is shown in **Table 5.2**.

In these experiments, the pulse plasma MIG welding system is used to conduct the welding. The details regarding to this system is explained in chapter 2.

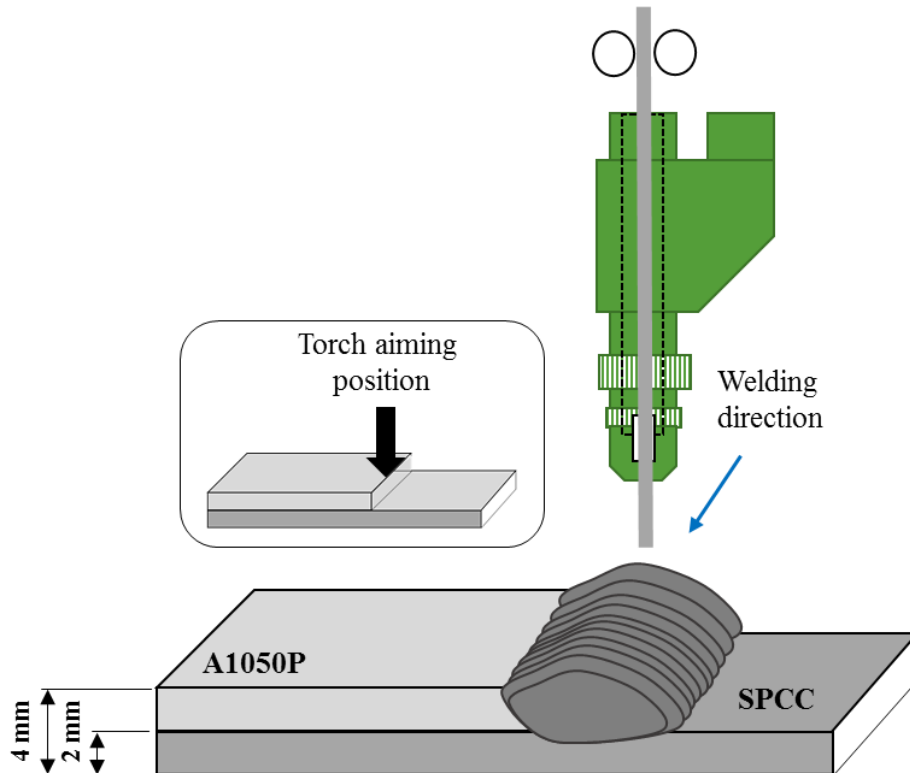


Fig. 5.1 Experiment set-up for dissimilar Al/Steel lapse joining

Table 5.1 Details of welding parameter for bead on plate welding

i.	Polarity	Pulse DCEP
ii.	Plasma current	Pulse MIG: 0 A Pulse plasma MIG: 25 A
iii.	Plasma Electrode Diameter (PED)	Pulse MIG: 7 mm Pulse plasma MIG: 3 mm
iv.	MIG current	100 A, 130 A, 160 A
v.	Wife Feeding Speed (WFS)	Pulse MIG: 80 – 130 cm/min Pulse plasma MIG: 150 – 250 cm/min
vi.	MIG voltage	8 – 25 V
vii.	Contact Tip to Work Distance (CTWD)	10 mm
viii.	Argon gas flow rate	Center gas: 5 litre per min Plasma gas: 10 litre per min Shielding gas: 10 litre per min
ix.	Materials	Base metal: A1050P (300x50x15 mm) Filler wire: A4047WY (Dia.1.2 mm)

Table 5.2 Details of welding parameter for dissimilar welding

i.	Polarity	Pulse DCEP
ii.	Plasma current	Pulse MIG: 0 A Pulse plasma MIG: 25 A
iii.	Plasma Electrode Diameter (PED)	Pulse MIG : 7 mm Pulse plasma MIG: 3 mm
iv.	MIG current	70 A to 190 A
v.	Wife Feeding Speed (WFS)	80 – 200 cm/min
vi.	MIG voltage	8 – 25 V
vii.	Contact Tip to Work Distance (CTWD)	10 mm
viii.	Argon gas flow rate	Center gas: 5 liter per min Plasma gas: 10 liter per min Shielding gas: 10 liter per min
ix.	Materials	Base metal : A1050P (300x50x2 mm) Base metal : SPCC (300x100x2 mm) Filler wire : A4047WY (Dia.1.2 mm)

5.3 Experimental Results

5.3.1 Observation of metal transfer behavior in aluminum pulse plasma MIG welding

As being concluded in chapter 3 and 4, the factors that affect the reduction of droplet temperature in plasma MIG welding are the decrease of heat content in droplet due to the dispersion of heat to the MIG wire as well as the decrease in current density in the droplet due to the increase in the droplet diameter. Meanwhile, the gradual taper formation before the droplet detachment contributes to the smooth metal transfer. The smooth metal transfer includes the detachment of small deviation of droplet diameter and the stable impingement position.

In chapter 4, it is confirmed that the use of pulse DCEP system capable to reduce the droplet temperature in pulse plasma MIG welding for another hundreds Kelvin. The phenomena that associated with the reduction of the droplet temperature were observed to be similar to the one in DCEN system. Since the property of the aluminum wire is different compared with the mild steel wire and there is a possibility of aluminum welding to show the different behavior. Therefore, to ensure the occurrence of the same phenomena in aluminum pulse plasma MIG welding, the observations of the metal transfer in aluminum pulse plasma MIG welding were conducted and the results are shown in **Fig. 5.2** and **Fig. 5.3**. **Fig. 5.2** shows the WFS as a function of MIG current and **Fig. 5.3** shows the droplet diameter as a function of MIG current. The blue line refers to the droplet in pulse plasma MIG welding and the red line refers to the one in pulse MIG welding. Since the experiment was done under the same MIG current, the higher value of WFS and the larger droplet diameter in pulse plasma MIG welding simply showed that the melting rate in pulse plasma MIG welding was higher than the pulse MIG welding. It is considered that the divergence of MIG current which causes the dispersion of heat and electromagnetic force to a higher position of aluminum MIG wire attributes to this behavior. The dispersion of the heat is able to avoid the fluctuation of the heat at wire tip, thus the arc disturbance at the wire tip can be prevented. The dispersion of heat also results in the decrement of heat content in the droplet which in turn leads to the reduction of the droplet temperature. Meanwhile, the dispersion of electromagnetic force leads to a formation of larger droplet temperature, which eventually contributes to the reduction of the droplet temperature.

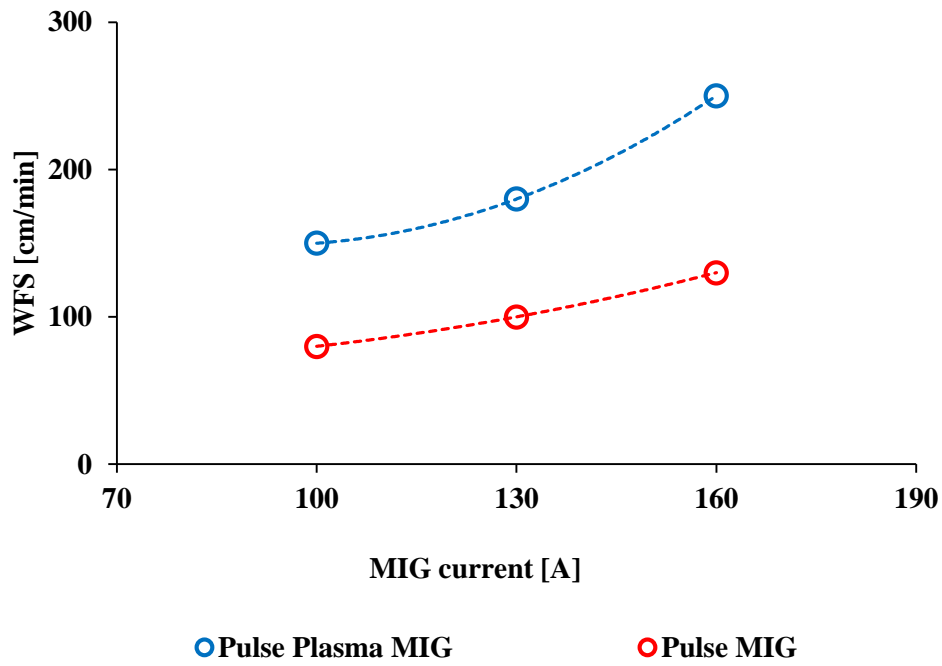


Fig. 5.2 Dependence of WFS to MIG current in pulse plasma MIG and pulse MIG welding

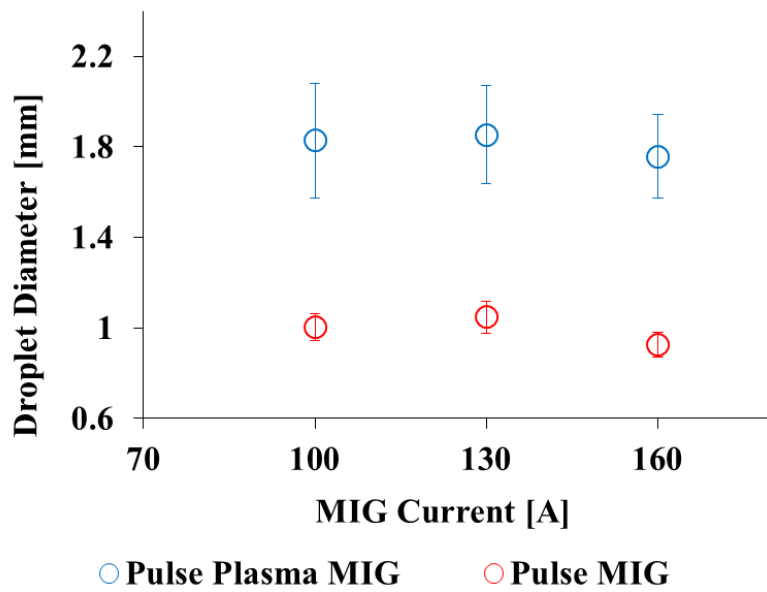


Fig. 5.3 Droplet diameter in pulse plasma MIG and pulse MIG welding

Fig. 5.4 shows the droplet impingement to base metal in pulse plasma MIG and pulse MIG welding and **Fig. 5.5** shows the analysis of drop position of the droplet during impingement process. The drop position refers to the distance of the droplet fall position from an arc axis. The blue line mentions the droplet in pulse plasma MIG and the red one in pulse MIG welding. The graph shows that the deviation of drop position in pulse plasma MIG welding is from 0.2 to the left and 0.8 to the right of the arc axis. Meanwhile, the drop position of pulse MIG welding deviates from 1.1 to the left and 1.4 to the right of the arc axis. The small deviation range of drop position confirms the stability of the droplet detachment process in pulse plasma MIG welding. This behavior can be explained by the dispersion of the electromagnetic force to the higher position of aluminum MIG wire. This dispersion causes the less magnetic pinch force acted in inward direction at necking area, thus enhance the smoothness of the droplet detachment. The smooth detachment then contributes to the small deviation of the drop position during impingement on base metal.

From these preliminary experiment's results, since the same behavior of metal transfer can be observed in aluminum welding, we consider that the use of pulse plasma MIG welding in aluminum welding also capable to reduce the aluminum droplet temperature. Also, the stable droplet impingement position can stabilize the heat input distribution into base metal.

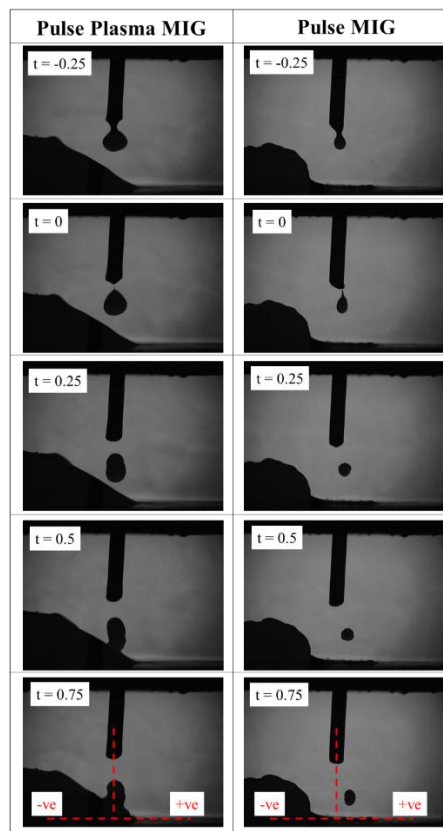


Fig. 5.4 Droplet impingement to base metal in pulse plasma MIG and pulse MIG welding

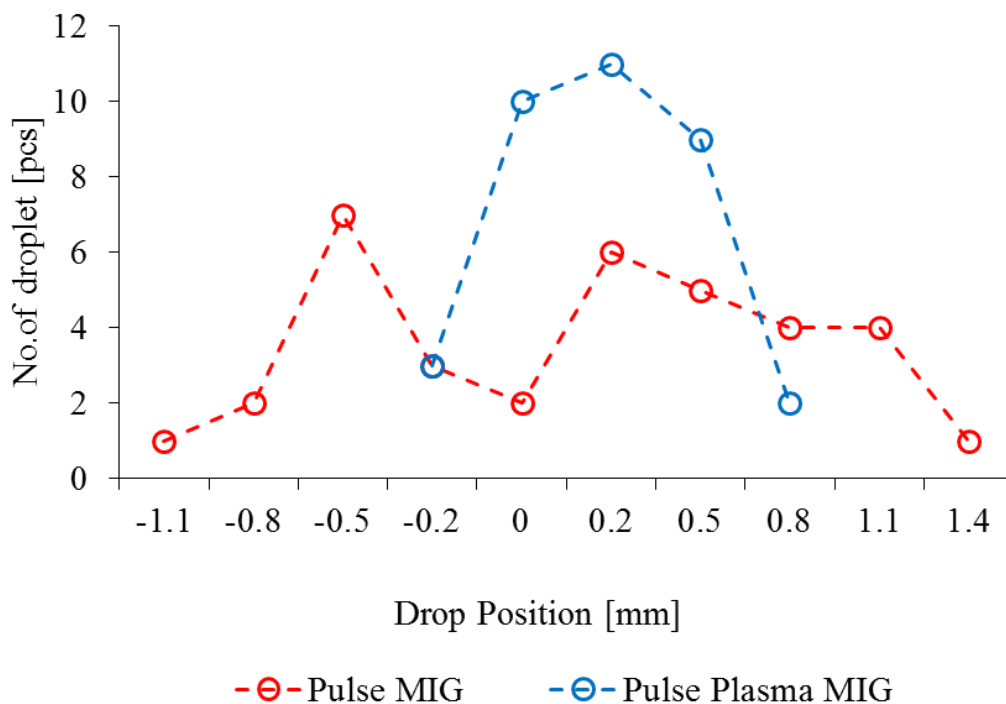
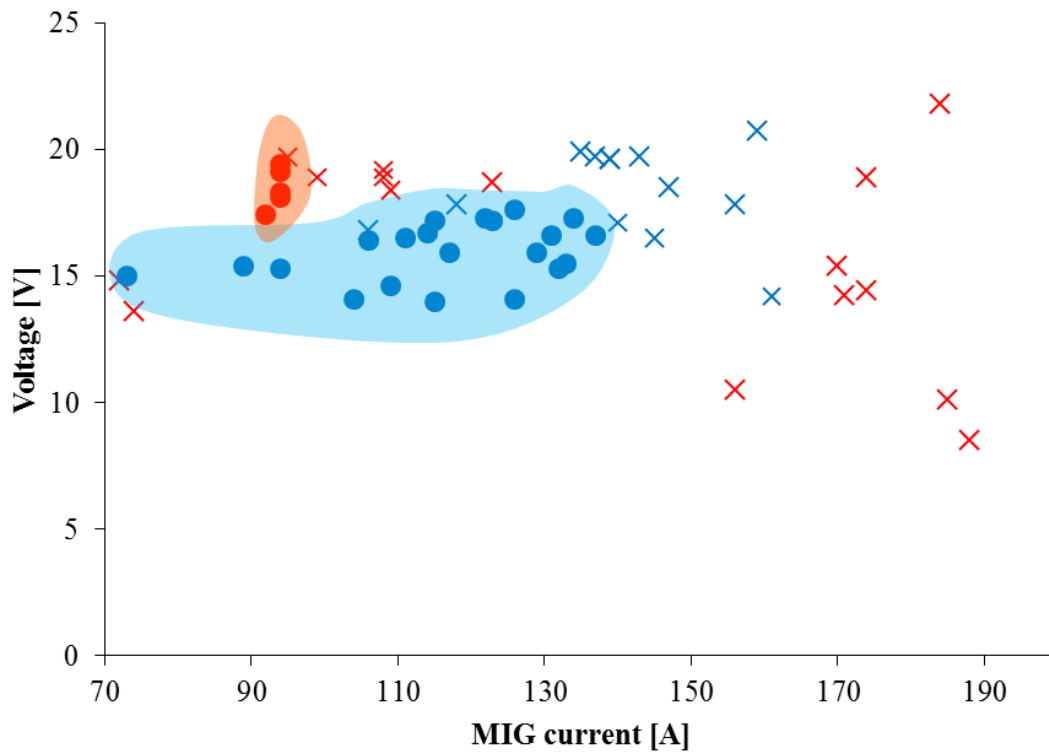


Fig. 5.5 Analysis of drop position of the droplet during impingement process

5.3.2 Study on the weldability of Al/Steel dissimilar welding

Fig. 5.6 shows the weldability of both processes ranging from 70 A to 190 A. The consideration was done visually based on the bead formation and its profile. The good weld condition refers to a proper weld bead forms between aluminum plate and steel plate, meanwhile bad weld condition refers to the improper weld bead formation or the presence of the welding defect as shown in **Fig. 5.7**. In this graph, blue color represents a pulse plasma MIG welding process and the red color represents a pulse plasma MIG welding process.

The graph clearly showed that the use of pulse plasma MIG welding process capable to join the aluminum and steel in a wide range of MIG current from 70 A to 160 A. Meanwhile, pulse MIG welding can only join the aluminum and steel plate in a small range of MIG current, from approximately 80 A to 110 A. During welding, the arc length of both processes was kept at almost same value, and from the observation, the optimum arc length for both processes were about 2 or 3 mm. If the arc length was too short, the short circuit occurred which led to unstable arc and eventually caused the arc stop. If the arc length was higher than 4 mm, the proper weld bead was hard to be formed and results in poor weld condition.



- Good weld condition (pulse MIG)
- Good weld condition (pulse plasma MIG)
- ✕ Poor weld condition (pulse MIG)
- ✕ Bad condition (pulse plasma MIG)

Fig. 5.6 Weldability of pulse plasma MIG and pulse MIG welding for the MIG current ranging from 70 A to 190 A

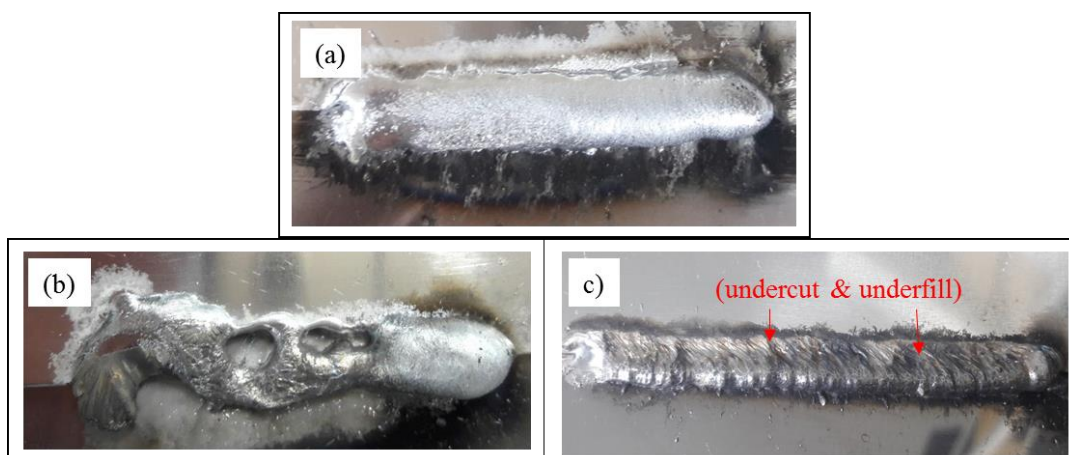


Fig. 5.7 (a) Example of good weld condition in pulse plasma MIG welding, (b) example of bad weld condition in pulse plasma MIG welding at the MIG current more than 140 A, and (c) example of bad weld condition in pulse MIG welding at MIG current less than 70 A

5.3.3 Formation of Intermetallic Compound (IMC)

In order to examine the intermetallic compound (IMC) in all good weld condition joints, the cross section of the joint have been prepared. However, almost all the joints that was prepared by using pulse MIG welding peeled off during cutting process, except only one joint that was prepared at 92 A (WFS 80 cm/min). While, only the joints welded below 140 A by using pulse plasma MIG welding were cut without peeling off. Therefore, the analysis below will only consider one joining prepared by pulse MIG welding at 92 A and six joining prepared by pulse plasma MIG welding at the MIG welding ranges from 70 A to 140 A.

5.3.3.1 Pulse MIG welding

Fig. 5.8 shows the bead appearance, cross section and bead height of the joint that welded by using pulse MIG welding process. Through visual inspection, straight bead profile without other visual defect is observed, however the whole bead surface is covered by weld smut. The smut also clearly can be seen beside the weld bead. The formation of the weld smut on the bead surface as well as beside the weld bead is thought to be related to the evaporation and oxidation of aluminum and magnesium during welding [56]. The bead height is measured to be 3.13 mm. The measurement of the bead height here is done from the top of the reinforcement until the surface of steel base metal.


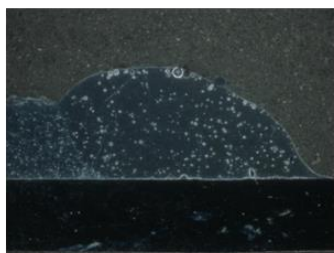
MIG Current	Bead Appearance	Cross Section	Bead Height
92 A			3.13 mm

Fig. 5.8 Bead appearance, cross section and bead height of the weld joint by using pulse MIG welding

5.3.3.2 Pulse plasma MIG welding

Fig. 5.9 shows the cross section and bead height of the joint that welded by using pulse plasma MIG welding process. Through visual inspection, the straight bead profile without any other visual defect is observed. The bright and shiny weld bead can be seen with a smut beside of the weld bead. Compared with the weld smut formation on the surface of the weld bead as a result of using the pulse MIG welding as shown in **Fig. 5.8** above, the absence of the weld smut whilst welding using pulse plasma MIG is thought to be caused by the cleaning effect by plasma current during MIG base current [57]. The cleaning effect prevents the formation of aluminum oxide and magnesium oxide on the relatively cool weld bead. Thus, the bright and shiny weld bead can be observed when the joining is done by using pulse plasma MIG welding. Meanwhile, the bead height shows a significant increment by the increase of the MIG current as shown in **Fig. 5.10**. This is because of the increase in MIG current increases a wire melting rate, thus more wire deposited into the weld metal [58].

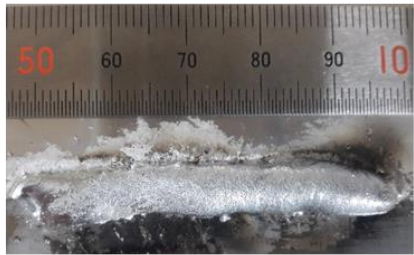
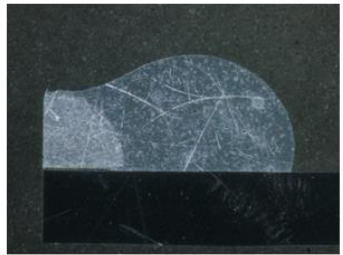
MIG Current	Bead Appearance	Cross Section	Bead Height
89 A			3.17 mm

Fig. 5.9 Bead appearance, cross section and bead height of the weld joint by using pulse plasma MIG welding at 89 A

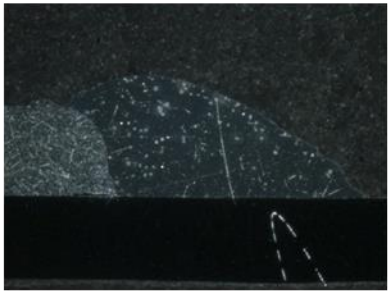
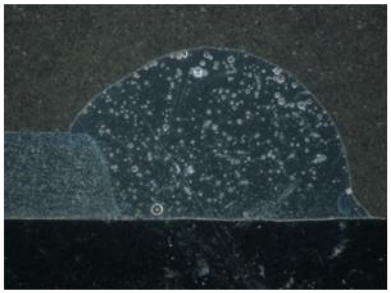
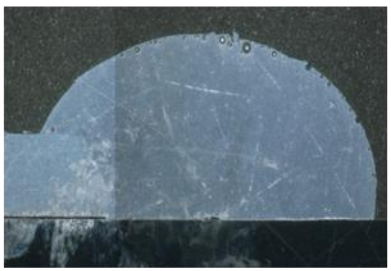
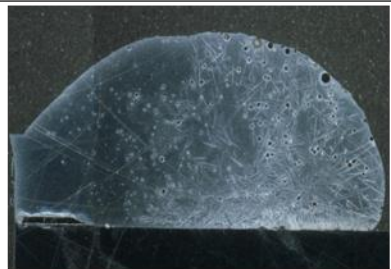
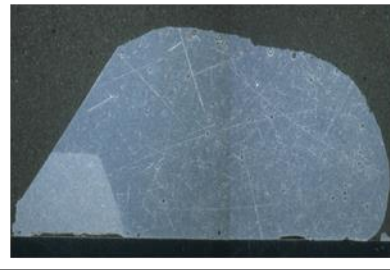
MIG Current	Cross Section	Bead Height
73 A		2.92 mm
104 A		4.2 mm
117 A		4.55 mm
131 A		4.81 mm
140 A		5.35 mm

Fig. 5.10 Cross section and bead height of the weld joint by using pulse plasma MIG welding

5.3.3.3 IMC thickness measurement

The results for the IMC thickness measurement in pulse MIG and pulse plasma MIG welding are shown in **Fig. 5.11**. The IMC thickness was measured randomly at 10 different points at Al/Steel interface. The graph shows the IMC thickness as a function of MIG current. The red dot refers to the IMC thickness in pulse MIG welding and the blue dots refer to that in pulse plasma MIG welding. Since there was a difficulty in getting the non-peel off cross section of the joint by pulse MIG welding, the IMC thickness measurement done to the only one specimen we got was recorded as $8.8 \mu\text{m}$.

Nevertheless, the IMC formation in the joint by pulse plasma MIG welding can be observed in a wider range of MIG current. The graph clearly showed that, the MIG current affects the IMC thickness, in which the higher the MIG current results in the thicker IMC. At low MIG current (70 A), the average of IMC thickness was measured as $4.7 \mu\text{m}$. By the increase of MIG current, the IMC thickness increases gradually until it reaches the highest average value at $14.9 \mu\text{m}$. It is very interesting to note that, the standard deviation of the IMC thickness of the joint at the MIG current below 100 A is very small which less than $1 \mu\text{m}$ compared with the one at the MIG current above 100 A. This value suggests that stable IMC thickness formed when the welding was conducted under the relatively low MIG current.

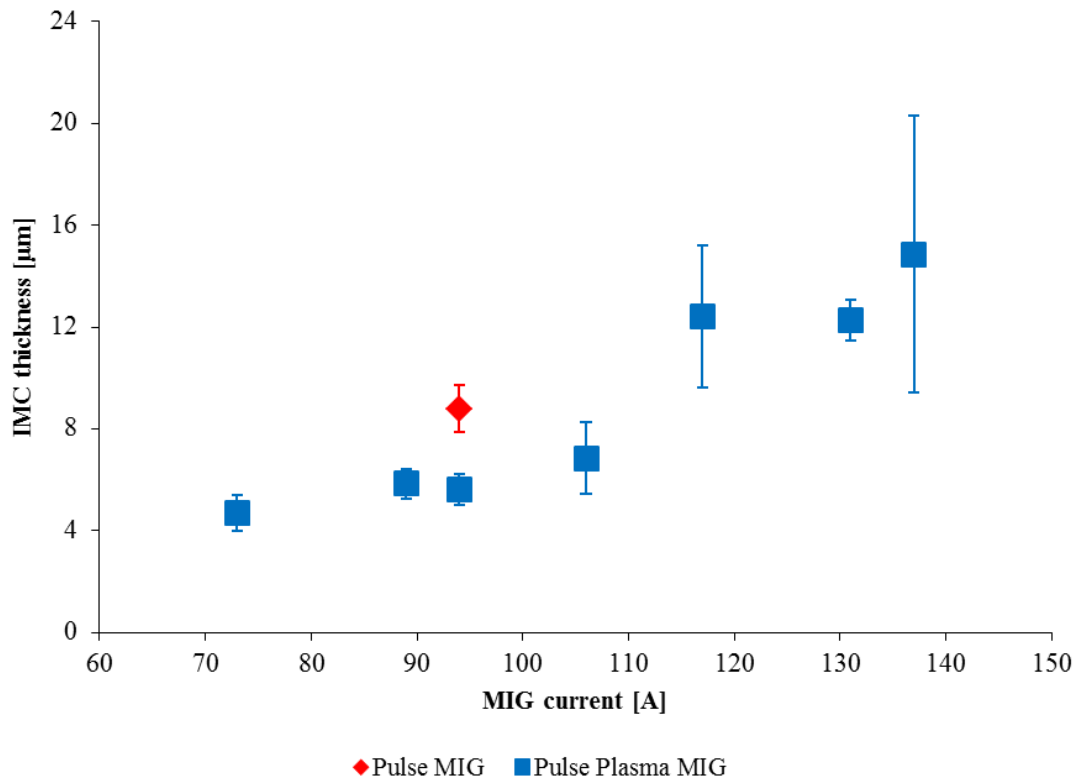


Fig. 5.11 IMC thickness measurement in pulse MIG and pulse plasma MIG welding at interface of Al/Steel

Fig. 5.12 shows the micrograph taken by microscopy at magnification of 500 times and the micrograph taken by SEM for the specimen welded by using pulse MIG welding. The micrograph taken by SEM clearly shows the formation of IMC layer at the boundary of Al/Steel. The plate like structure also can be seen formed at the aluminum weld metal. Meanwhile, the IMC layer also observed to exhibit an irregular shape as if it moving upwards.

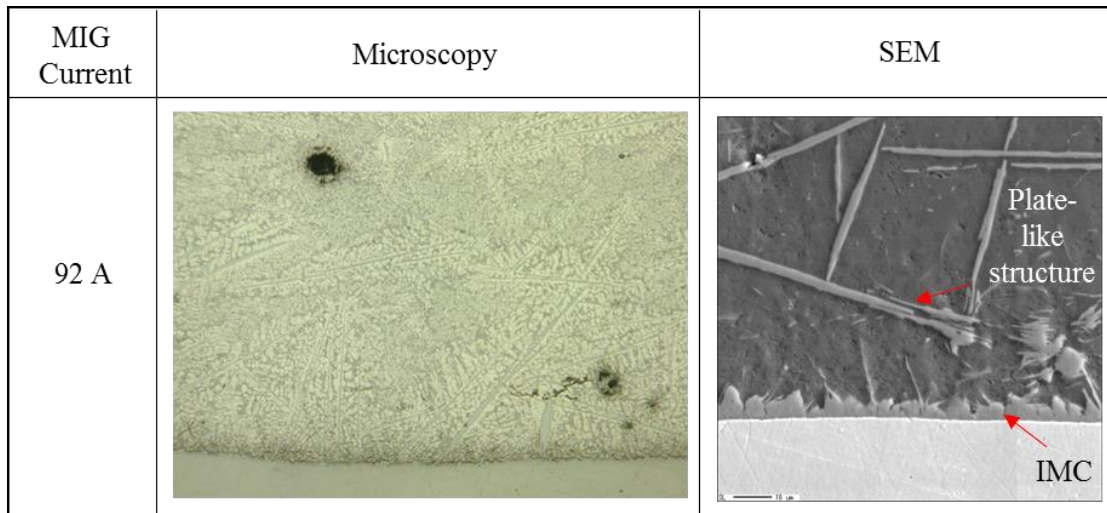


Fig. 5.12 Micrograph taken by microscopy at magnification of 500 times and the micrograph taken by SEM for the specimen welded by using pulse MIG welding

Following, **Fig. 5.13** and **Fig. 5.14** show the micrograph taken by microscopy at magnification of 500 times and the micrograph taken by SEM for the specimens welded by using pulse plasma MIG welding under different MIG current. At 73 A of MIG current, very thin IMC was observed to be formed at the boundary of Al/Steel surface. While, the small portions of needle-like structure also observable at the aluminum weld metal. At 89 A of MIG current, the IMC layer seen to be thicker. The formation of the needle-like structure also can be seen much more compared with the previous one, and at some extent the IMC layer is connected to this structure. The thickness of the IMC becomes larger with the increase of the MIG current. The formation of the plate-like structure which connected to the IMC is really stands out despite of the formation of needle-like structure at aluminum weld metal. As a result of further increase in MIG current, the size of plate-like structure becomes larger and the portion of needle-like structure becomes lesser. At 140 A of MIG current, there is no IMC formation observed in the intermediate area and the plate-like structure is predominant at aluminum weld metal. Here, the SEM pictures show a very good tendency in terms of the IMC formation and its thickness, and the formation of different structure at aluminum weld metal that grows larger from needle-like structure to plate-like structure by the increase of the MIG current.

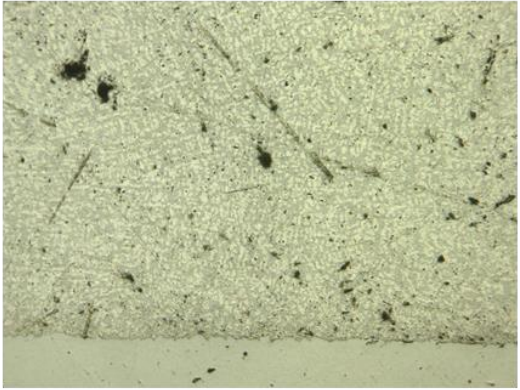
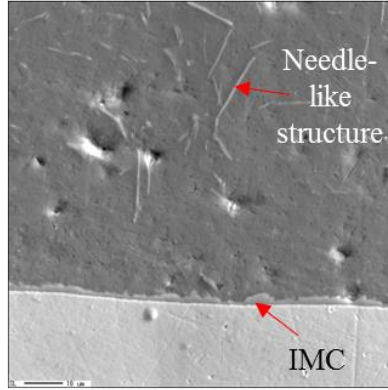
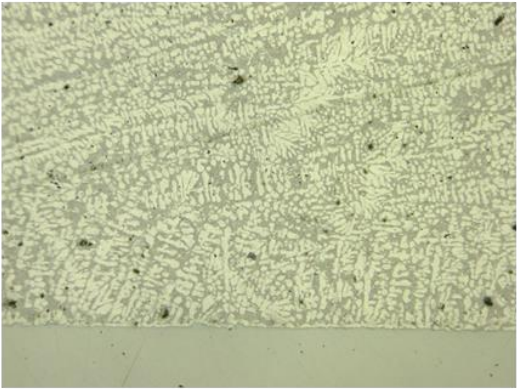
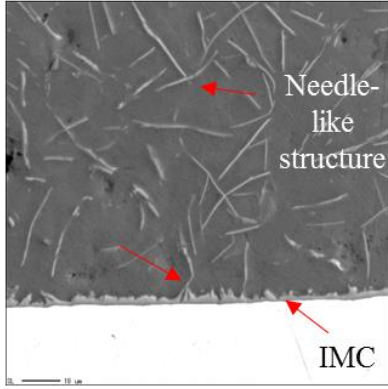
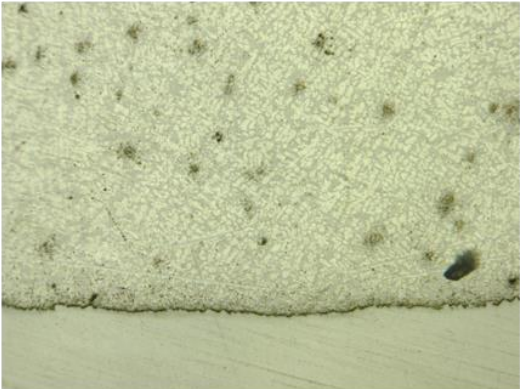
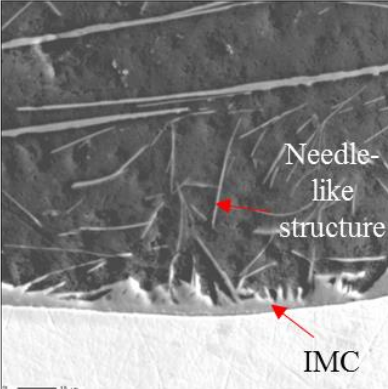
MIG Current	Microscopy	SEM
73 A		
89 A		
106A		

Fig. 5.13 Micrograph taken by microscopy at magnification of 500 times and the micrograph taken by SEM for the specimen welded by using pulse plasma MIG welding


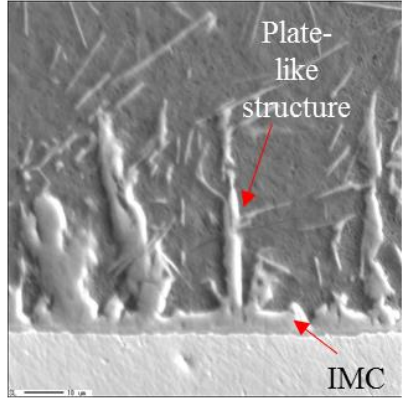

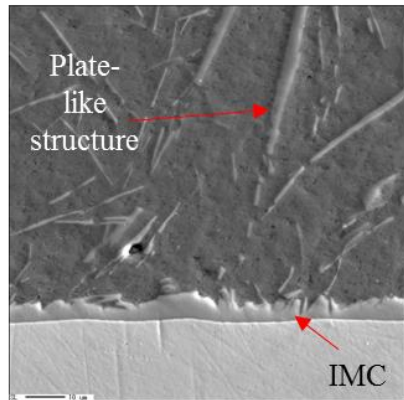

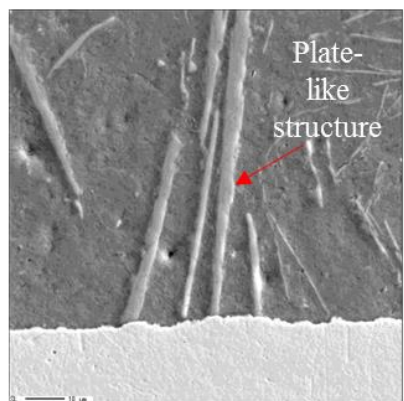
MIG Current	Microscopy	SEM
117 A		
131 A		
140 A		

Fig. 5.14 Micrograph taken by microscopy at magnification of 500 times and the micrograph taken by SEM for the specimen welded by using pulse plasma MIG welding

5.3.4 Characterization of IMC through EPMA

5.3.4.1 Pulse MIG welding

Fig. 5.15 shows the EPMA analysis of the specimen welded by using pulse MIG welding at the intermediate area. The mapping picture shows the concentration of Fe, Al and Si in IMC layer as well as in aluminum weld metal. Here, the diffusion of Fe into aluminum and vice-versa forms the Fe-Al IMC layer at interface area with three different morphology of Fe-Al IMC. These three strips shape of different Fe-Al IMC morphology are shown clearly in **Fig. 5.16** which is denoted as I in **Fig. 5.15**. Through the EPMA quantitative analysis, these three types of IMCs were estimated as FeAl/Fe₃Al, Fe₂Al₅ and FeAl₃, in ascending sequence from the Al/Steel interface. The formation of these IMCs agree with other researchers [27, 59–61]. The sequence showed that the formation of each IMCs was depending on the amount of Fe diffused into Al. The FeAl/Fe₃Al layer was observed to form a thin layer at the interface and almost flat to the steel surface. The Fe₂Al₅ formed in the second layer and gradually the formation of FeAl₃ took place. The FeAl₃ formed a tongue-like shape and seemed to move forward into aluminum area. The combination of these IMCs was measured approximately 9 μ m with Fe₂Al₅ and FeAl₃ were dominant IMC. Basically, in EPMA quantitative analysis, there was an element of Si especially at Fe₂Al₅ and FeAl₃ layer. Si reacted with Al to form Al-Si eutectic structure and at some area formed Fe-Al-Si. The presence of Si inhibit the formation of brittle Fe-Al phase through the formation of Fe_{1.8}Al_{7.2}Si and Fe(Al,Si)₃. The formations of these phases which property are less detrimental enhance the quality of the joining [62]. However, in this study, we only concentrate on the Fe-Al binary system and ignore the Fe-Al-Si ternary system.

From the Fe-Al phase diagram (refer Appendix **Fig. A1**) and the EPMA analysis results, it could be understood that, the formation of FeAl is facilitated by the high peak temperature in pulse MIG welding at the area close to the steel. This is because, the formation of this type of IMC only occurs at high temperature above 1200 K [25] instead of the transformation through diffusion control at low temperature. The high amount of Fe at the area promotes the formation besides the high cooling rate that may affects the formation as well.

Meanwhile, in the area close to the aluminum, the formation of Fe₂Al₅ preceded the transformation although the formation of FeAl₃ also possible at the same time. However, the formation of FeAl₃ that necessitate of higher amount of Al might be one of the reasons for the Fe₂Al₅ preceded the transformation. The formation of these IMCs was also believed to be influenced by the heating rate and peak temperature. Since this measurement was done in intermediate area, the peak temperature was considered as the highest compared with the other area due to the concentration of arc energy as well as the heat content from metal droplet, caused the cooling rate in this area was the highest. Therefore, in the case of pulse MIG welding, the high temperature in the intermediate area facilitated the formation of thick Fe₂Al₅ layer. The high temperature also facilitated the aluminum to diffuse into Fe₂Al₅ to form FeAl₃ instead of the formation through reaction with the unreacted Fe [63].

Regarding to the plate-like structure that can be seen clearly formed in the aluminum weld metal, the Fe element in the microstructure is thought to come from the steel sheet that moves into aluminum molten area through the convection during welding process. The size of this microstructure is closely related to the amount of heat input into the weld metal, thus the larger amount of heat input results in the larger microstructure size.

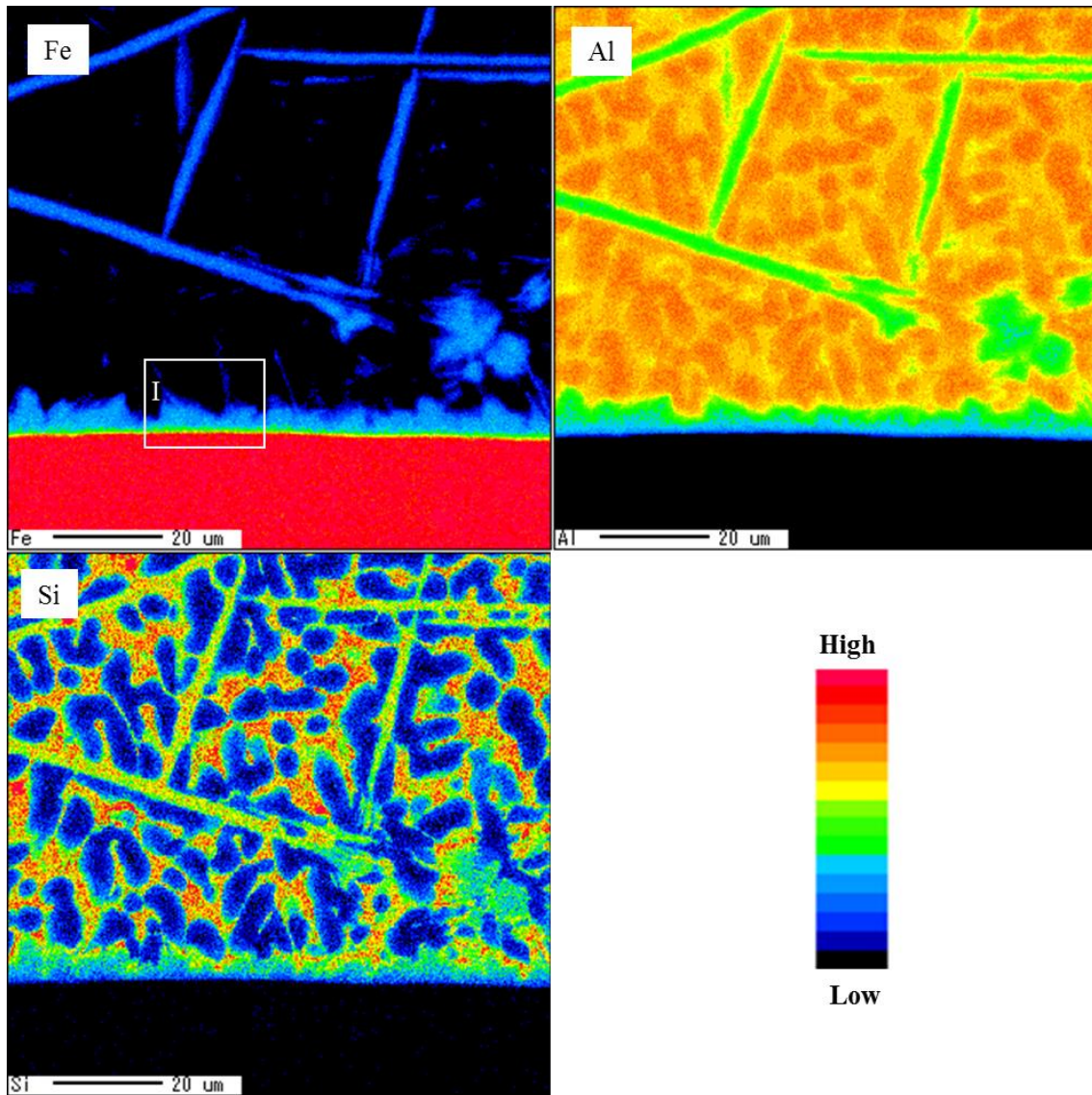


Fig. 5.15 EPMA analysis for the specimen welded at 92 A by using pulse MIG welding process with the enlargement area marked as I

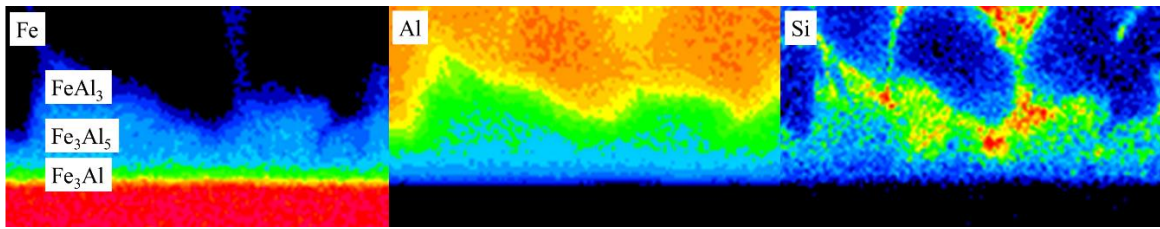


Fig. 5.16 Enlarge area denoted by I in **Fig.5.15**

5.3.4.2 Pulse plasma MIG welding

Fig. 5.17 shows the EPMA analysis of the specimen welded by using pulse plasma MIG welding at the intermediate area. The specimen was welded at 89 A of MIG current. The EPMA analysis result clearly shows that the IMC thickness at the Al/Steel interface area is thinner than the one in the specimen that was prepared by pulse MIG welding above. **Fig. 5.18** shows the enlarge picture at the area denoted by J in **Fig. 5.17**. The strip shape of three morphologies of IMC in the area can also be observed in this specimen. Through the EPMA quantitative analysis, the same morphology of Fe-Al IMC as being observed in pulse MIG welding is verified. There was, FeAl/Fe₃Al adjacent to the steel sheet, Fe₂Al₅ and FeAl₃ with some element of Si adjacent to the aluminum weld metal. These combination of three IMCs made the thickness of about 5 μm. The FeAl/Fe₃Al layer was observed to form a thin layer followed by the formation of Fe₂Al₅ and FeAl₃. Compared to the one in pulse MIG welding, the thickness of Fe₂Al₅ was not a dominant phase and its thickness was almost similar to FeAl₃. The same thickness of these two IMCs suggested the simultaneous transformation occurred during heating. Indeed, the short time transformation of Fe₂Al₅ could be caused by the less amount of Fe in the area. Therefore, the transformation to FeAl₃ which consumed less Fe was promoted.

In regards to the formation of the microstructures in aluminum weld metal, apparently the use of pulse plasma MIG welding capable to reduce the formation of plate-like structure in the weldment. However, the formation of needle-like structure was still could be observed in aluminum weld metal in small amount surrounded by eutectic Al-Si structure.

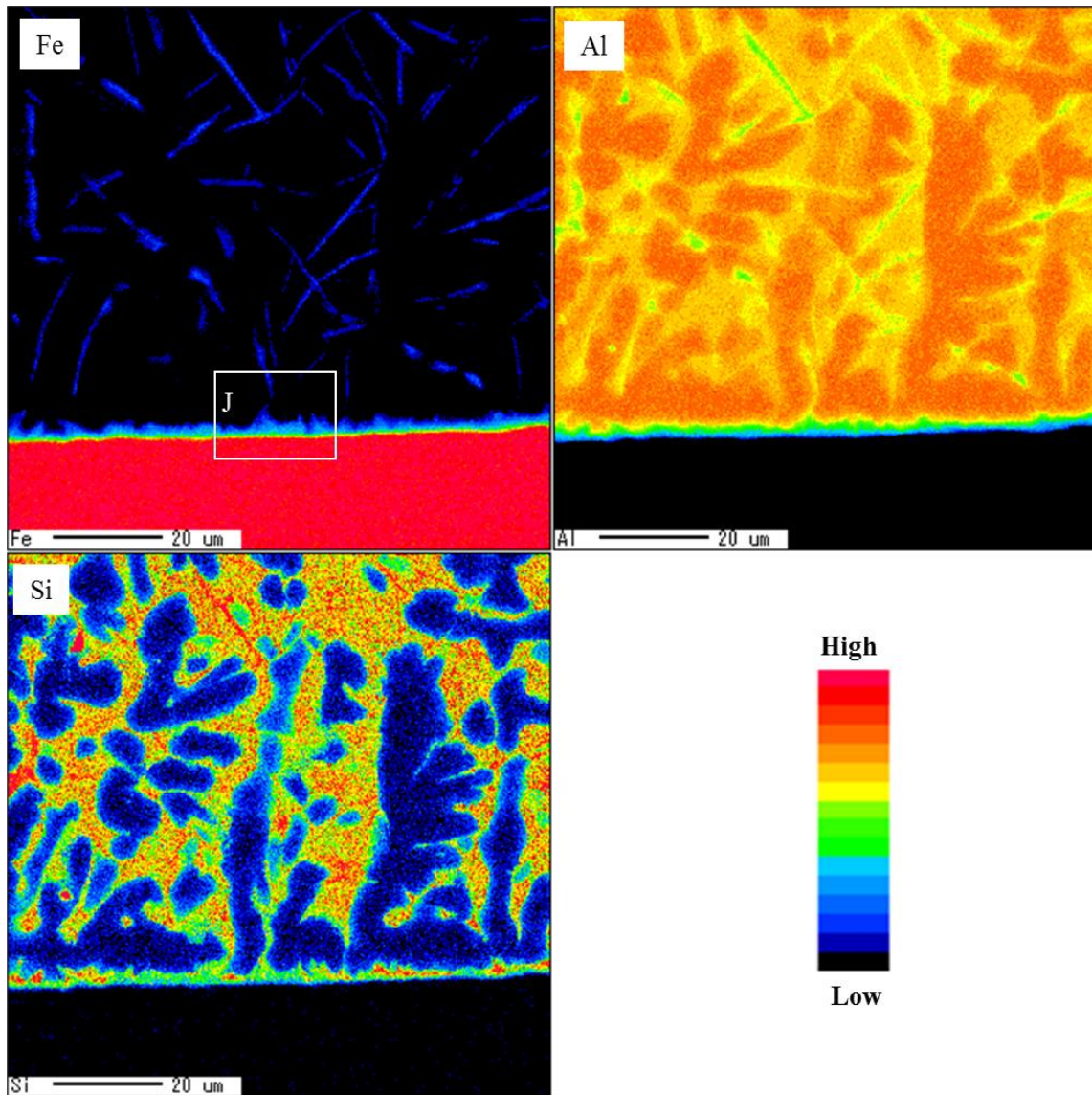


Fig. 5.17 EPMA analysis for the specimen welded at 89 A (WFS 110 cm/min) by using pulse MIG welding process with the enlargement area marked as J

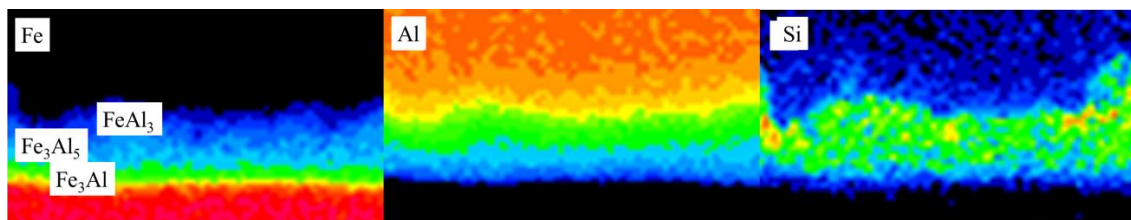


Fig. 5.18 Enlarge area denoted by J in **Fig. 5.17**

5.3.4.3 IMC formation under different MIG current in pulse plasma MIG welding

The formation of IMC layer under the different MIG current in pulse plasma MIG welding are shown in **Fig. 5.19** to **Fig. 5.23** for the MIG current ranging from 73 A to 140 A. From these figures, apparently the increase of MIG current increases the thickness of IMC and influences the tendency of microstructure formation in aluminum weld metal. The diffusion of Fe element from steel into molten aluminum and diffusion of Al element into steel can be clearly observed in these figures. The enlarge area for all these figures are summarized in **Fig. 5.24**.

Fig. 5.24 shows the enlarge area of each current ranging from 73 A to 137 A. The increase of MIG current increased the diffusion rate of both iron and aluminum, and this effect could be seen clearly in the analysis results below. For the MIG current below than 100 A, the thickness of IMC was almost the same. However, the IMC thickness increased markedly when the MIG current became more than 100 A. This is simply because of the increase of MIG current causes the increase in the peak temperature and thus accelerates the diffusion of Fe into molten aluminum. The presence of Fe element in the molten aluminum area facilitates the formation of Fe_2Al_5 , and the increase of Fe element in the area allows the formation of thicker Fe_2Al_5 . The formation of FeAl_3 was observed sandwiched between the layer of Fe_2Al_5 and aluminum as well as $\text{FeAl}/\text{Fe}_3\text{Al}$ between Fe_2Al_5 and steel sheet.

At 140 A of MIG current, the IMC layer is not observed to be formed at intermediate area. However, the formation of many plate-like structures with a large size is observed at aluminum weld area. The formation of this plate-like structure that at some area starts from the interface of Al/Steel, suggests the preferential direction for growth of Fe_2Al_5 [8,10,11].

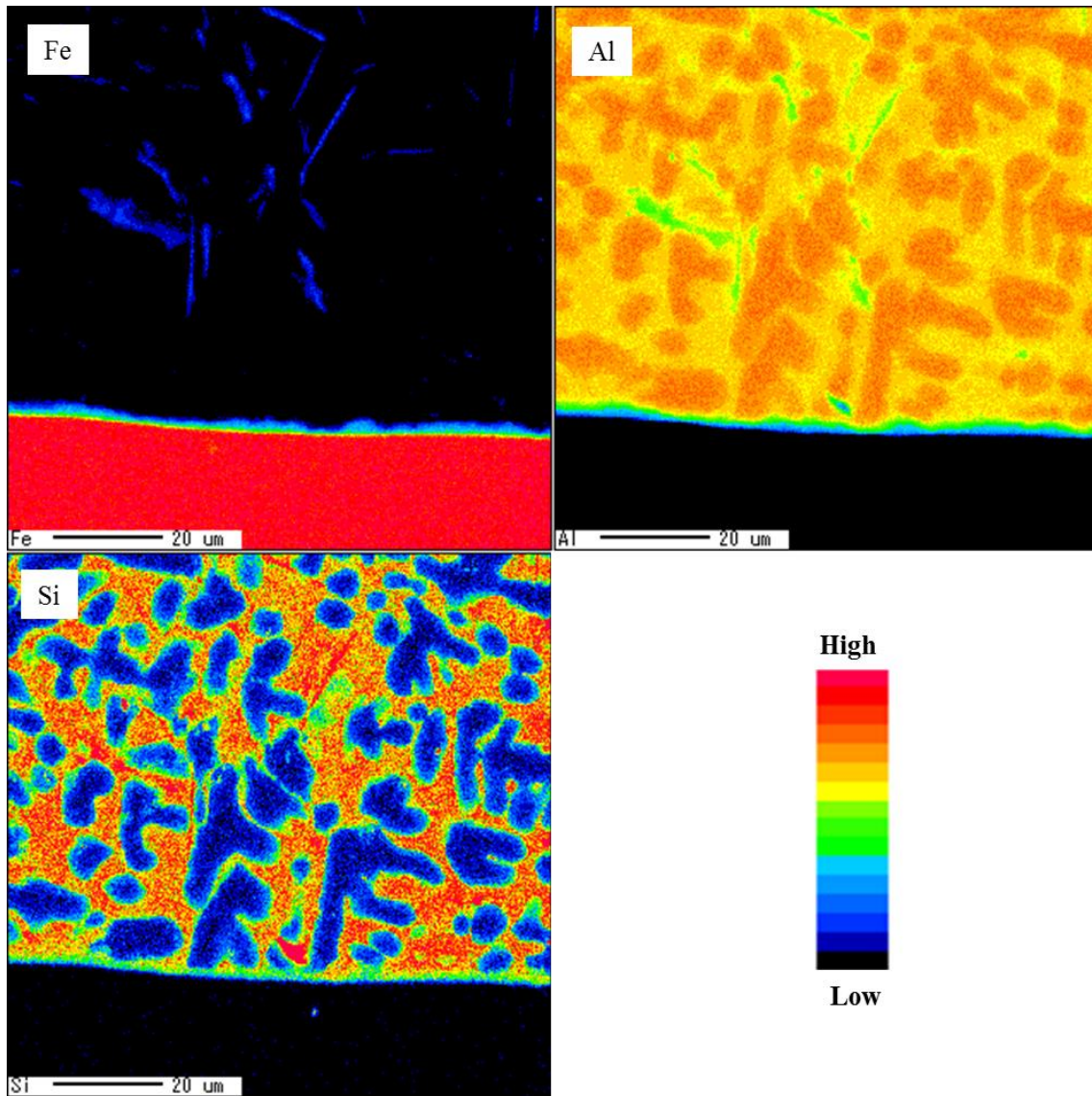


Fig. 5.19 EPMA analysis for the specimen welded at 73 A (WFS 90 cm/min) by using pulse plasma MIG welding process

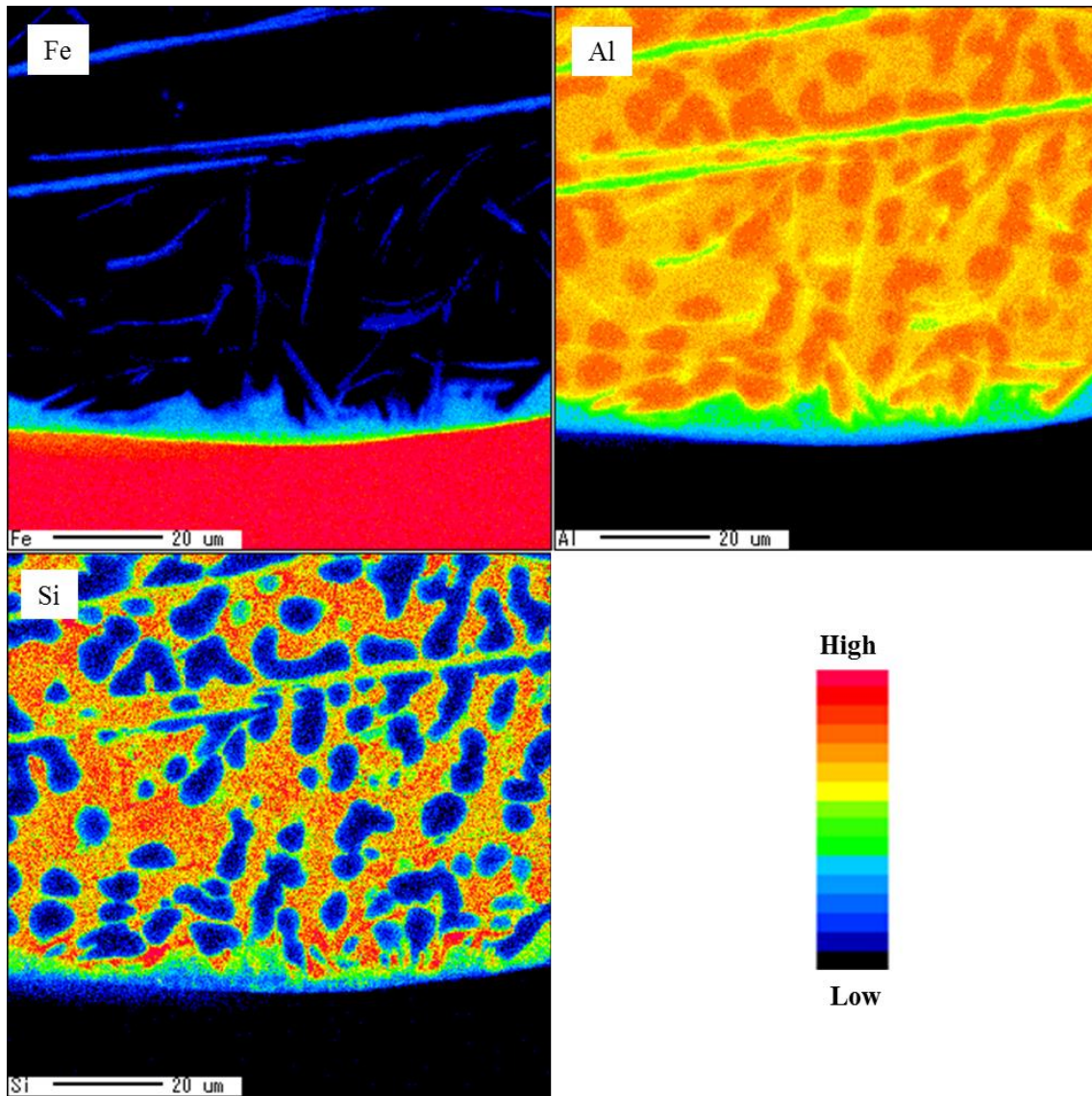


Fig. 5.20 EPMA analysis for the specimen welded at 106 A (WFS 120 cm/min) by using pulse plasma MIG welding process

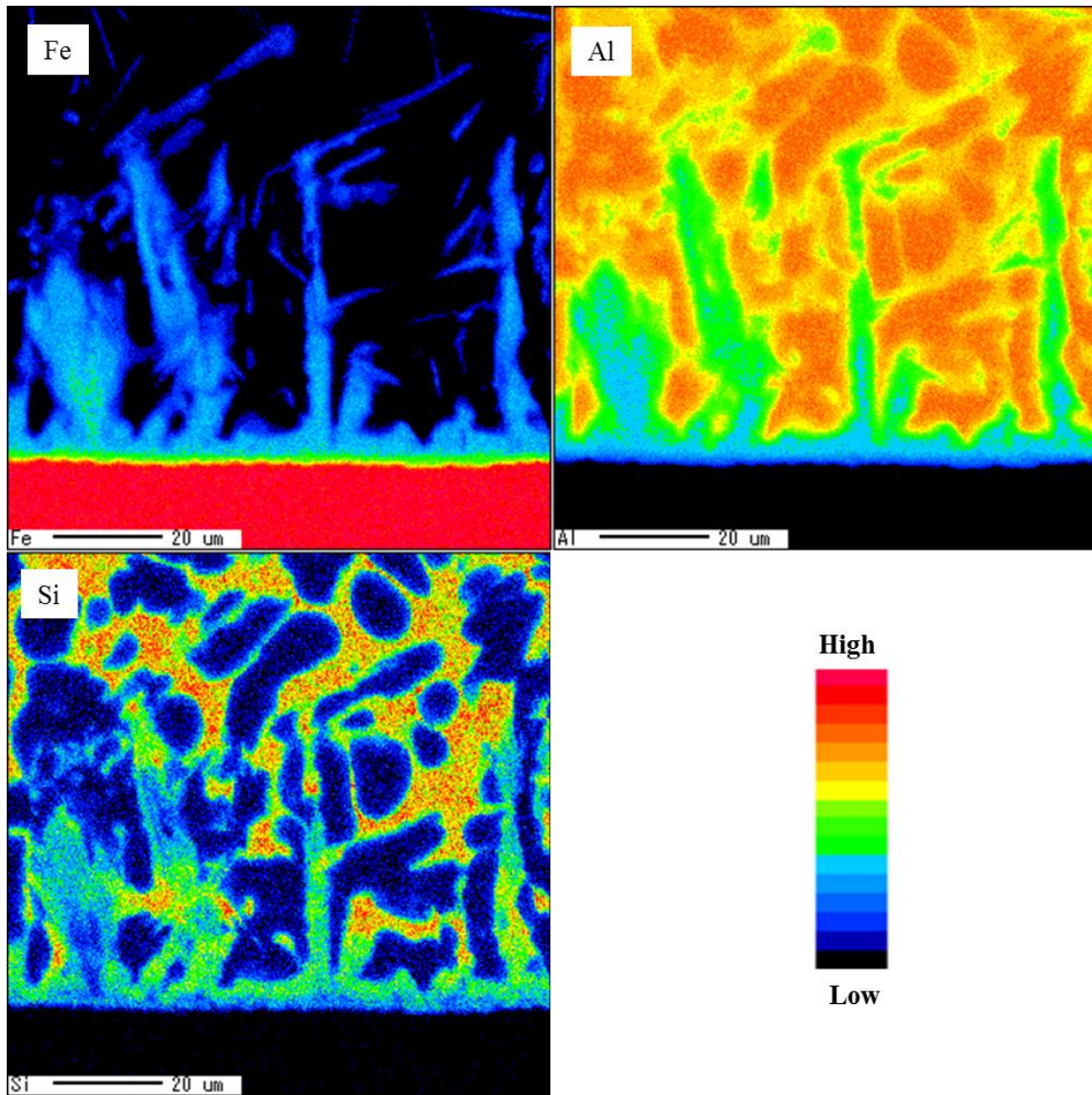


Fig. 5.21 EPMA analysis for the specimen welded at 117 A (WFS 140 cm/min) by using pulse plasma MIG welding process

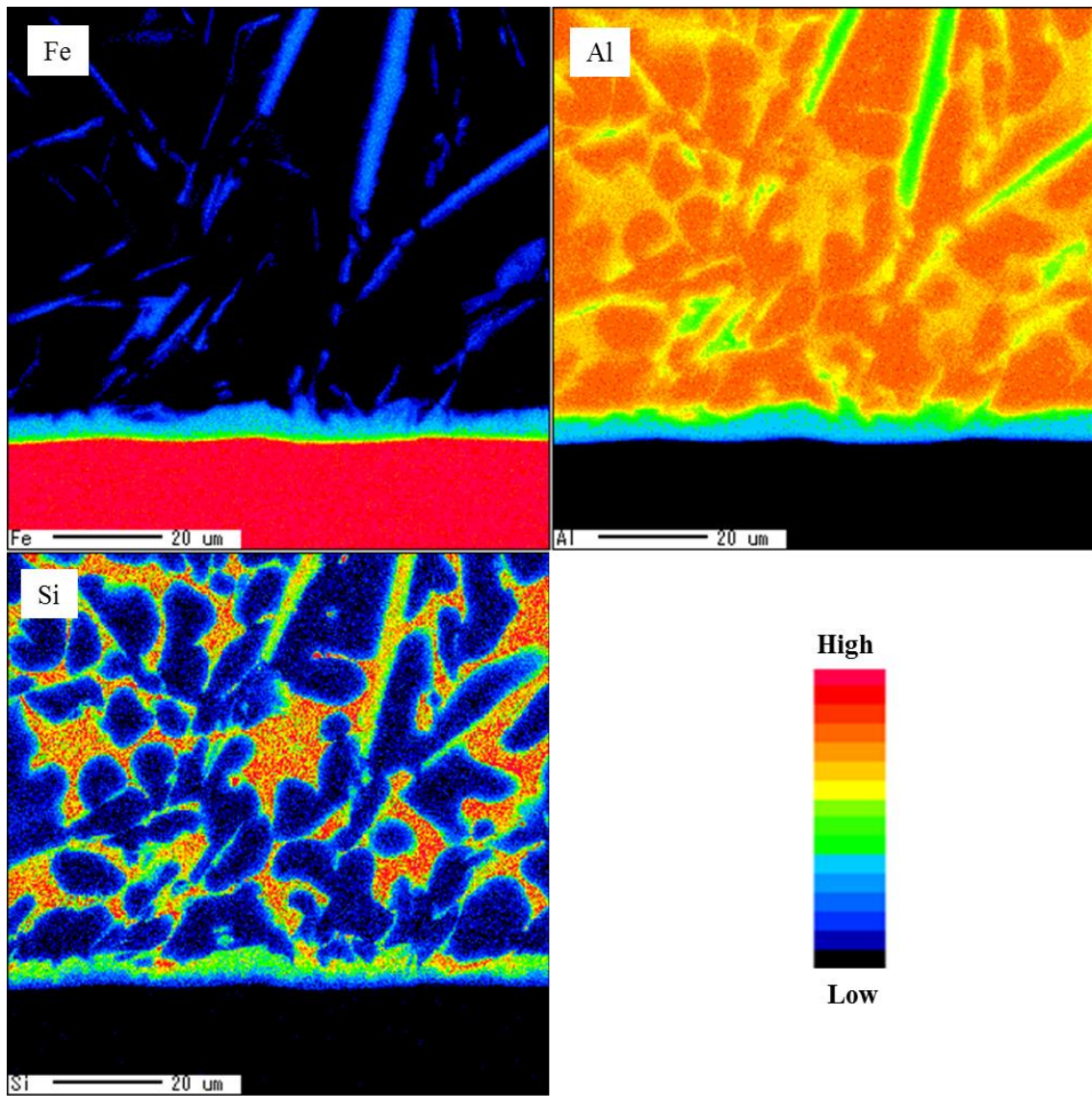


Fig. 5.22 EPMA analysis for the specimen welded at 131 A (WFS 180 cm/min) by using pulse plasma MIG welding process

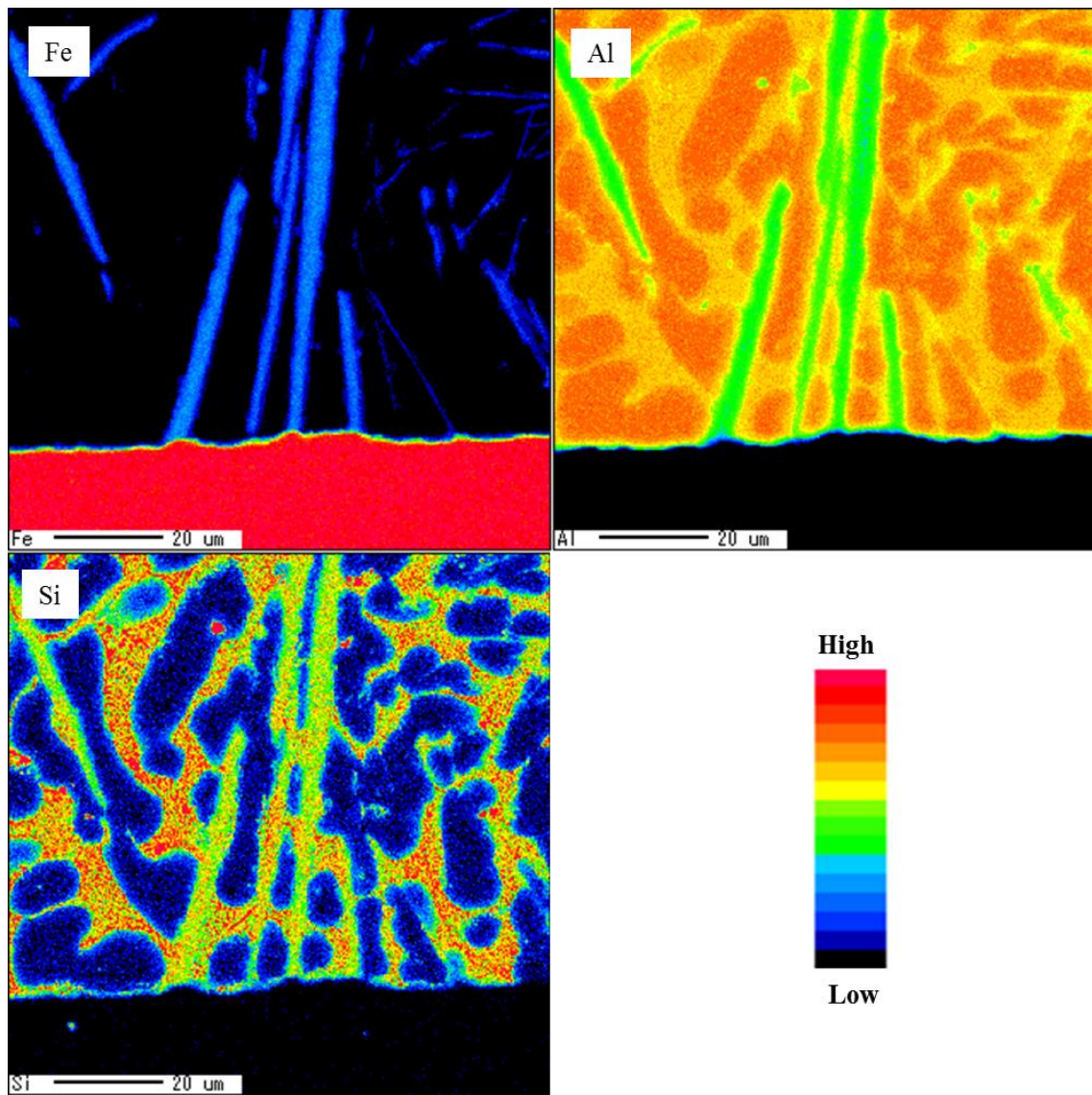


Fig. 5.23 EPMA analysis for the specimen welded at 140 A (WFS 200 cm/min) by using pulse plasma MIG welding process

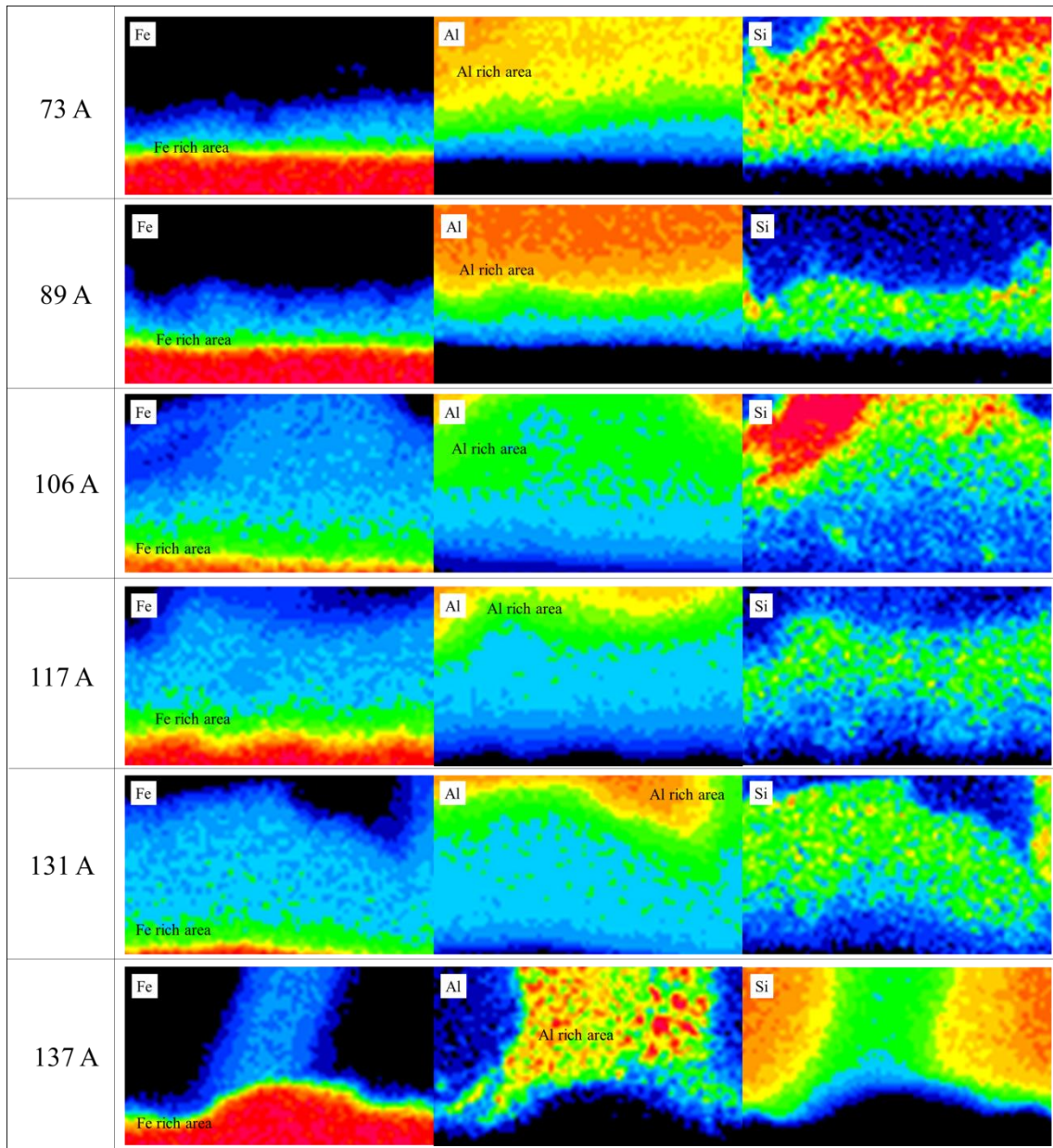


Fig. 5.24 Enlarge area of each MIG current ranging from 73 A to 140 A

Meanwhile, **Fig. 5.25** shows the concentration of Fe, Al and Si as a function of the distance, depicting the thickness of the IMCs that formed during welding process. The data is taken from the EPMA analysis results and pointing at the thickest area in the analysis. **Fig. 5.25 (a)** and (c) show the difference of IMC formation behavior in pulse MIG and pulse plasma MIG welding under the same MIG current. Fe_2Al_5 is a dominant IMC that formed during welding which covers $6 \mu\text{m}$ from the total IMC thickness of $9 \mu\text{m}$. Meanwhile in pulse plasma MIG welding, the thickness of FeAl_3 is almost the same with the thickness of Fe_2Al_5 . The total thickness for the IMC formed in (c) is $4.5 \mu\text{m}$. Likewise for the formation of Fe_3Al which tended to form thicker in pulse MIG welding process.

From **Fig. 5.25 (b)** to **Fig. 5.25 (h)** show the thickness and behavior of the IMCs in pulse plasma MIG welding under the different MIG current setting. **Fig. 5.25(g)** and **Fig. 5.25(h)** show the different IMC formation behavior in pulse plasma MIG welding at 140 A. These graphs verify the formation of thicker IMC by the increase of heat input. Interestingly, the behavior of the formation of Fe_2Al_5 in relatively high MIG current (above 100 A) in pulse plasma MIG welding resembles the behavior in pulse MIG welding, in which the Fe_2Al_5 is the dominant IMC and after some while, the FeAl_3 starts to transform. Subsequently, compared with the low MIG current (below 100 A) of pulse plasma MIG welding, the pulse plasma MIG welding with the higher MIG current (above 100 A) observed to form the thicker Fe_3Al by the increase of MIG current. From approximately 130 A, the thickness of IMC at Al/Steel interface seems to decrease and only about $2 \mu\text{m}$ of total IMC is measured at 140 A. However, as shown in **Fig. 5.20(g)**, the concentration of Fe keeps at about 10 at % while Al concentration is about 80 at% with the silicon about 10 at %. This shows that the formation of IMC is associated with the plate-like structure which the content is similar to the IMC formed at Al/Steel interface.

(a)

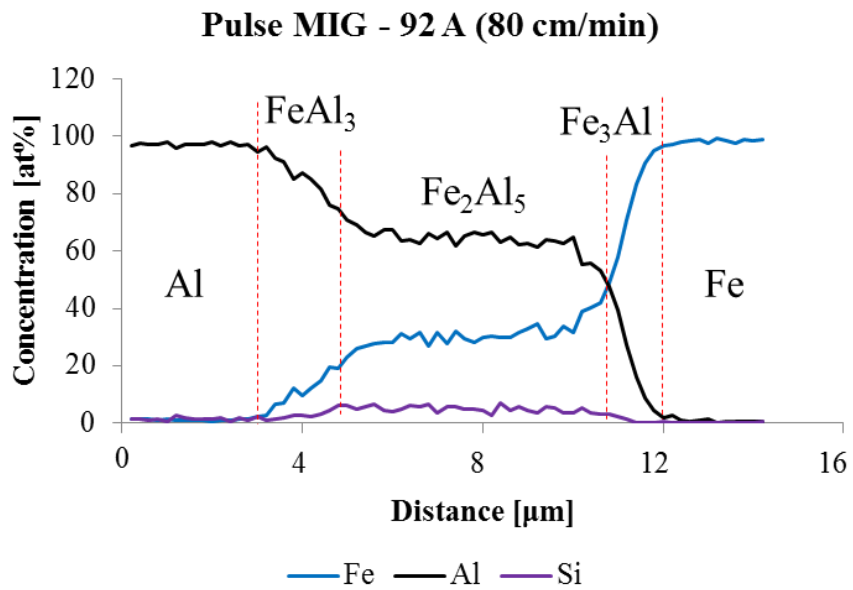


Fig. 5.25 (a) Formation of IMCs in pulse MIG welding at 92 A (80 cm/min)

(b)

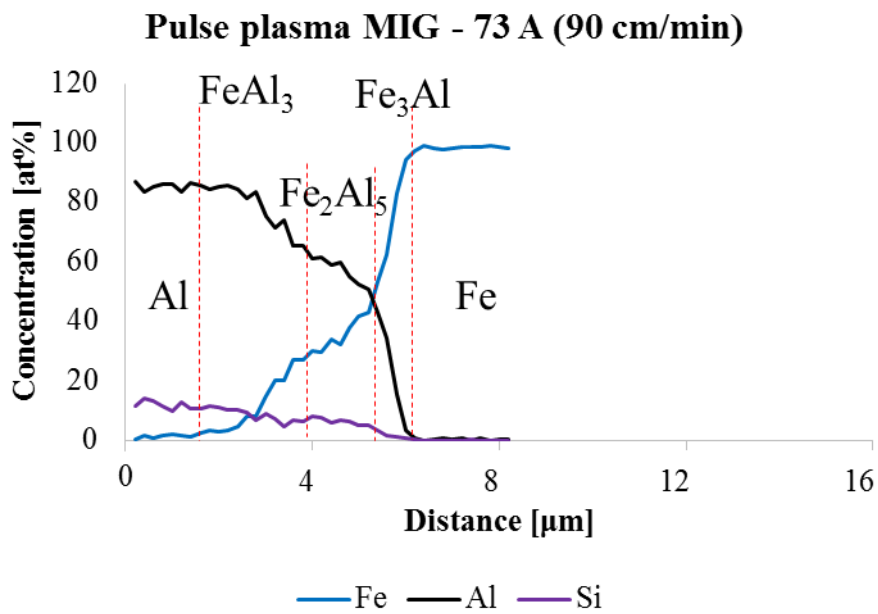


Fig. 5.25 (b) Formation of IMCs in pulse plasma MIG welding at 73 A (90 cm/min)

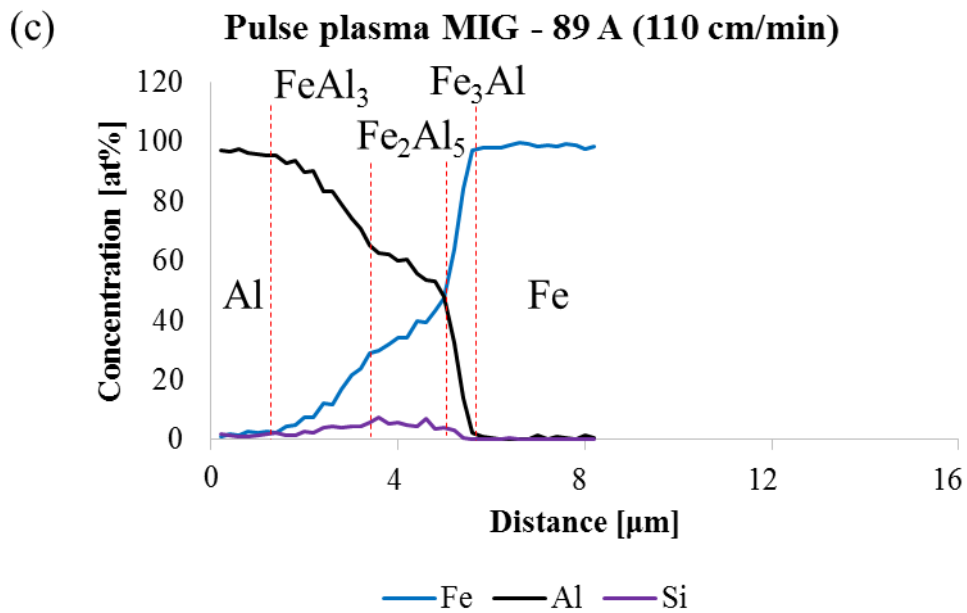


Fig. 5.25 (c) Formation of IMCs in pulse plasma MIG welding at 89 A (110 cm/min)

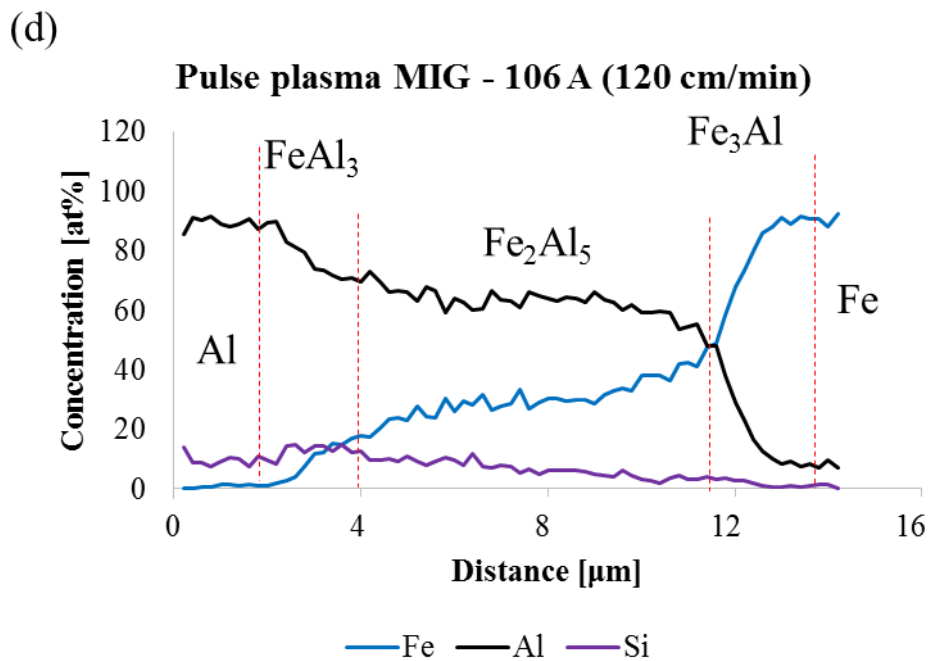


Fig. 5.25 (d) Formation of IMCs in pulse plasma MIG welding at 106 A (120 cm/min)

(e)

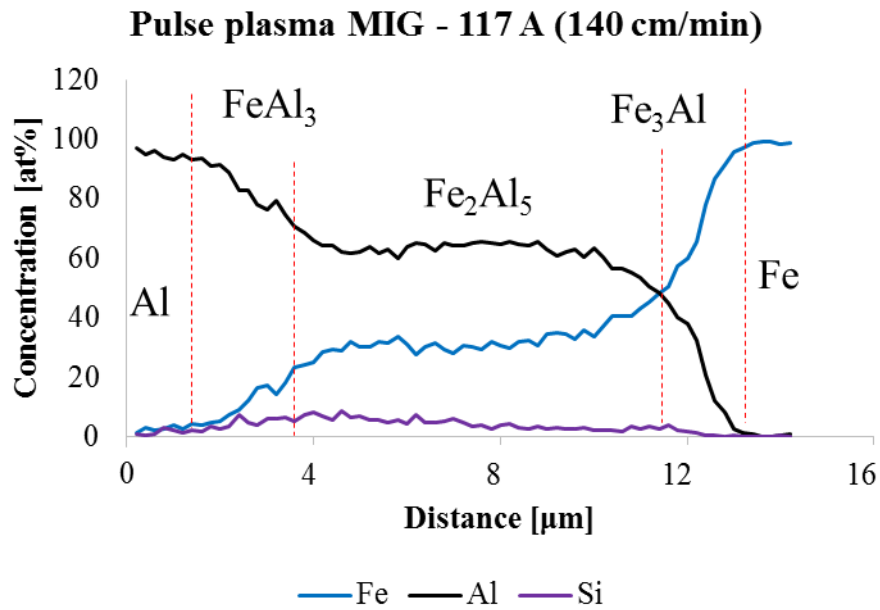


Fig. 5.25 (e) Formation of IMCs in pulse plasma MIG welding at 117 A (140 cm/min)

(f)

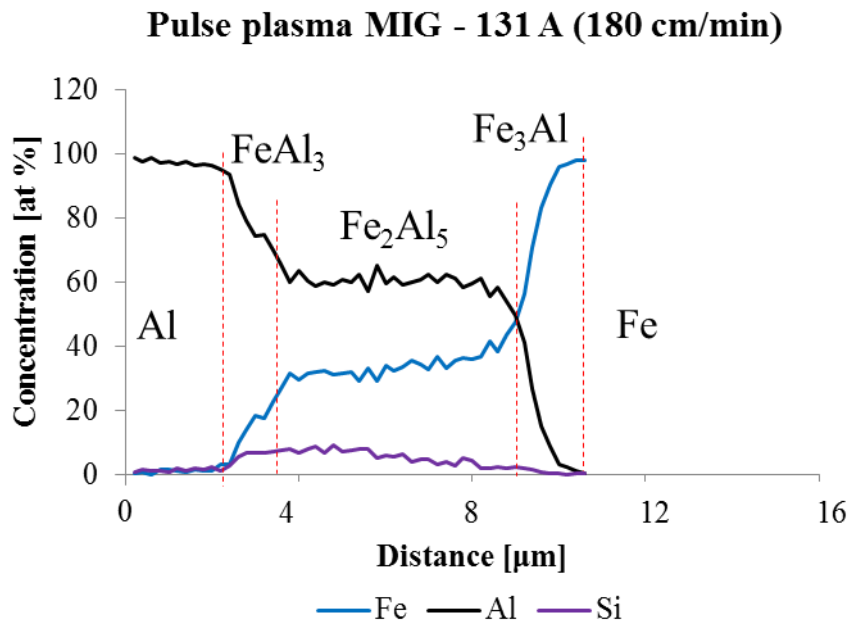


Fig. 5.25 (f) Formation of IMCs in pulse plasma MIG welding at 131 A (180 cm/min)

(g)

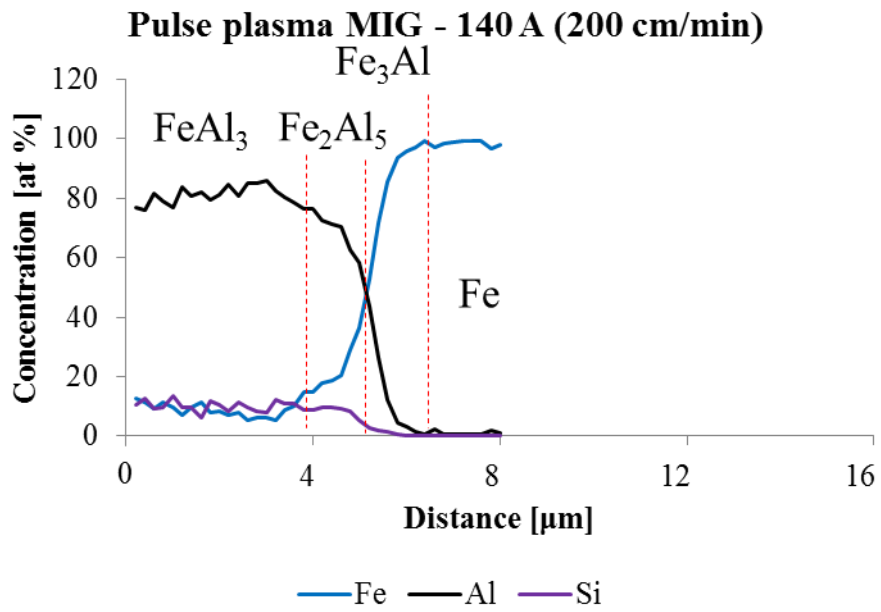


Fig. 5.25 (g) Formation of IMCs in pulse plasma MIG welding at 140 A (200 cm/min) connected to plate-like structure

(h)

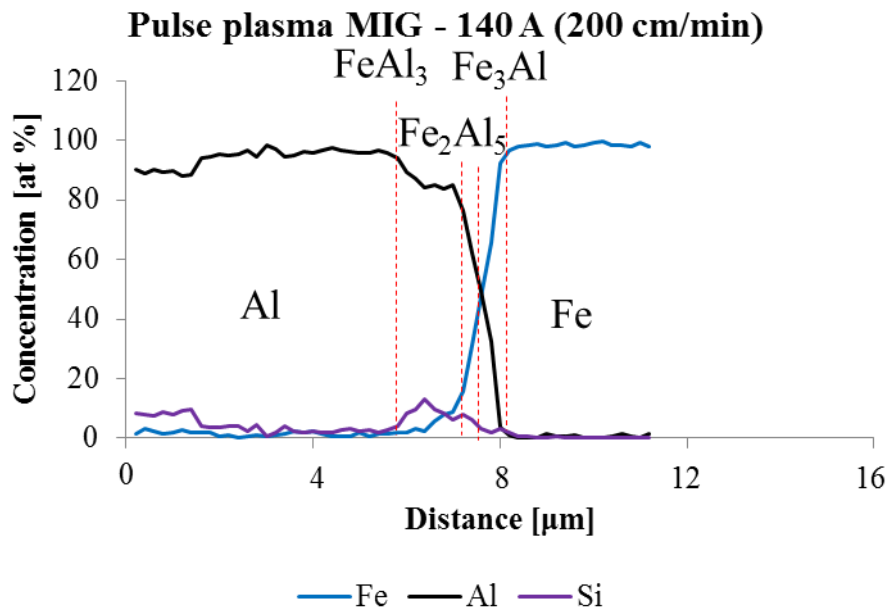


Fig. 5.25 (h) Formation of IMCs in pulse plasma MIG welding at 140 A (200 cm/min)

5.4 Discussion

Generally, the formation of IMC layer in joining the aluminum and steel is an inevitable, however its thickness can be controlled by optimizing the parameter of the welding to the extent that not affects the quality of the joining. In this study, the IMC thickness at Al/Steel interface that formed during welding by using pulse plasma MIG and pulse MIG welding was compared. The experimental results have shown that under the same MIG current, the IMC thickness formed during welding by using pulse MIG welding is thinner than the one in pulse plasma MIG welding. The formation of plate-like structure also prominent in pulse MIG welding compared with that in pulse plasma MIG welding. Meanwhile, the increase of MIG current in pulse plasma MIG welding results in the increase of the IMC thickness as well as the plate-like structure.

5.4.1 Formation of IMC in pulse plasma MIG welding

In this study, although we did not conduct any droplet temperature measurement in pulse plasma MIG welding, but the phenomena observed during aluminum welding show the similar behavior with the one in steel welding. Through these findings, under the same setting of MIG current, we consider that the droplet temperature in pulse plasma MIG welding is lower than the one in pulse MIG welding.

Base on the IMC thickness at interface of Al/Steel during welding, it can be confirmed that the use of pulse plasma MIG welding capable to reduce the IMC thickness. The low temperature in pulse plasma MIG welding limits the diffusivity of Fe into aluminum thus limits the formation of Fe_2Al_5 . In rapid heating, the formation of Fe_2Al_5 only starts to form after the aluminum melts [66]. The formation is temperature dependence, and accelerates by the increase of temperature. Therefore, the high peak temperature in pulse MIG welding results in the more formation of Fe_2Al_5 and is maximized until it saturation temperature at about 1073 K [25].

The FeAl_3 is suggested to be formed after the formation of Fe_2Al_5 . One of the reasons is the crystallography habit orientation of Fe_2Al_5 which almost similar to the Fe crystallography orientation facilitates the formation [65]. Since the formation of Fe_2Al_5 consumes high amount of Al, the unreacted Fe at the area of high concentration of Al facilitates the formation of FeAl_3 . The rapid cooling in pulse MIG welding then suppresses the further formation of Fe_3Al . Therefore, the thickness of this IMC is lesser than the thickness of Fe_2Al_5 . However, lower peak temperature in pulse plasma MIG welding limits the formation of Fe_2Al_5 , besides facilitates the formation of FeAl_3 . Due to this, the thickness of FeAl_3 is almost similar to the thickness of Fe_2Al_5 in pulse plasma MIG welding.

The formation of Fe_3Al starts at slightly high temperature, above 1200 K [25]. In pulse MIG welding, the formation of Fe_3Al is suggested mainly occurred when the temperature reaches up to 1200 K. The formation rate reduces when the pulse arc stop and the temperature decreases rapidly. The high cooling rate limits the solid state diffusion of Fe into Fe_2Al_5 to form Fe_3Al , thus the only

small fraction of Fe_3Al formed due this factor. In pulse plasma MIG welding, the formation of Fe_3Al is suggested driven by the diffusion of Fe into Fe_2Al_5 [3,13,14] during cooling process. **Fig. 5.26 (a)-(d)** show the mechanism of slower cooling rate in pulse plasma MIG welding in comparison with pulse MIG welding. The presence of plasma flow in pulse plasma MIG welding after the pulse arc stop heats the weld bead at the minimum extent, thus reduce the cooling rate. Since the diffusion of Fe into Fe_2Al_5 is the solid state diffusion, the slower cooling rate allows higher diffusivity of Fe, thus thicker Fe_3Al formed in pulse plasma MIG welding compared with the one in pulse MIG welding.

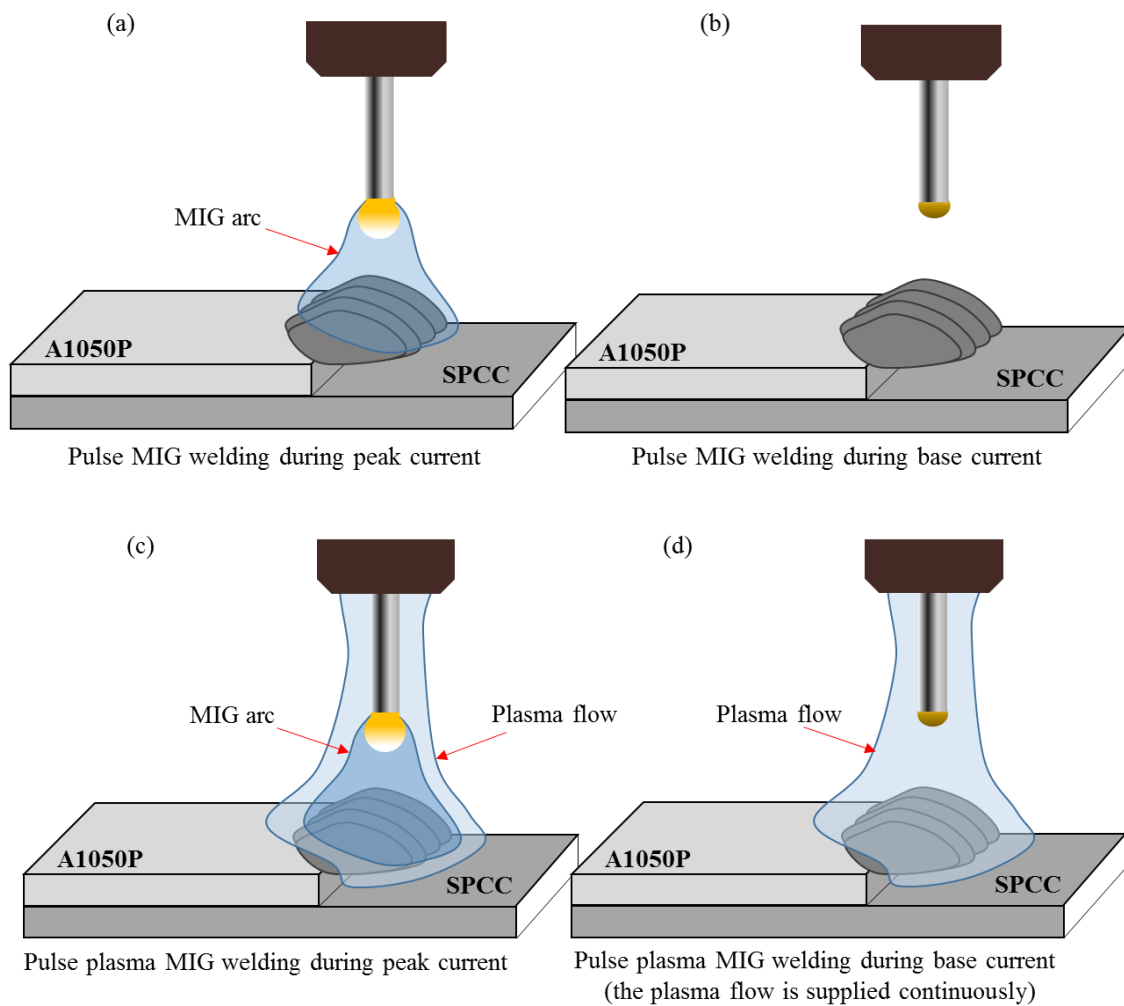


Fig. 5.26 Illustration of pulse MIG during welding, (a) the presence of MIG arc during peak current, (b) the absence of MIG arc during base current and illustration of pulse plasma MIG during welding, (c) the presence of plasma flow overwhelms the MIG wire, MIG arc and aluminum weld bead during peak current, (d) the presence of plasma flow during base current

As mentioned earlier, the increase of MIG current in pulse plasma MIG welding increase the peak temperature and results in the formation of thicker IMC at Al/Steel interface. Since the process involves the higher peak temperature, the tendency of the IMC formation (Fe_2Al_5 , FeAl_3 and Fe_3Al) during heating process is markedly close to the one in pulse MIG welding. Meanwhile, the presence of plasma flow causes the slower cooling rate, thus facilitate the formation of Fe_3Al . Here, the formation of relatively large fraction Fe_3Al is thought to be the reason in improving the weldability of dissimilar welding by using the pulse plasma MIG welding. The involvement of both factors during pulse plasma MIG welding leads to the formation of thick IMC at Al/Steel interface.

5.4.2 Control of IMC thickness by plasma MIG welding process

It is suggested that, the presence of plasma flow in pulse plasma MIG welding is a main factor to influence the formation of IMC at interface of aluminum and steel. The presence of plasma flow enables the divergence of MIG current and results in the dispersion of heat as well as the magnetic force towards the MIG wire [58]. This mechanism is effective to reduce the droplet temperature. In joining the aluminum and steel, the control of heat input is crucial to keep the good quality of joining. Therefore, the mechanism of the droplet temperature reduction in pulse plasma MIG welding is an important factor and capable to control the formation of IMC especially Fe_2Al_5 and FeAl_3 .

Instead of reducing the droplet temperature, the plasma flow also brings a pre-heat effect to the weld metal. The joining of aluminum that involves a low melting temperature, the minimum heat affects the cooling rate significantly. The slower cooling rate initiates more diffusion of Fe, thus leads to a thicker formation of Fe_3Al . Since the Fe_3Al layer has relatively high fracture resistance and oxidation resistance properties, the formation of this IMC is preferable and is considered to improve the weldability of the joining by using the pulse plasma MIG welding.

To summarize, **Fig. 5.27** shows the factors that control the thickness of IMC by using pulse plasma MIG welding. To facilitate the understanding, the phenomena in pulse plasma MIG welding is compared with the one in pulse MIG welding.

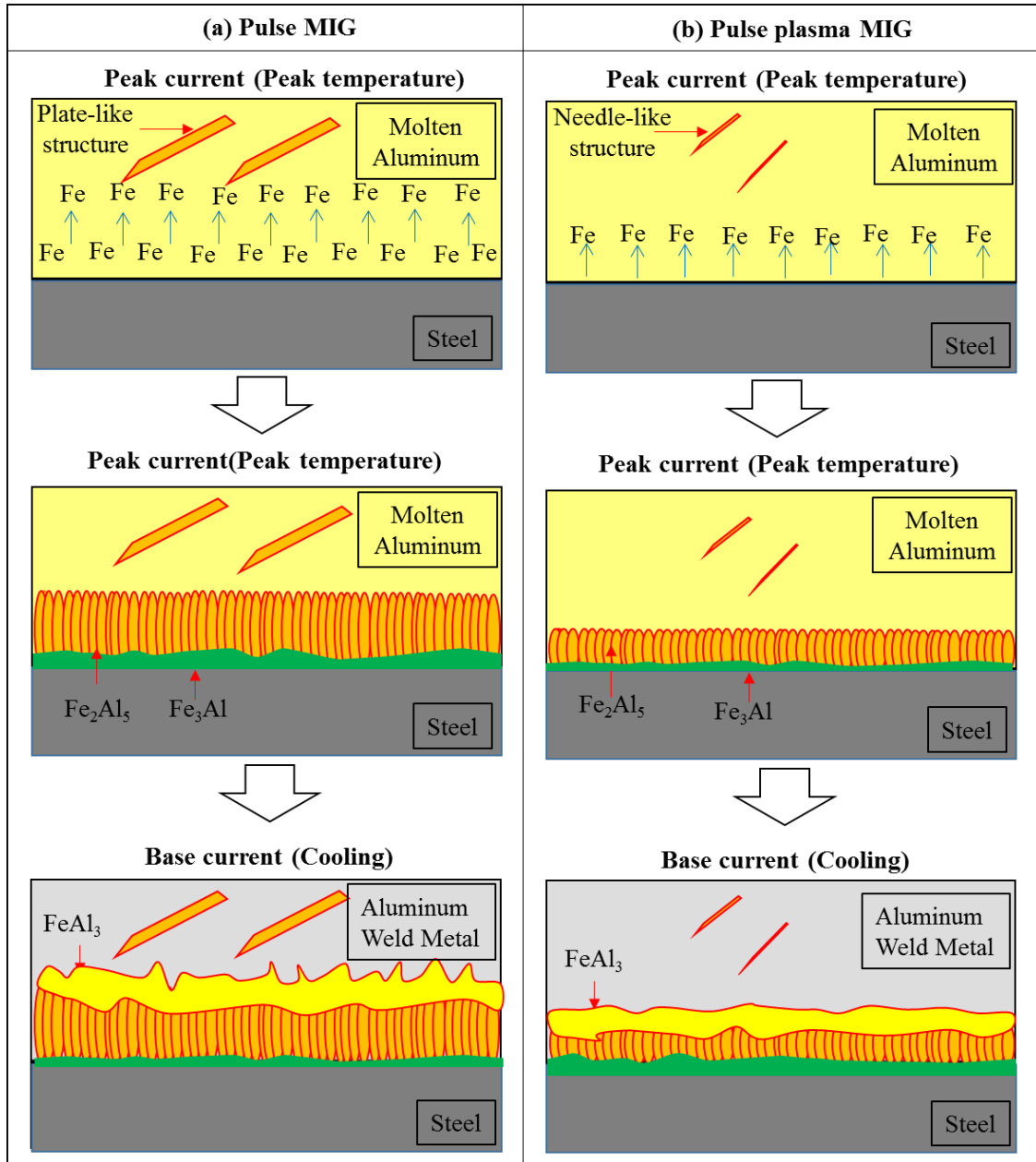


Fig. 5.27 Factors that control the thickness of IMC by using pulse plasma MIG welding compared with the one in pulse MIG welding

5.5 Conclusion

In this chapter, the mechanism to control the IMC thickness in the pulse plasma MIG welding was discussed based on the analysis to the IMC layer at the interface of aluminum and steel for a wide range of MIG currents. The following conclusions can be drawn from the results obtained :

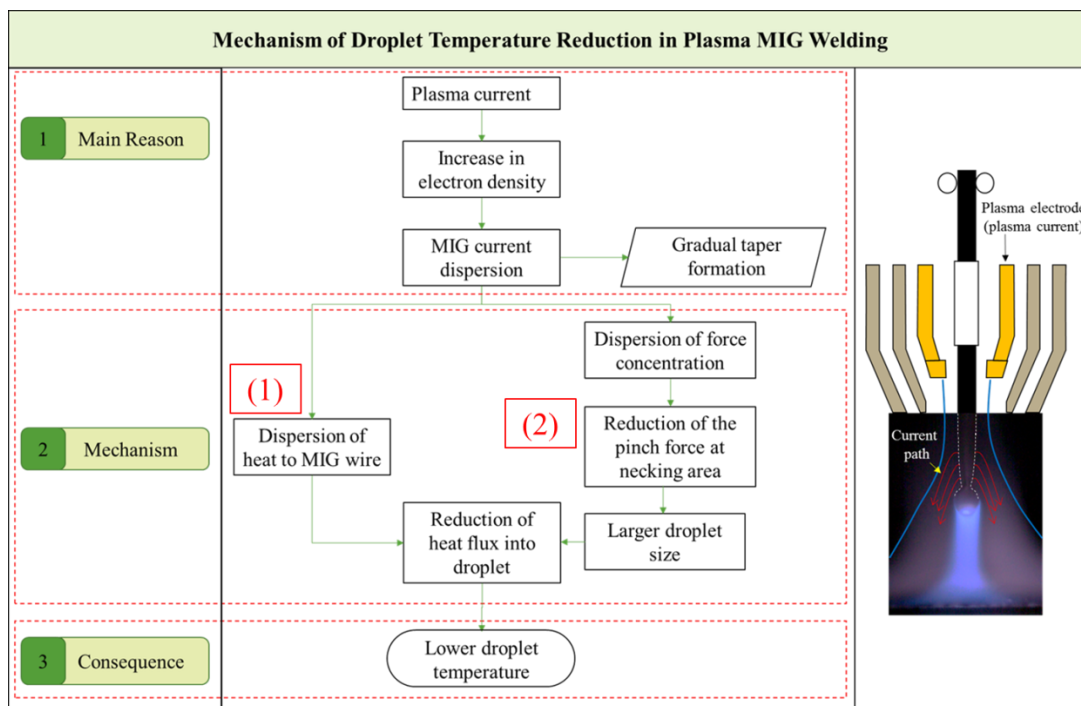
1. The use of pulse plasma MIG process improves the weldability of the Al/Steel dissimilar welding in terms of its visual appearance. The smut formation on the surface of the aluminum weld bead can be avoided when welding by using this pulse plasma MIG.
2. The use of plasma MIG welding reduces the thickness of IMC compared with the one in pulse MIG welding under the same MIG current. The formation of plate-like structure in aluminum weld metal also reduced.
3. The increase in MIG current in pulse plasma MIG welding increases the thickness of IMC at Al/Steel interface as well as the plate-like structure in aluminum weld metal. However, the increase in the thickness of Fe_3Al by increasing of MIG current up to certain limit gives a good weldability to the joint that welded by using this process.
4. It is suggested that the formation of IMC at Al/Steel interface mainly influenced by the amount of Fe diffusivity into aluminum region. The diffusivity of Fe into aluminum determines by the temperature. Therefore, the higher the achievable temperature results in the more diffusion of Fe which eventually results in the formation of thicker IMC.
5. It is suggested the IMC thickness in Al/steel dissimilar welding can be controlled by using pulse plasma MIG welding through its low droplet temperature and its ability to decrease the cooling rate during welding. The use of pulse plasma MIG welding is able to reduce the achievable peak temperature by its mechanism to reduce the droplet temperature. The low temperature suppresses the formation of Fe_2Al_5 and FeAl_3 , and decrease the IMC thickness in total.

Chapter 6

Conclusion

In this thesis, the comprehensive works have been done towards plasma MIG welding process to study the appropriateness of the welding method to be applied in Al/Steel dissimilar welding. Since the Al/Steel dissimilar welding is susceptible to the high heat input, the welding process that has a capability to reduce the heat input is needed, and in this study, the plasma MIG welding with freely adjustable welding parameter is used as a tool to realize a temperature controllable welding process. During welding, there are many ways of the heat input into base metal, among them is the droplet heat content, which covers almost 40% of the total heat input. Therefore, by focusing to the droplet temperature measurement, the approach of this research can be divided into 3 stages : 1) to study the factors that affects the droplet temperature and suggests the mechanism of droplet temperature reduction through the use of plasma MIG welding system, 2) to validate the findings regarding to the factors and the droplet temperature reduction mechanism, the difference welding system is used, instead of using the DCEN, the system is changed to pulse DCEN and 3) to apply the findings in previous experiments in Al/Steel dissimilar welding.

Flow chart below summarizes the findings in stage one. The main reason for the droplet temperature reduction in plasma MIG welding is the presence of plasma flow surrounding the MIG wire at all the time during welding. The plasma flow causes an increase of the electron density in surrounding of the MIG wire, resulting in the arc attachment to expand towards the contact tip. This phenomenon enables the divergence of the MIG current, and as an effect, the dispersion of the heat and force concentration to the MIG wire. These two mechanisms eventually caused a reduction of heat flux into droplet, and reduce the droplet temperature.



Through this mechanism, the droplet temperature in plasma MIG welding can be reduced up to 500 K maximally in comparison with conventional MIG welding. Besides of the mentioned findings, the visualized of metal transfer by means of high speed video camera has revealed the formation of gradual taper and smooth droplet detachment in plasma MIG welding compared with the conventional MIG welding that sometimes detached by eruption and produced a spatter. The gradual taper formation seems to be one of the important characteristics of the plasma MIG welding and the effect of plasma flow prevent the arc disturbance at wire tip after detachment. This leads to the stable formation and growth of the next droplet, results in the stable droplet size in every cycle of droplet detachment.

To validate this finding, the pulse DCEN was used instead of DCEN in first stage. In second stage, the droplet temperature also was measured and the metal transfer was visualized by using high speed video camera. Through the droplet temperature measurement results and the metal transfer observation, it can be concluded that the use of pulse DCEN plasma MIG welding is able to reduce the droplet temperature for another hundreds Kelvin maximally. The combination of the plasma MIG welding system and pulse system bring multiple effects to the droplet reduction mechanism. In this stage, we found three main factors that play an important role to reduce the droplet temperature. Namely, the effect by plasma MIG welding system itself that becomes a dominant factor during peak current, the limitation of heat flux due into droplet due to the current reduction during base current period, and lastly the radiative effect that cooled the droplet during base current.

The last stage is, to apply the findings in previous stages to join the Al/Steel dissimilarly. In this stage, the aluminum filler wire is used to perform a joining by using pulse plasma MIG welding

process. The appropriateness of the plasma MIG welding system to be applied in Al/Steel dissimilar welding is validated by the formation of IMC at the interface of aluminum and steel. From the analysis, it can be concluded that the use of pulse plasma MIG welding capable to reduce the IMC thickness to be less than $10\ \mu\text{ m}$ at the welding current below 100 A. The low temperature reduce the diffusivity of Fe into Al area, thus suppress the formation of Fe_2Al_5 and FeAl_3 . This phenomenon leads to the formation of thinner IMC in total.

To conclude, the droplet temperature is controllable in plasma MIG welding process by its flexible adjustable parameter. Due to its capability to reduce the droplet temperature, therefore the plasma MIG welding process is suitable to join the aluminum and steel dissimilarly.

Reference

- [1] S. Terashima and H. K. D. H. Bhadeshia, “Changes in toughness at low oxygen concentrations in steel weld metals,” *Sci. Technol. Weld. Join.*, vol. 11, no. 5, pp. 509–516, 2006.
- [2] W. G. Essers, “New process combines plasma with GMA welding,” *Weld. J.*, vol. 55, no. 5, pp. 394–400, 1976.
- [3] W.G.Esser, G.Jelmorini, and G.W.Tichelaar, “The plasma-MIG welding process,” *Tool Alloy Steels*, vol. 12, no. 8, pp. 275–277, 1978.
- [4] W. G. Essers, G. A. M. Willems, J. J. C. Buelens, and M. R. M. van Gompel, “Plasma-MIG welding - a new torch and arc starting method,” *Met. Constr.*, vol. 13, no. 1, pp. 36–42, 1981.
- [5] H. Ton, “Physical properties of the plasma-nm welding arc,” vol. 8, pp. 922–933, 1975.
- [6] Z. Liu, K. Ono, T. Ueyama, T. Era, and M. Tanaka, “Development of Plasma GMA welding system,” *J. Japan Weld. Soc.*, vol. 27, no. 2, p. 45s–49s, 2009.
- [7] K. Ono *et al.*, “Development of a plasma MIG welding system for aluminium,” *Weld. Int.*, vol. 23, no. 11, pp. 805–809, Nov. 2009.
- [8] Y. Tsujimura and M. Tanaka, “Numerical Simulation of heat source property with metal vapor behavior in GMA Welding(in japanese),” *J. Japan Weld. Soc.*, vol. 30, no. 1, pp. 68–76, 2012.
- [9] Y. Hirata, M. Onda, H. Nagaki, and T. Ohji, “In-situ measurement of metal drop temperature in GMA short circuiting welding (in Japanese),” *J. High Temp. Soc.*, vol. 30, no. 3, pp. 140–147, 2004.
- [10] K. Yamazaki *et al.*, “The Measurement of Metal Droplet Temperature in GMA Welding by Infrared Two-Colour Pyrometry,” *Weld. Int.*, vol. 24, no. 2, pp. 81–87, 2010.
- [11] E. Siewert, J. Schein, and G. Forster, “Determination of enthalpy, temperature, surface tension and geometry of the material transfer in PGMAW for the system argon-iron,” *J. Phys. D Appl. Phys. J. Phys. D Appl. Phys.*, vol. 46, no. 46, pp. 224008–16, 2240.
- [12] R. Monier, F. Thumerel, J. Chapuis, P. Gilles, F. Soulie, and C. Bordreuil, “In situ experimental measurement of temperature field and surface tension during pulsed GMAW,” *Weld. World*, vol. 60, no. 5, pp. 1021–1028, 2016.
- [13] E. J. Soderstrom, K. M. Scott, and P. F. Mendez, “Calorimetric Measurement of Droplet Temperature in GMAW,” *Weld. J.*, vol. 90, no. 4, p. 77S–84S, 2011.
- [14] S.Tashiro, M.Seto, A.Aoki, and M.Tanaka, “Numerical simulation of new welding process with duplex current feeding (in Japanese),” *J. Japan Weld. Soc.*, vol. 34, no. 4, pp. 223–230, 2016.
- [15] M.Seto, A. Aoki, M. Tanaka, S. Tashiro, and T.Era, “Study on new GMA welding process with duplex current feeding (in Japanese),” *J. Japan Weld. Soc.*, vol. 34, no. 2, pp. 150–157, 2016.
- [16] Y. Zhao and H. Chung, “Investigation of arc and droplet transfer in variable polarity GMAW process using numerical approach,” *Proc. Int. Symp. Vis. Join. Weld. Sci. through Adv. Meas.*

- Simulation, Osaka, Japan*, vol. 1, pp. 47–48, 2016.
- [17] G. Huismann, “Determining cooling time $t_{8/5}$ on AC-GMAW in comparison to DC-pulse welding,” *Proc. Int. Symp. Vis. Join. Weld. Sci. through Adv. Meas. Simulation, Osaka, Japan*, vol. 1, pp. 45–46, 2016.
- [18] A. Ikram and H. Chung, “The Effect of EN Ratio and Current on Microstructural and Mechanical Properties of Weld Joined by AC-GMAW on Square Groove Butt Joints,” *Appl. Sci.*, vol. 7, no. 261, pp. 1–14, 2017.
- [19] L. O. Vilarinho, A. S. Nascimento, D. B. Fernandes, and C. A. M. Mota, “Methodology for Parameter Calculation of VP-GMAW,” *Weld. Res.*, vol. 88, p. 92s–98s, 2009.
- [20] P. Praveen and P. K. D. V. Yarlagadda, “Meeting challenges in welding of aluminum alloys through pulse gas metal arc welding,” *J. Mater. Process. Technol.*, vol. 164–165, pp. 1106–1112, May 2005.
- [21] M. M. Atabaki, M. Nikodinovski, P. Chenier, J. Ma, M. Harooni, and R. Kovacevic, “Welding of Aluminum Alloys to Steels: An Overview,” *J. Manuf. Sci. Prod.*, vol. 14, no. 2, Jan. 2014.
- [22] J. Li, H. Li, C. Huang, T. Xiang, Y. Ni, and H. Wei, “Welding process characteristics of pulse on pulse MIG arc brazing of aluminum alloy to stainless steel,” *Int. J. Adv. Manuf. Technol.*, vol. 91, no. 1–4, pp. 1057–1067, Jul. 2017.
- [23] T. Murakami, K. Nakata, H. Tong, and M. Ushio, “Dissimilar metal joining of aluminum to steel by MIG arc brazing using flux cored wire,” *ISIJ Int.*, vol. 10, pp. 1596–1602, 2003.
- [24] S. Sasabe, T. Iwase, T. Matsumoto, Y. Hattori, and T. Miono, “Dissimilar Metal Joining of Aluminum Alloys to Steel in MIG Braze Welding by using the advanced Hot-dip Aluminized Steel Sheet,” *Q. J. JAPAN Weld. Soc.*, vol. 27, no. 2, p. 55s–59s, 2009.
- [25] S. Kobayashi and T. Yakou, “Control of intermetallic compound layers at interface between steel and aluminum by diffusion-treatment,” *Mater. Sci. Eng. A*, vol. 338, no. 1–2, pp. 44–53, Dec. 2002.
- [26] Y. Su, X. Hua, and Y. Wu, “Influence of alloy elements on microstructure and mechanical property of aluminum–steel lap joint made by gas metal arc welding,” *J. Mater. Process. Technol.*, vol. 214, no. 4, pp. 750–755, Apr. 2014.
- [27] J. Yang, Z. Yu, Y. Li, H. Zhang, W. Guo, and N. Zhou, “Influence of alloy elements on microstructure and mechanical properties of Al/steel dissimilar joint by laser welding/brazing,” *Weld. World*, vol. 62, no. 2, pp. 427–433, Mar. 2018.
- [28] L. H. Shah and M. Ishak, “Review of research progress on aluminum-steel dissimilar welding,” *Mater. Manuf. Process.*, vol. 29, no. 8, pp. 928–933, 2014.
- [29] H. T. Zhang, J. C. Feng, and P. He, “Interfacial phenomena of cold metal transfer (CMT) welding of zinc coated steel and wrought aluminium,” *Mater. Sci. Technol.*, vol. 24, no. 11, pp. 1346–1349, 2008.

- [30] S. Bozzi, A. L. Helbert-Etter, T. Baudin, B. Criqui, and J. G. Kerbiguet, "Intermetallic compounds in Al 6016/IF-steel friction stir spot welds," *Mater. Sci. Eng. A*, vol. 527, no. 16–17, pp. 4505–4509, Jun. 2010.
- [31] S. Katayama, "Laser welding of aluminium alloys and dissimilar metals," *Weld. Int.*, vol. 18, no. 8, pp. 618–625, 2004.
- [32] H. J. Park, S. Rhee, M. J. Kang, and D. C. Kim, "Joining of Steel to Aluminum Alloy by AC Pulse MIG Welding," *Mater. Trans.*, vol. 50, no. 9, pp. 2314–2317, 2009.
- [33] A. Mathieu, S. Mattei, A. Deschamps, B. Martin, and D. Grevey, "Temperature control in laser brazing of a steel/aluminium assembly using thermographic measurements," *NDT E Int.*, vol. 39, no. 4, pp. 272–276, 2006.
- [34] A. Szczepaniak, J. Fan, A. Kostka, and D. Raabe, "On the correlation between thermal cycle and formation of intermetallic phases at the interface of laser-welded aluminum-steel overlap joints," *Adv. Eng. Mater.*, vol. 14, no. 7, pp. 464–472, 2012.
- [35] N. P. Long, Y. Katada, and Y. Tanaka, "Cathode diameter and operating parameter effects on hafnium cathode evaporation for oxygen plasma cutting arc," *J. Phys. D. Appl. Phys.*, vol. 45, no. 435203, pp. 1–14, 2012.
- [36] S. Yamashita, M. Yamamoto, K. Shinozaki, K. Kadoi, K. Mitsui, and H. Usui, "In-situ Temperature Measurement using a Multi-sensor Camera during Laser Welding," *J. Japan Weld. Soc.*, vol. 33, no. 2, p. 93s–97s, 2015.
- [37] K. Nomura, K. Yoshii, K. Toda, K. Mimura, Y. Hirata, and S. Asai, "3D measurement of temperature and metal vapor concentration in MIG arc plasma using a multidirectional spectroscopic method," *J. Phys. D. Appl. Phys.*, vol. 50, no. 42, 2017.
- [38] M. Tanaka *et al.*, "Time-dependent calculations of molten pool formation and thermal plasma with metal vapour in gas tungsten arc welding," *J. Phys. D. Appl. Phys.*, vol. 43, no. 43, p. 434009, Nov. 2010.
- [39] M. Hertel, A. Spille-Kohoff, U. Füssel, and M. Schnick, "Numerical simulation of droplet detachment in pulsed gas–metal arc welding including the influence of metal vapour," *J. Phys. D. Appl. Phys.*, vol. 46, no. 22, p. 224003, Jun. 2013.
- [40] Y. Ogino, Y. Hirata, and A. B. Murphy, "Numerical simulation of GMAW process using Ar and an Ar–CO₂ gas mixture," *Weld. World*, vol. 60, no. 2, pp. 345–353, Mar. 2016.
- [41] J. Ni and H. M. Gao, "Effect of the Wire Temperature on the Weld Formation in GMAW," *Adv. Mater. Res.*, vol. 652–654, pp. 2289–2292, 2013.
- [42] F. Valensi *et al.*, "Study of the spray to globular transition in gas metal arc welding: a spectroscopic investigation," *J. Phys. D Appl. Phys. J. Phys. D Appl. Phys.*, vol. 46, no. 224005, pp. 1–12, 2013.
- [43] S. W. Simpson, P. Zhu, Q. Lin, and X. Li, "Metal transfer measurements in gas metal arc

- welding,” *J. Phys. D Appl. Phys. J. Phys. D Appl. Phys.*, vol. 34, pp. 347–353, 2001.
- [44] J. J. Lowke, “Physical basis for the transition from globular to spray modes in gas metal arc welding,” *J. Phys. D. Appl. Phys.*, vol. 42, no. 13, pp. 1–7, Jul. 2009.
- [45] S. Bin Mamat, T. Methong, S. Tashiro, and M. Tanaka, “Droplet Temperature Measurement in Metal Inert Gas Welding Process by Using Two Color Temperature Measurement Method,” *J. Japan Weld. Soc.*, vol. 35, no. 2, p. 160s–164s, 2017.
- [46] M. Hertel, M. Trautmann, S. Jäckel, and U. Füssel, “The Role of Metal Vapour in Gas Metal Arc Welding and Methods of Combined Experimental and Numerical Process Analysis,” *Plasma Chem. Plasma Process.*, vol. 37, no. 3, pp. 531–547, May 2017.
- [47] M. E. Rouffet, “Spectroscopic investigation of the high-current phase of a pulsed GMAW process,” *J. Phys. D Appl. Phys. J. Phys. D Appl. Phys.*, vol. 43.
- [48] S. Zielińska *et al.*, “Investigations of GMAW plasma by optical emission spectroscopy,” *Plasma Sources Sci. Technol.*, vol. 16, no. 4, pp. 832–838, Nov. 2007.
- [49] M. Schnick, U. Füssel, M. Hertel, A. Spille-Kohoff, and A. B. Murphy, “Metal vapour causes a central minimum in arc temperature in gas–metal arc welding through increased radiative emission,” *J. Phys. D. Appl. Phys.*, vol. 43, no. 2, p. 022001, Jan. 2010.
- [50] A. Boutaghane, K. Bouhadef, F. Valensi, S. Pellerin, and Y. Benkedda, “Theoretical model and experimental investigation of current density boundary condition for welding arc study,” *Eur. Phys. J. Appl. Phys.*, vol. 54, no. 1, p. 10802, Apr. 2011.
- [51] P. C. Wang, “Modelling and analysis of metal transfer in gas metal arc welding,” *J. Phys. D Appl. Phys.*, vol. 36, pp. 1143–1152, 2003.
- [52] M. Hertel, S. Rose, and U. Füssel, “Numerical simulation of arc and droplet transfer in pulsed GMAW of mild steel in argon,” *Weld. World*, vol. 60, no. 5, pp. 1055–1061, 2016.
- [53] H. Shimizu, Y. Yokota, T. Itoh, T. Kurokawa, and M. Ushio, “Joule heating of solid wires in MAG welding,” *Weld. Int.*, vol. 19, no. 10, pp. 761–772, 2005.
- [54] Y. Hirata, “Physics of Welding. (III). Melting rate and temperature distribution of electrode wire,” *J. Japan Weld. Soc.*, vol. 63, no. 7, pp. 484–488, 1994.
- [55] A. B. Murphy, “Influence of metal vapour on arc temperatures in gas–metal arc welding: convection versus radiation,” *J. Phys. D. Appl. Phys.*, vol. 46, no. 22, p. 224004, Jun. 2013.
- [56] H. Lee, S. Park, and C.-Y. Kang, “Effect of plasma current on surface defects of plasma-MIG welding in cryogenic aluminum alloys,” *J. Mater. Process. Technol.*, vol. 223, pp. 203–215, Sep. 2015.
- [57] S. Tashiro and M. Tanaka, “Development of plasma MIG brazing process for dissimilar metal joining of aluminum to steel,” *IOP Conf. Ser. Mater. Sci. Eng.*, vol. 61, p. 012018, Aug. 2014.
- [58] S. Bin Mamat, S. Tashiro, M. Tanaka, and M. Yusoff, “Study on factors affecting the droplet temperature in plasma MIG welding process,” *J. Phys. D. Appl. Phys.*, vol. 51, no. 13, p. 135206,

- Apr. 2018.
- [59] Y. Su, X. Hua, Y. Wu, Y. Zhang, and Y. Guo, "Characterization of intermetallic compound layer thickness at aluminum–steel interface during overlaying," *Mater. Des.*, vol. 78, pp. 1–4, Aug. 2015.
- [60] G. Sierra, P. Peyre, F. D. Beaume, D. Stuart, and G. Fras, "Steel to aluminium braze welding by laser process with Al–12Si filler wire," *Sci. Technol. Weld. Join.*, vol. 13, no. 5, pp. 430–437, Jul. 2008.
- [61] H. J. Park, S. Rhee, M. J. Kang, and D. C. Kim, "Joining of Steel to Aluminum Alloy by AC Pulse MIG Welding," *Mater. Trans.*, vol. 50, no. 9, pp. 2314–2317, 2009.
- [62] J. L. Song, S. B. Lin, C. L. Yang, and C. L. Fan, "Effects of Si additions on intermetallic compound layer of aluminum–steel TIG welding– brazing joint," *J. Alloys Compd.*, vol. 488, no. 1, pp. 217–222, Nov. 2009.
- [63] G. Zhang, M. Chen, Y. Shi, J. Huang, and F. Yang, "Analysis and modeling of the growth of intermetallic compounds in aluminum–steel joints," *RSC Adv.*, vol. 7, no. 60, pp. 37797–37805, 2017.
- [64] N. Cinca, C. R. C. Lima, and J. M. Guilemany, "An overview of intermetallics research and application: Status of thermal spray coatings," *J. Mater. Res. Technol.*, vol. 2, no. 1, pp. 75–86, Jan. 2013.
- [65] H. Springer, A. Kostka, E. J. Payton, D. Raabe, A. Kaysser-Pyzalla, and G. Eggeler, "On the formation and growth of intermetallic phases during interdiffusion between low-carbon steel and aluminum alloys," *Acta Mater.*, vol. 59, no. 4, pp. 1586–1600, Feb. 2011.
- [66] P. Novák *et al.*, "On the formation of intermetallics in Fe–Al system – An in situ XRD study," *Intermetallics*, vol. 32, pp. 127–136, Jan. 2013.
- [67] Y. Su, X. Hua, and Y. Wu, "Quantitative characterization of porosity in Fe–Al dissimilar materials lap joint made by gas metal arc welding with different current modes," *J. Mater. Process. Tech.*, vol. 214, pp. 81–86, 2014.
- [68] Y. Su, X. Hua, and Y. Wu, "Influence of alloy elements on microstructure and mechanical property of aluminum–steel lap joint made by gas metal arc welding," *J. Mater. Process. Tech.*, vol. 214, pp. 750–755, 2014.
- [69] Henager Charles and H. Charles, "Hydrogen Permeation Barrier Coatings", 2018.

Appendix

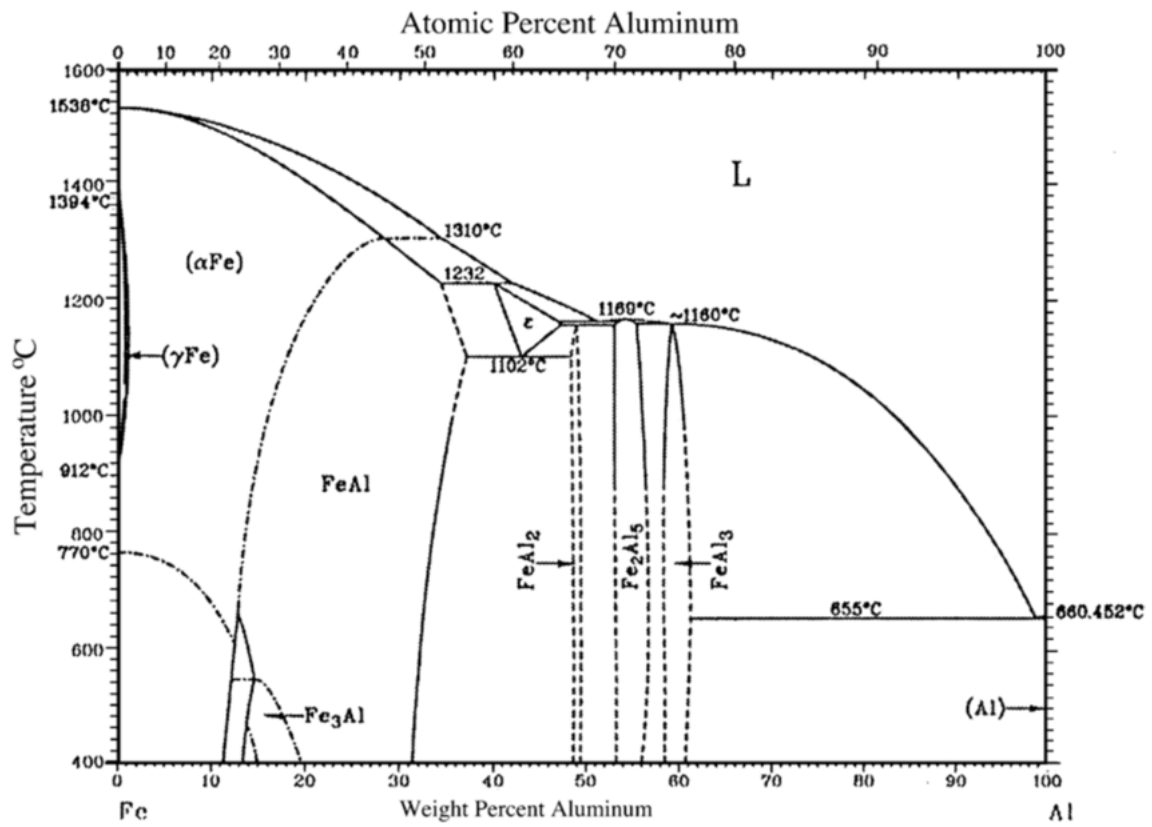


Fig. A1 Fe-Al phase diagram [69]

Appendix

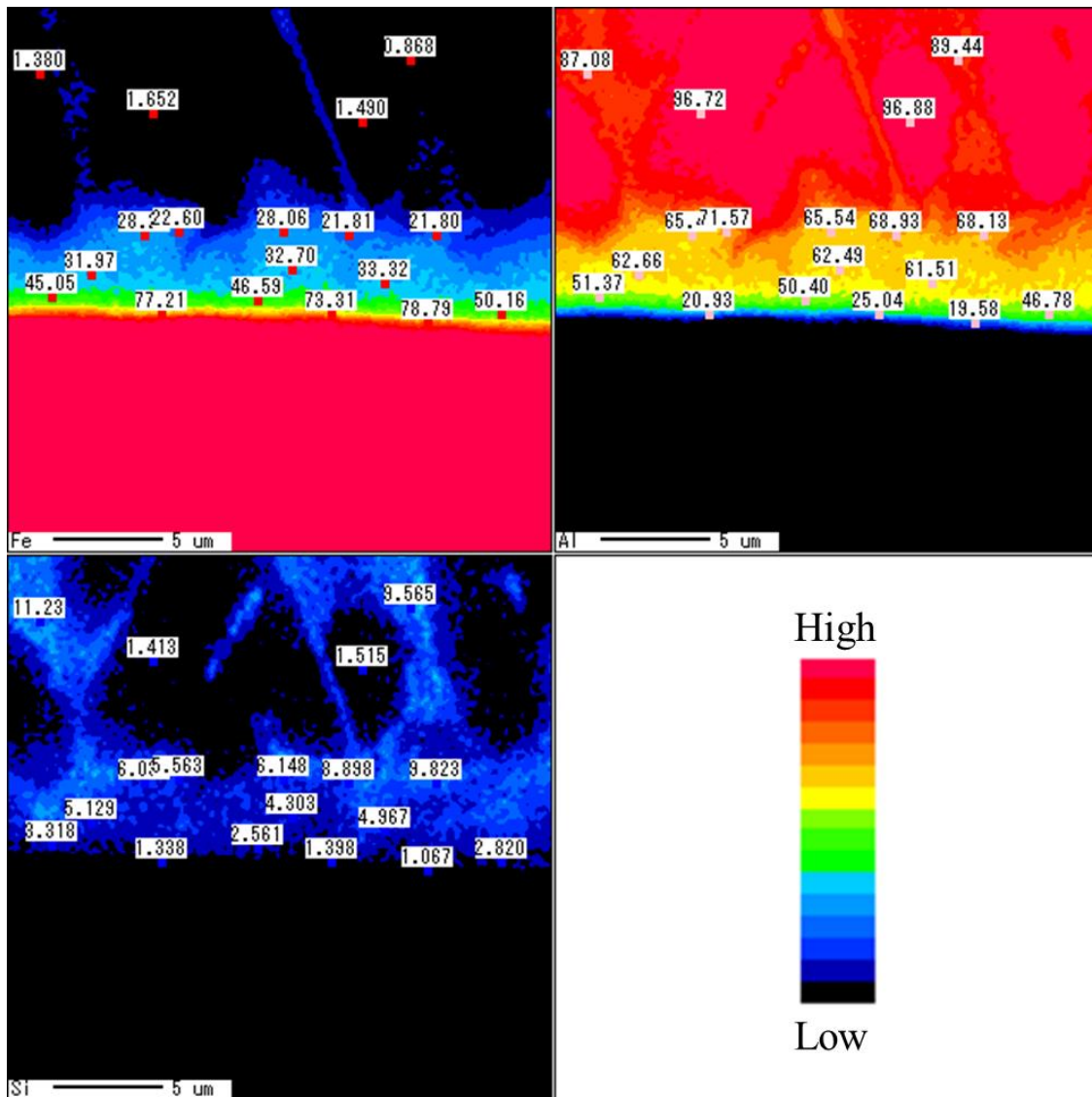


Fig. A2 EPMA quantitative analysis of the sample welded by pulse MIG welding (92 A)

Appendix

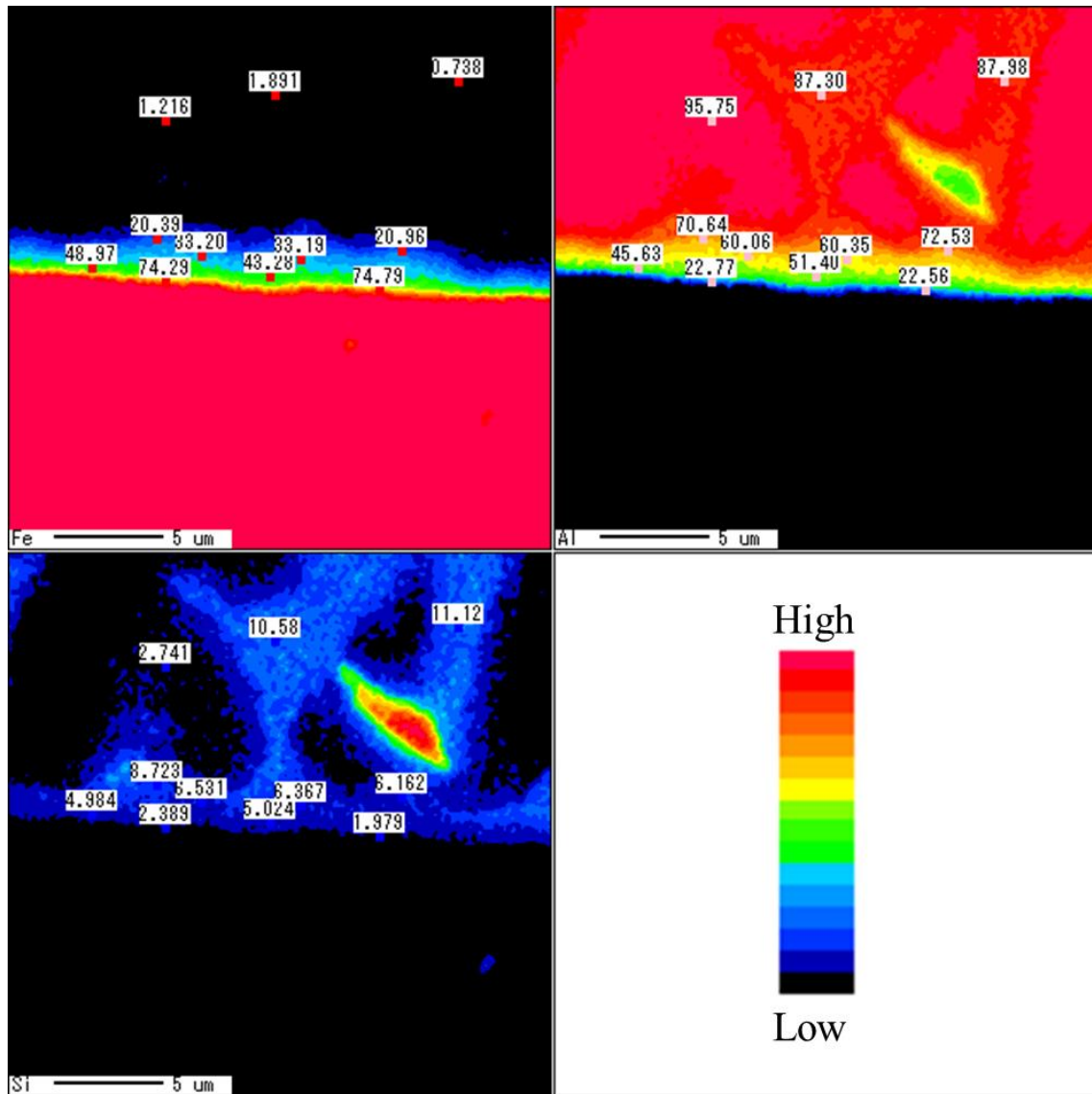


Fig. A3 EPMA quantitative analysis of the sample welded by pulse plasma MIG welding (73 A)

Appendix

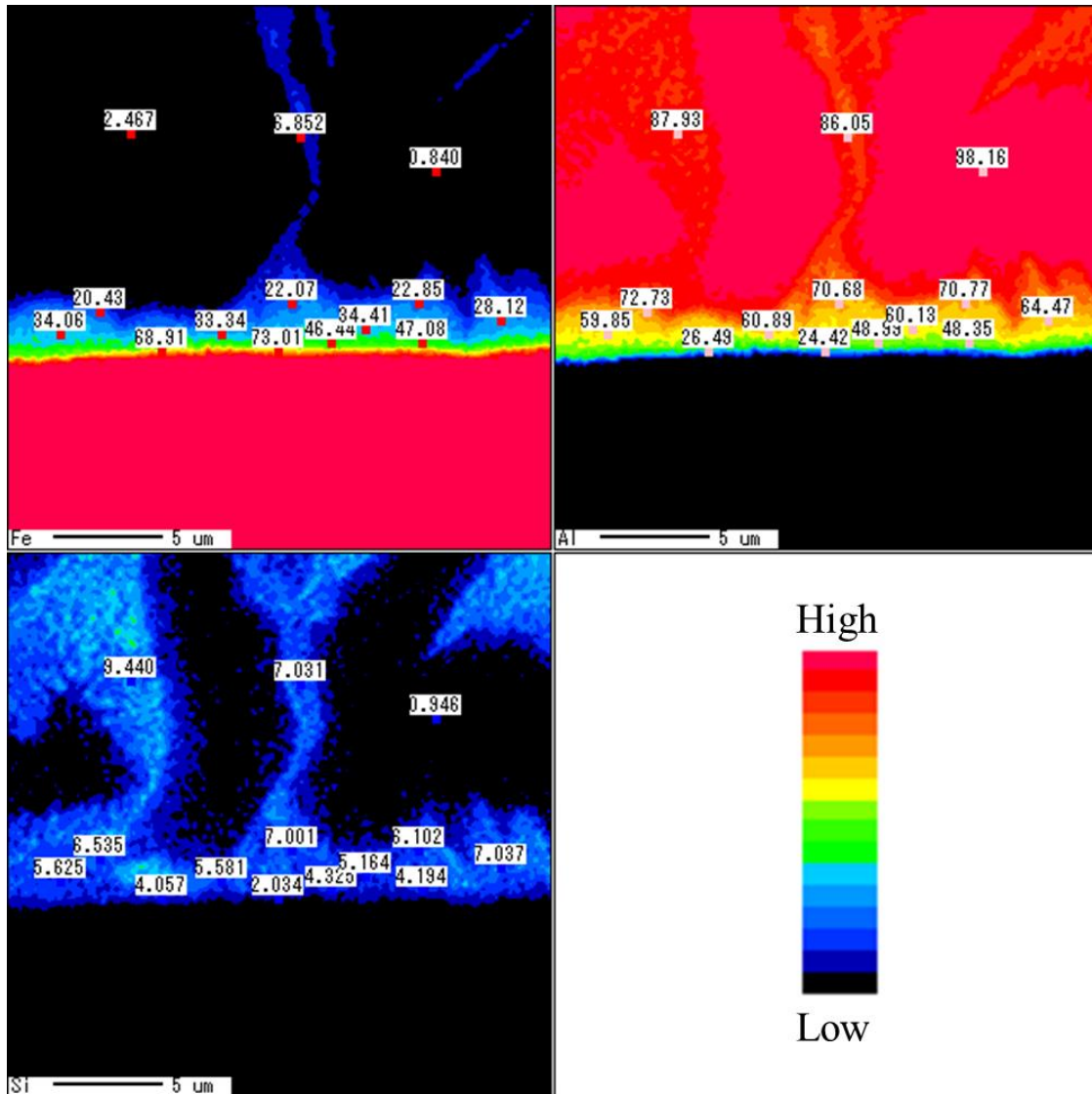


Fig. A4 EPMA quantitative analysis of the sample welded by pulse plasma MIG welding (89 A)

Appendix

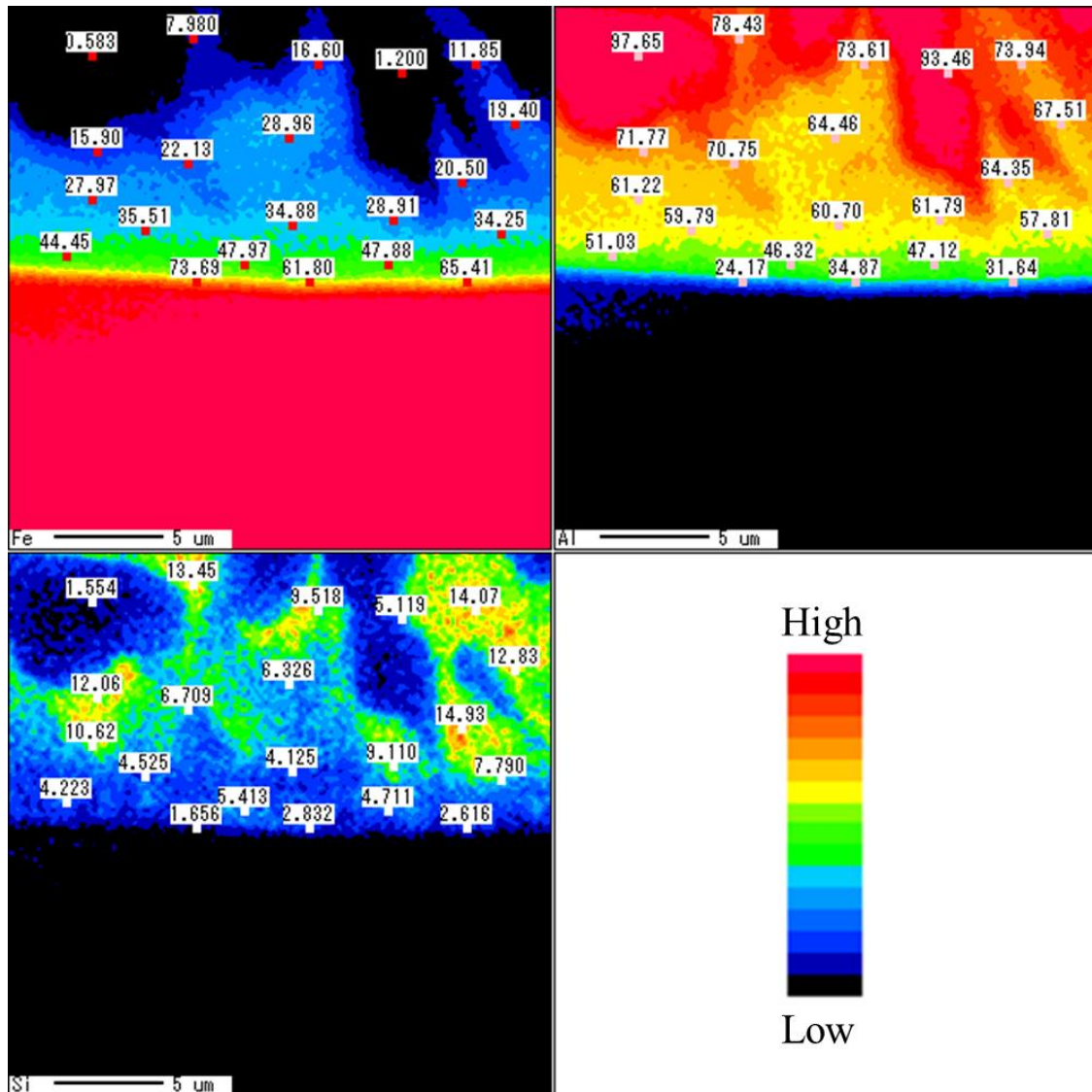


Fig. A5 EPMA quantitative analysis of the sample welded by pulse plasma MIG welding (106 A)

Appendix

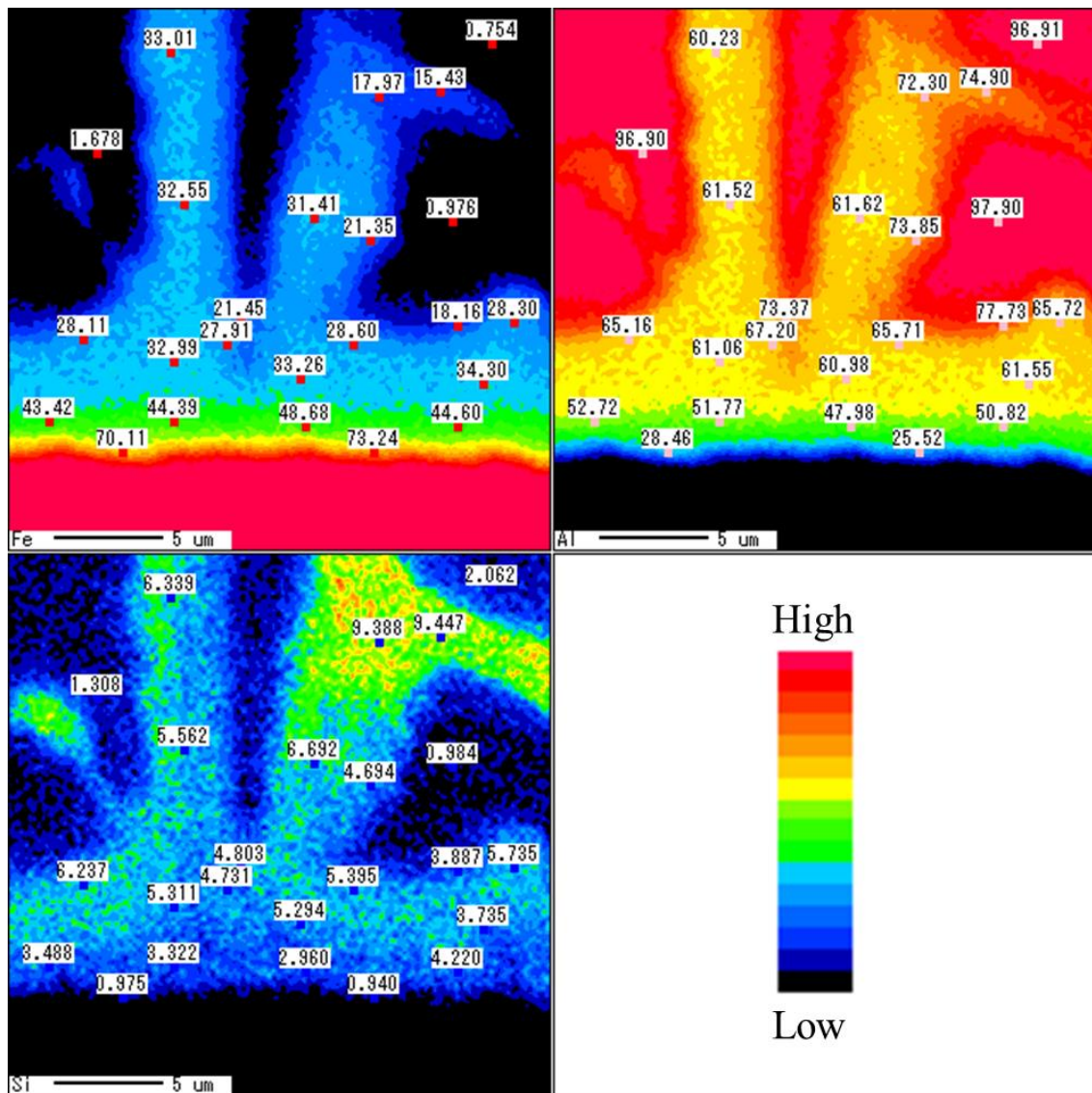


Fig. A6 EPMA quantitative analysis of the sample welded by pulse plasma MIG welding (117 A)

Appendix

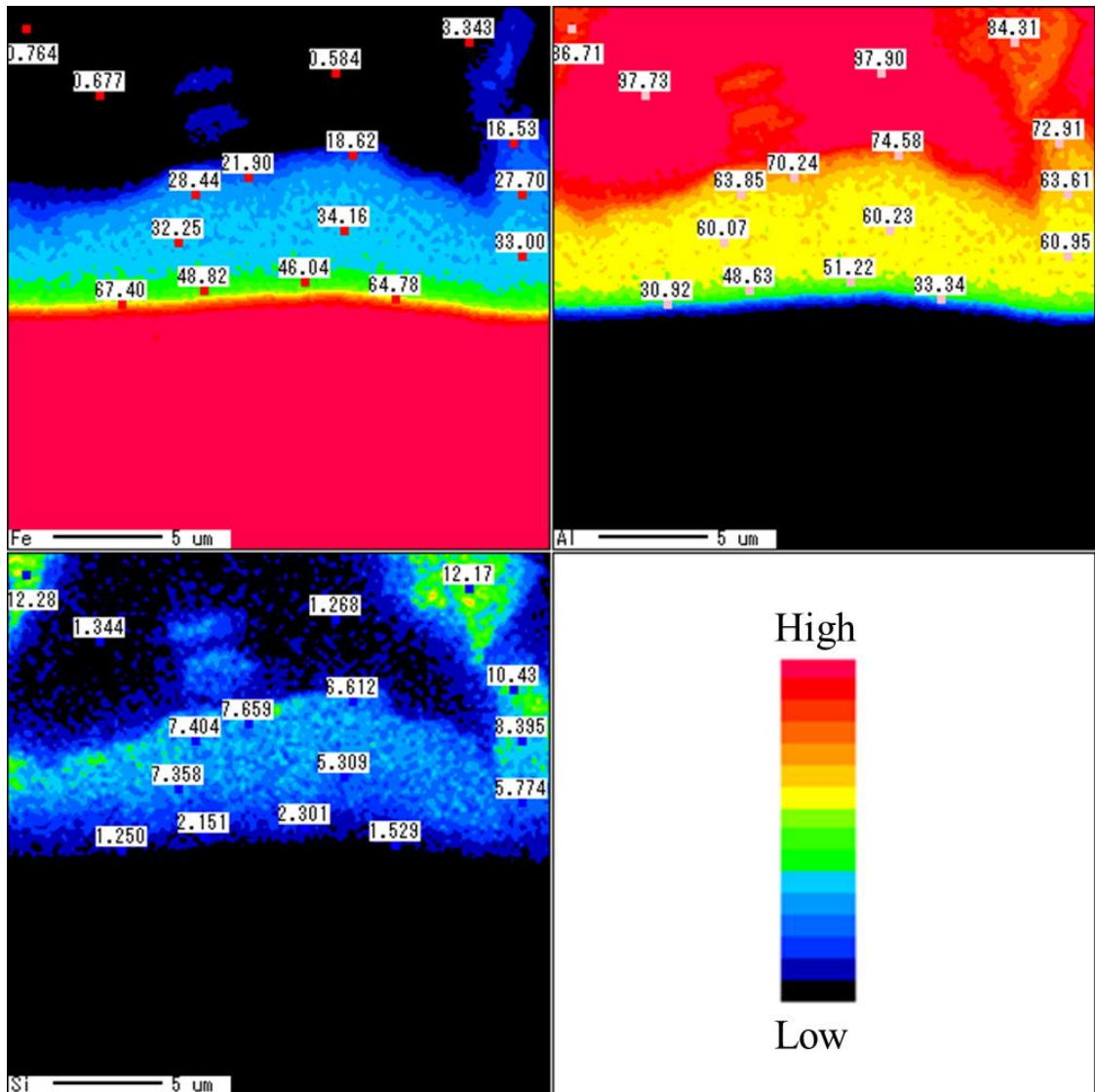


Fig. A7 EPMA quantitative analysis of the sample welded by pulse plasma MIG welding (131 A)

Appendix

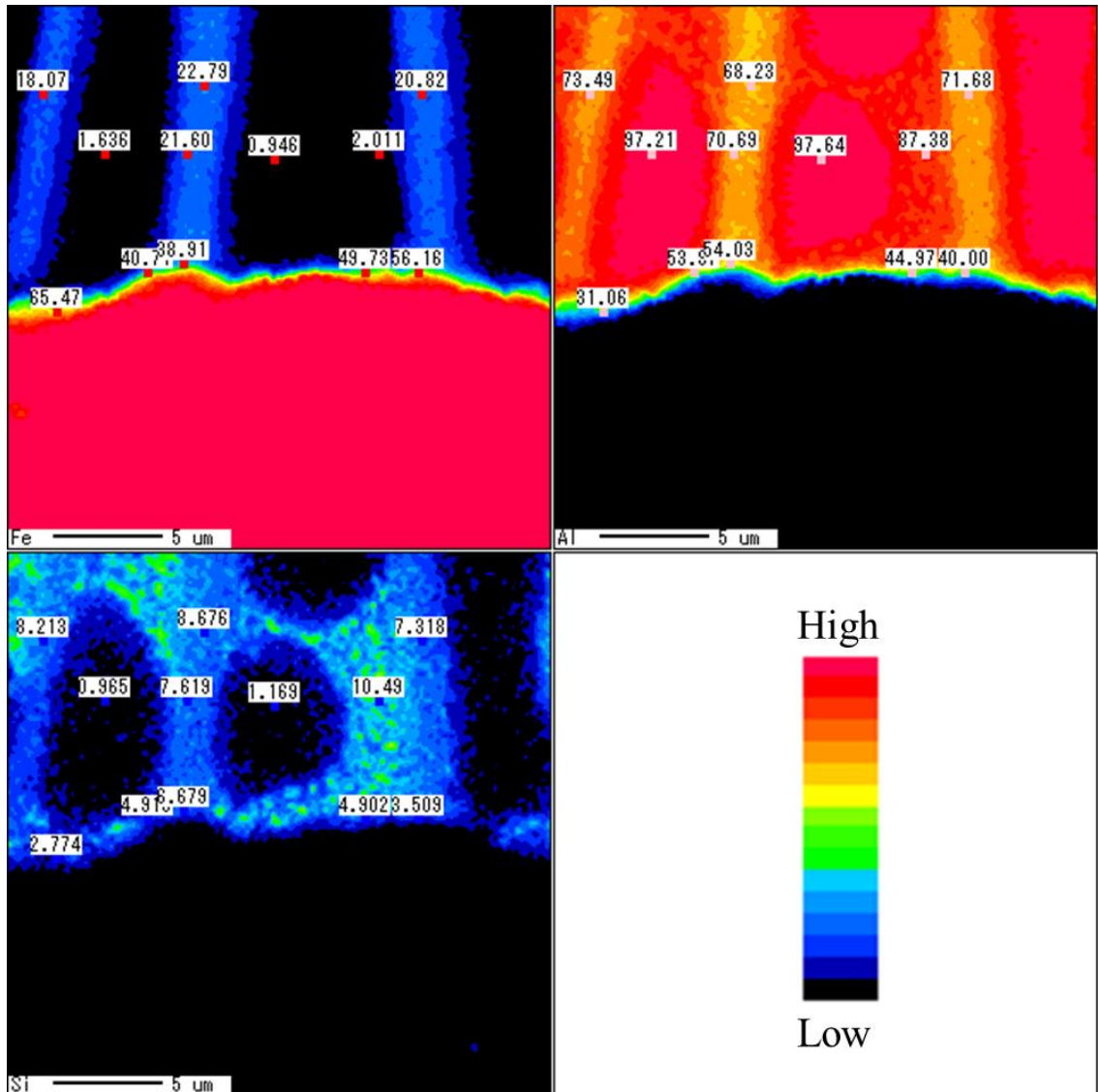


Fig. A8 EPMA quantitative analysis of the sample welded by pulse plasma MIG welding (140 A)

List of Publications

1. **Sarizam Bin Mamat**, Shinichi Tashiro, Manabu Tanaka, Mahani Yusoff, “**Study on Factors Affecting the Droplet Temperature in Plasma MIG Welding Process**”, Journal of Physics D : Applied Physics, 51, 2018, 135206, (23pp), DOI No : 10.1088/1361-6463/aab128
2. **Sarizam Bin Mamat**, Shinichi Tashiro, Manabu Tanaka, “**Observation of Metal Transfer in Plasma MIG Welding Process**”, Journal of The Japan Welding Society, Vol.35, No.2, 2017, pp 33s-37s
3. **Sarizam Bin Mamat**, Titinan Methong, Shinichi Tashiro, Manabu Tanaka, “**Droplet Temperature Measurement in Gas Metal Inert Gas by Using Temperature Measurement Method**”, Journal of The Japan Welding Society, Vol.35, No.2, 2017, pp 160s-164s

List of Proceedings

1. **Sarizam Bin Mamat**, Shinichi Tashiro, Manabu Tanaka, “**Metal Transfer Observation in Aluminum Pulse Plasma MIG Welding**”, Paper presented at Spring 2018 National Meeting of Japan Welding Society, Tokyo, Japan, 2018.04.24-2018.04.26, pp 152-153, Printed
2. **Sarizam Bin Mamat**, Shinichi Tashiro, Manabu Tanaka, “**Development of Advanced Control Technology of Plasma MIG Process and Application to Dissimilar Joining**”, Paper presented at Symposium on Creation of Life Innovation Materials for Interdisciplinary and International Researcher Development, Osaka, Japan, 2018.03.30, pp125-126 ,Printed
3. **Sarizam Bin Mamat**, Shinichi Tashiro, Manabu Tanaka, “**Study on Factors in Controlling the Droplet Temperature in Plasma MIG Welding Process**” , Paper presented at Joint Intermediate Meeting of International Institute of Welding Comm.I,IV, XII and SG212, Malibor, Slovenia, 2018.03.12-2018.03.13
4. Shinichi Tashiro, **Sarizam Bin Mamat**, Manabu Tanaka, Anthony B. Murphy, “**Numerical Simulation on Plasma MIG Welding Process**” , Paper presented at Joint Intermediate Meeting of International Institute of Welding Comm.I,IV, XII and SG212, Malibor, Slovenia, 2018.03.12-2018.03.13
5. Shinichi Tashiro, **Sarizam Bin Mamat**, Manabu Tanaka, Yuichiro Koizumi, “**Development of Advanced Control Technology of Plasma MIG Process and Application to Dissimilar Joining**”, Paper presented at National Symposium on Creation of Life Innovation Materials for Interdisciplinary and International Researcher Development, Nagoya University, 2017.03.30, pp 152-153, Printed
6. **Sarizam Bin Mamat**, Shinichi Tashiro, Manabu Tanaka, “**Droplet Temperature Measurement in Plasma MIG Welding**”, Paper presented at International Welding and Joining Conference, IWJC 2017, Gyeong Ju, South Korea, 2017.04.11-2017.04.14, CD-ROM
7. **Sarizam Bin Mamat**, Shinichi Tashiro, Manabu Tanaka, “**Study on Factors in Controlling the Droplet Temperature in Plasma MIG Welding Process**” , Paper presented at Spring 2017 National Meeting of Japan Welding Society, Tokyo, Japan, pp 244-245, https://doi.org/10.14920/jwstaikai.2017s.0_86

8. **Sarizam Bin Mamat**, Shinichi Tashiro, Manabu Tanaka, “ **Effect of Plasma Electrode Diameter to Droplet Temperature in Plasma MIG Welding**” , Paper presented at Autumn 2017 National Meeting of Japan Welding Society, Kita Kyushu, Japan, http://www.jstage.jst.go.jp/article/jwstaikai/2017f/0/2017f_446
9. **Sarizam Bin Mamat**, Shinichi Tashiro, Manabu Tanaka, “**Effect of Plasma Electrode Diameter to Droplet Temperature in Plasma MIG Welding**” Paper presented at International Conference on Materials and System for Sustainability, ICMaSS 2017, Nagoya University, Nagoya, 2017.09.29 – 2017.10.01, Vol.1, p.p 79-80, Printed
10. **Sarizam Bin Mamat**, Shinichi Tashiro, Manabu Tanaka, “**Factors in Controlling the Droplet Temperature in Plasma MIG Welding Process**”, Paper presented at Autumn 2017 Smart Process Society Meeting, Tokyo, Japan, 2017.11.28, pp.55-56, Printed
11. **Sarizam Bin Mamat**, Shinichi Tashiro, Manabu Tanaka, “**Basic Characterization of Plasma MIG Welding Process**” , Paper presented at Autumn 2016 National Meeting of Japan Welding Society, Gunma, Japan, pp 244-245, https://doi.org/10.14920/jwstaikai.2016f.0_244
12. **Sarizam Bin Mamat**, Shinichi Tashiro, Manabu Tanaka, “**Measurement of Droplet Temperature in Plasma MIG Welding**”, Paper presented at The 172th Iron and Steel Institute of Japan Meeting 2016, 2016.09.22 – 2016.09.23, CAMP-ISIJ Vol.29(2016), 724 (CD-ROM)
13. **Sarizam Bin Mamat**, Titinan Methong, Shinichi Tashiro, Manabu Tanaka, “**Droplet Temperature Measurement in Gas Metal Arc Welding Process by Using Two Color Temperature Measurement Method**”, Paper presented at The International Symposium on Visualization in Joining & Welding Science through Advanced Measurements and Simulation (Visual-JW2016), Osaka, Japan, 2016.10.17 – 2016.10.18, Vol.1, pp 177-178, Printed
14. Shinichi Tashiro, **Sarizam Bin Mamat**, Manabu Tanaka, “**Basic Characteristics of Plasma MIG Welding Process**”, Paper presented at The 1st International Symposium on Creation of Life Innovation Materials for Interdisciplinary and International Researcher Development (iLIM-1), Osaka, Japan, 2016.10.17 – 2016.10.18, Vol.3, pp 108, Printed

ACKNOWLEDGEMENT

First and foremost, I would like to express my gratitude to my principal supervisor, Professor Dr. Manabu Tanaka for his extremely supportive and ever accessible throughout this research work. He provided a good study environment and offered plenty of opportunities for me to explore and pursue my research interest. An enormous and great appreciation are also presented to my immediate supervisor, Assistant Professor Dr. Shinichi Tashiro for his guidance. His expertise, understanding and patience, added considerably to my graduate experience and with his encouragement and personal guidance, it would have been provided a good basis for the present thesis. Besides that, I also wish to express my sincere appreciation to Associate Professor Dr. Masaya Shigeta for his encouragement and kindness during my time in this laboratory.

Special thanks are also presented to my seniors, Dr. Yuhei Konishi, Dr. Mithong Titinan, Dr. Nguyen Van Anh, for their kind sharing of experience. Additionally, my grateful thanks also go to my colleagues, Mr Hisaya Komen, Mr Phan Le Huy, Mr. Keigo Tanaka, Mr. Akitoshi Korukawa, Mr. Satoshi Miki, Mr. Katsuyuki Shimada, Mr Tomohiro Sugai and Mr. Tetsuya Yamada for their courage, sharing of knowledge and advice.

My family members have been the largest supporters throughout my PhD research. I am humbly indebted to my loving mother, Hajjah Che Munah Bt. Che Ali, my late father, Almarhum Haji Mamat Bin Ishak for their doa and blessing. Special thanks and gratitude to my wife, Che Rohayu Bt Che Mohd Apandi for her patience, encouragement and continuous support on this research work. To my loving kids, Minhalina Rasyada, Muhammad Mirza Razin, Muhammad Mifzal Raziq, Muhammad Mizal Rafiq and Maisara Raisya, thanks for being my strength during my study.

Thanks as well to all my immediate family in Osaka University, especially Mr. Wan Aminuddin Wan Ismail, Mr. Firdaus Mohamad, Mr. Mohd Natashah Norizan, Mr. Riyaz Ahmad Mohamed Ali, Mr. Shahrul Ismail, Mrs Hasyiya Karimah Adli and many others who are always available with their valuable advice in my difficult time throughout these years.

I gratefully acknowledge the financial support from The Ministry of Higher Education of Malaysia and University Malaysia Kelantan through the SLAB/SLAI scholarship program.

Sarizam Bin Mamat

May 2018